RECENT DEGLACIERIZATION OF THE UPPER WHEATON RIVER WATERSHED, YUKON

by

Amber Church
Double Honours B.Sc. with Distinction University of Victoria 2004

THESIS SUBMITTED IN PARTIAL FULFILLMENT OF
THE REQUIREMENTS FOR THE DEGREE OF

MASTER OF SCIENCE

In the
Department of Earth Sciences

SIMON FRASER UNIVERSITY

SPRING 2011

APPROVAL

Name: **Amber Church**

Degree: **Master of Science**

Title of Thesis: **Recent Deglacierization of the Upper Wheaton River Watershed, Yukon**

Examining Committee:

Chair: **Dr. Andy Calvert**
Professor, Department of Earth Sciences

Dr. John Clague
Senior Supervisor
Professor, Department of Earth Sciences

Dr. Brent Ward
Supervisor
Associate Professor, Department of Earth Sciences

Dr. Jeff Bond
Supervisor
Surficial Geologist, Yukon Geological Survey

Dr. Andrée Blais-Stevens
External Examiner
Geological Survey of Canada

Date Defended/Approved: November 8, 2010

Declaration of
Partial Copyright Licence

ABSTRACT

My research involves the study of Wheaton Glacier, the largest glacier in the Wheaton River watershed in southern Yukon Territory. Since the Little Ice Age, Wheaton Glacier has lost 50% of its area and 58% to 63% of its volume. Despite increasing winter snowfall, rising temperatures continue to drive the persistent negative mass balance of the glacier. Periglacial activity, precipitation events, and glacier recession are affecting sediment delivery in the upper Wheaton River watershed. Sediment is moving downstream from the Wheaton Glacier forefield and large, out-of-channel debris flows are impacting the fan at the mouth of the valley. Evidence from sediment cores collected on the distal part of the fan suggests that debris flows have dominated sedimentation at the mouth of the valley during the last half of the Holocene, coincident with Neoglacial advances and the historic period of rapid glacier retreat.

Keywords: Holocene deglacierization; climate change; debris flows; Wheaton River; Yukon

Subject Terms: Quaternary geology; geomorphology

DEDICATION

This work is dedicated to my loving and ever-patient friends and family who have always encouraged and supported me. In particular, my husband, Tyler Kuhn, saw me through every step of the thesis process; from keeping me sane as I waded through an increasingly overloaded schedule, to pounding cores into unyielding debris flow deposits, to gently prodding me to finish.

ACKNOWLEDGEMENTS

I wish to thank Dr. John Clague for his guidance and support throughout this project and my supervisory committee members – Jeff Bond and Dr. Brent Ward – for all of their help. I thank the Yukon Geological Survey, the National Science and Engineering Research Council of Canada, the Yukon Mining and Petroleum Environmental Research Group, the Association for Canadian Universities for Northern Studies, the Northern Scientific Training Program, and the Northern Research Institute for their financial, logistical, and moral support. Tyler Kuhn, Kayla Vickers, and Denny Capps provided excellent assistance in the field under often challenging conditions.

TABLE OF CONTENTS

LIST OF FIGURES

LIST OF TABLES

1: INTRODUCTION

1.1 Project Overview

The Arctic and sub-Arctic are experiencing greater climate warming than other parts of the world (Intergovernmental Panel on Climate Change, 2007). Over the past several decades, temperatures in these areas have increased at twice the rate of the rest of the planet. One of the manifestations of atmospheric warming in Yukon Territory is thinning and retreat of many glaciers (Arctic Climate Impact Assessment, 2005; Lemmen *et al*., 2008) and perennial snow banks (Hare at al., 2004). Glacier retreat in the Yukon is important because it is intimately linked to changes in geomorphology, hydrology, and biotic environments.

The Wheaton River watershed in southern Yukon supports several small glaciers, which are the northeastern most glaciers in the Coast Mountains. Glaciers in the Wheaton River watershed are located at the fringe of the region that today is able to support ice, making them highly responsive to recent and ongoing climate change. This study provides a perspective on the impacts of changing climate in southern Yukon by examining the largest of the glaciers in the Wheaton River watershed, hereafter referred to as Wheaton Glacier.

Periglacial activity, extreme precipitation events, and glacier recession are causing instability in the Wheaton Glacier forefield. A pulse of sediment is moving downstream as a series of debris flows that are affecting the fan at the valley

mouth. My research focuses on understanding the linkages between twentieth century glacier retreat and geomorphic changes in the valley below.

1.2 Objectives

This project involves a study of the impact of contemporary deglacierization on upper Wheaton River valley. The research addresses the following questions:

- How has Wheaton Glacier changed over the past century?
- What is the relationship between the historic activity of Wheaton Glacier and regional climate?
- What has been the impact of recent retreat of Wheaton Glacier on the valley below?

These questions will be addressed through a combination of aerial photograph analysis, geomorphic mapping, lichenometry, analysis of climate data, ground penetrating radar and sediment core analysis. These methods will be outlined in detail in subsequent chapters.

1.3 Wheaton River

1.3.1 Physiography

The Wheaton River watershed is in the transition zone between the Coast Mountains and the Yukon Plateau (Bond, 2003). It has an area of 875 km^2 and drains to Lake Bennett near Carcross (Figure 1; Ramage *et al*., 2006). The watershed is located within the Yukon-Stikine Highlands ecoregion, the Boundary Ranges physiographic region, and the Coast morphologic belt (Smith *et al*., 2004). This part of Yukon is an upland plateau with numerous cirques, arêtes,

and horns, and is dissected by narrow and deep river valleys (Bond, 2003). Broad summit areas lie 900 to 1200 m above valley floors at 760-900 m asl (Smith *et al.,* 2004).

1.3.2 Climate

The southern Yukon-Stikine Highlands region is affected by moist masses of maritime air, but the Wheaton River watershed is drier than most of this region. Most precipitation occurs during the fall and early winter; late winter and early spring are the driest seasons (Smith *et al*., 2004).

Mean annual temperature in the region is approximately -2.5 °C. Mean January temperature averages -18 °C at higher elevations and -25 °C on the valley floors (Smith *et al*., 2004). July is typically the warmest month of the year, with temperatures averaging 12 °C in the valley and 5 °C at high elevations. Annual temperature extremes at valley-bottom sites are -45 and 35 °C; corresponding values at higher elevations are -30 to 15 °C (Smith *et al*., 2004). Frost can occur at any time of the year, but is least common in July (Smith *et al*., 2004).

1.3.3 Bedrock Geology

The Wheaton River watershed is within the Stikinia Terrane (Smith *et al*., 2004). Stikinia in southern Yukon includes three sub-circular volcanic caldera complexes located along the west arm of Bennett Lake (Lambert, 1974), at

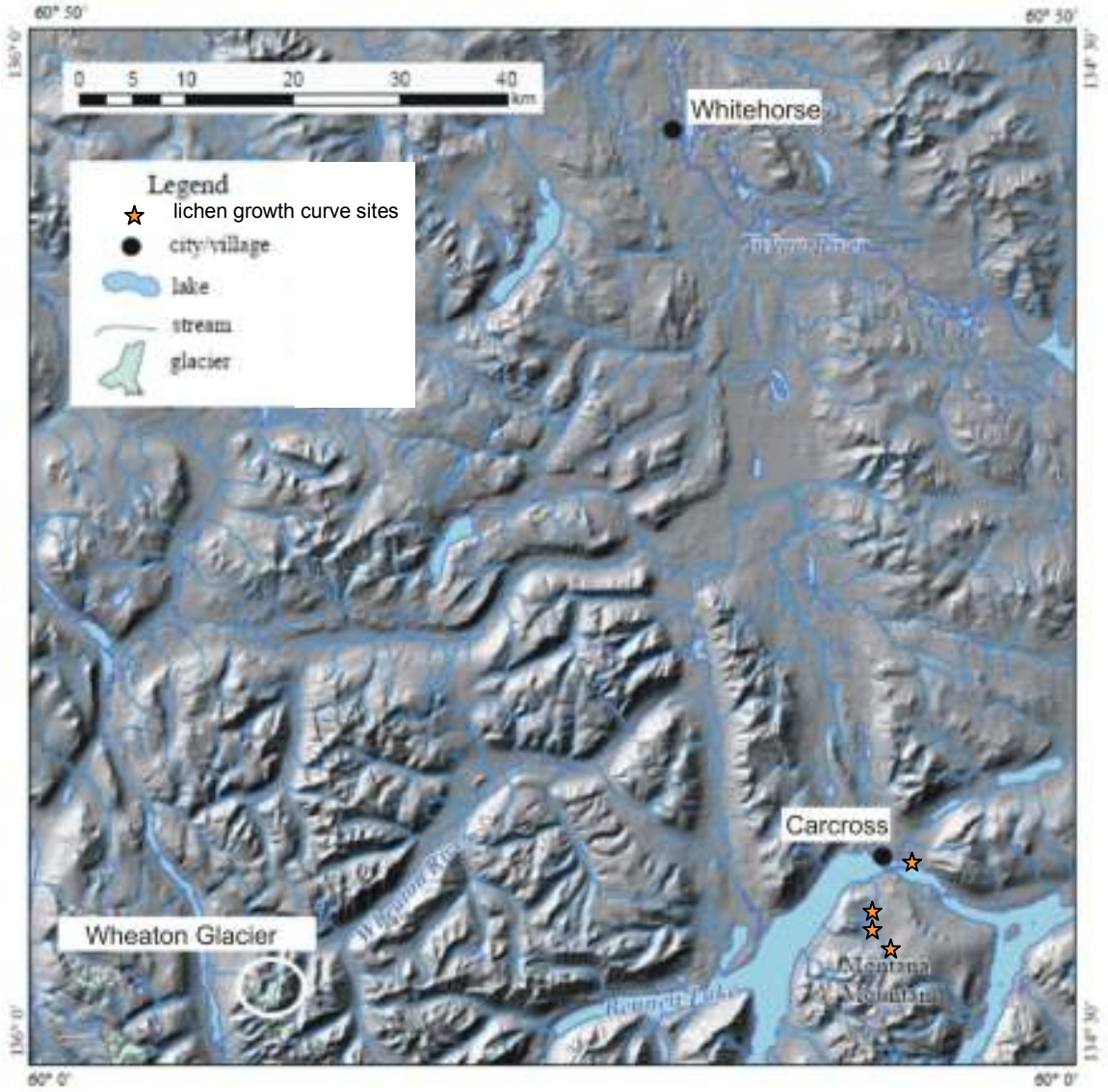

Figure 1 Location of the Wheaton Glacier study site. Orange stars indicate sample sites used to construct lichen growth curve.

Mount Skukum (Pride, 1985), and at Montana Mountain (Hart and Radloff, 1990). These volcanic complexes are correlated with the Bennett Lake Caldera Complex (Pride and Clark, 1985). The volcanic complexes consist of andesite and dacite flows and breccia. Steep faults separate the volcanic complexes from Jurassic Laberge Group sandstone and conglomerate and Upper Triassic Lewes

River Group augite porphyritic basalt and limestone (Smith *et al.*, 2004). Quartz veins at Mount Skukum and Montana Mountain have been mined for gold, silver, and antimony (MacDonald, 1990), and many metal occurrences have been documented in the watershed (Hart and Radloff, 1990).

1.3.4 Glacial Geology

The Cordilleran Ice Sheet covered the entire Wheaton River watershed, with the possible exception of the highest peaks, during the Late Wisconsinan McConnell Glaciation (Bond, 2003). During deglaciation, the Cassiar lobe of the Cordilleran Ice Sheet advanced into a zone vacated by the Coast Mountain lobe flowing from the west. A series of proglacial lakes developed throughout southern Yukon at this time (Figure 2). Wheaton River valley hosted a lake that initially drained via an outlet at the headwaters of Wheaton River, and later through Cowley Creek northward into the Yukon River valley (Bond, 2003).

Wheaton Glacier either disappeared or shrank to near its present size during the early Holocene, when climate was warmer than today (Denton and Stuiver, 1966). It reformed or advanced during Neoglaciation and reached its maximum Holocene extent during the Little Ice Age (Bond, 2003).

1.4 Holocene Climate

Earth's climate changed on different timescales during postglacial time (Figure 3). The most significant change was at the end of the Younger Dryas

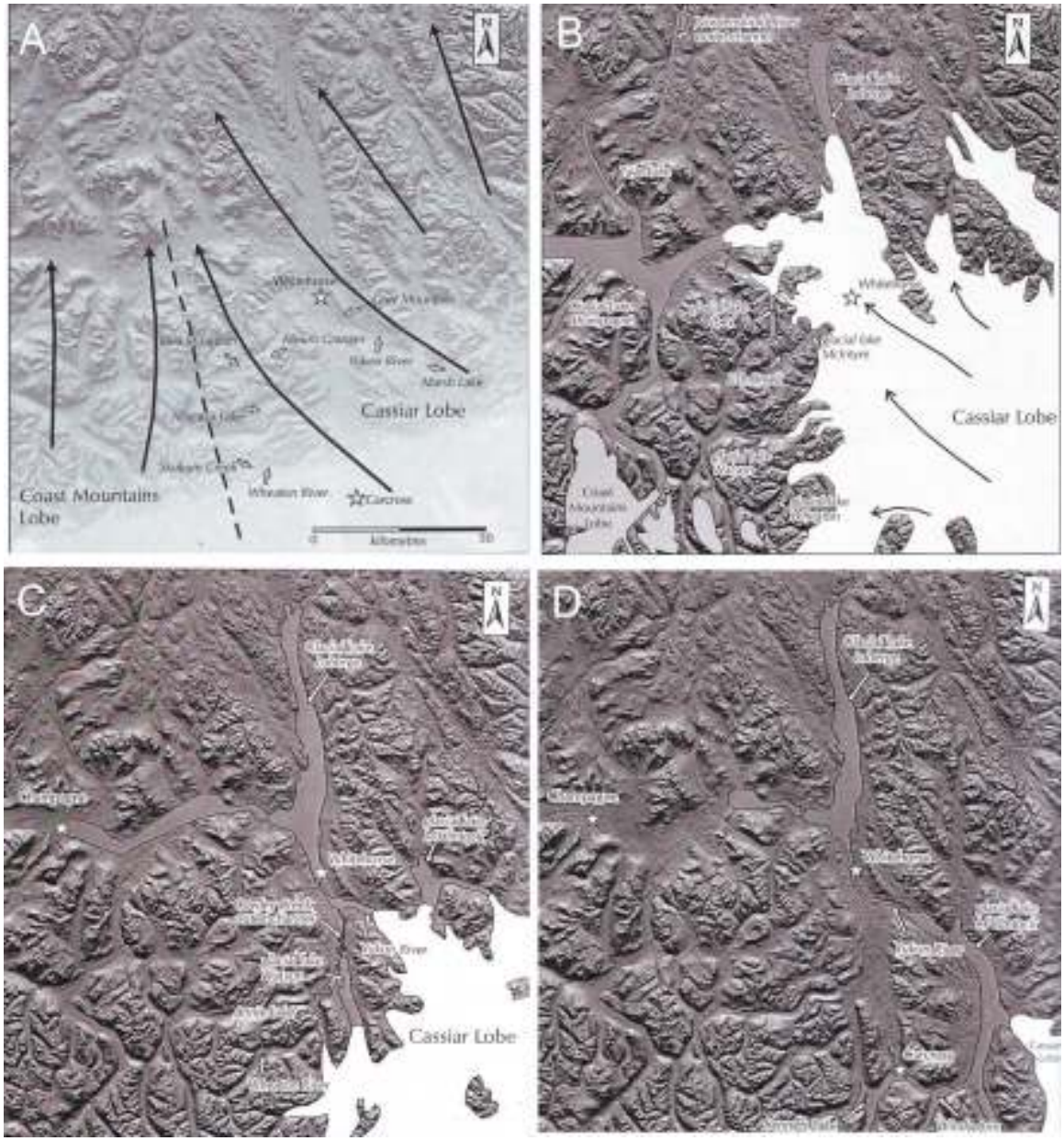

Figure 2 Regional glacial history. 3A: McConnell glacial maximum. 3B: Ibex stage. 3C: Cowley stage. 3D: M'Clintock stage. (From Bond, 2003).

Chronozone, when rapid stepwise warming occurred over a period of several decades in the Northern Hemisphere. Perhaps half of the warming took place in less than 15 years (Taylor et al., 1997). There is evidence that the Yukon

experienced similar warming from work done in Jellybean and Marcella lakes (Anderson, 2005).

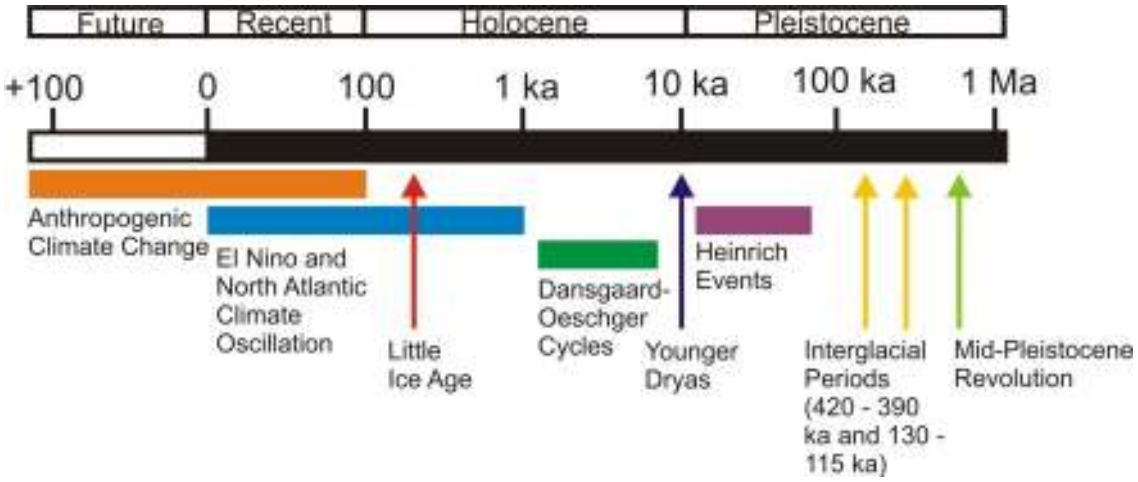

Figure 3 Major climatic events during the past million years. Data from Taylor *et al.* (1997).

Early Holocene warmth was interrupted, about 8200 years ago, by cool dry conditions that persisted for about 200 years before climate warmed again (Alley *et al*., 1997; Mayewski *et al*., 1997). The generally warmer period of the early Holocene has been termed the Climatic Optimum and is well documented in proxy climate records from the Arctic and sub-Arctic (Kaufman *et al.*, 2004).

1.4.1 Neoglaciation

The Holocene Climatic Optimum was followed by climate cooling and episodic glacier advances (Neoglaciation of Porter and Denton, 1967; Table 1).

Palynological evidence suggests that wetter and possibly cooler conditions became established as early as 7000 years ago in coastal British Columbia and Yukon (Mathewes, 1985; Pellatt and Mathewes, 1994; Anderson, 2005).

Neoglaciation culminated with the major glacier advances of the Little Ice Age (Grove, 1988; Luckman, 2000).

The Little Ice Age began about 800 years ago; most glaciers achieved their maximum Neoglacial extents in the eighteenth or nineteenth century (Grove, 1988; Grove and Switsur, 1994; Bradley and Jones, 1995). The Little Ice Age was the most significant climatic event of the late Holocene, with major impacts on civilization. Norse colonies in Greenland disappeared early during the Little Ice Age (Barlow *et al*., 1997); colder winters in Europe and North America caused harbours and canals to freeze; and crop failures across the Northern Hemisphere resulted in periodic famine (Fagan, 2001).

1.4.2 Historic Climate Change

Warming at the end of the nineteenth century terminated the Little Ice Age. Minor warming during the first two decades of the twentieth century was followed by accelerated warming between the 1930s and 1960s (Intergovernmental Panel on Climate Change, 2007). Climate cooled slightly in the 1960s and 1970s, but warmed again in the 1980s. Warming appears to be accelerating – several of the years 2001 through 2009 rank among the ten warmest years of the past 130 years (1880-2009; National Oceanic and Atmospheric Administration, 2010). The 2000-2009 decade is the warmest on record – the average global surface temperature over this decade is 0.54°C above the long-term (twentieth century) average and 50 percent higher than the value for the 1990s, which itself was well

Table 1 Late-Glacial and Neoglacial advances in western North America.

Site	Geographic Area	Radiocarbon Age	Reference
I. Pre-Neoglacial Advances			
Crowfoot Advance; estimated at 12 - 6.8 ka yrs BP (Osborn and Luckman, 1988)			
Crowfoot Glacier	Rocky Mountains	> 6800 yr BP	Luckman and Osborn, 1979
Waterton Lakes National Park	Rocky Mountains	> 6800 yr BP	Osborn, 1985
Glacier National Park	Rocky Mountains	> 6800 yr BP	Carrara, 1987; Osborn, 1985
Upper Elk Valley	Rocky Mountains	> 6800 yr BP	Ferguson, 1978
Mt. Rae	Rocky Mountains	> 6800 yr BP	Gardner *et al.* , 1983
Bugaboo Glacier	Purcell Mountains	> 6800 yr BP	Osborn and Karlstrom, 1986
Dunn Peak Advance (may correlate with the Crowfoot Advance) (Alley, 1976)			
Shuswap Highland	Monashee Mountains	5000 - 4000	Alley, 1976
Dunn Peak	Monashee Mountains	7390 +/- 250	Duford and Osborn, 1978
Germansen Lake	Omineca Mountains	8210 +/- 80	Blake, 1983
Garibaldi Provincial Park	Coast Mountains	7700-7300	Koch *et al.* , 2007
II. Neoglacial Advances			
Early Neoglacial Expansion: Garibaldi Phase (Ryder and Thompson, 1986)			
Mt. Garibaldi	Coast Mountains	5260 +/- 200	Stuiver *et al.* , 1960
Sentinel Glacier	Coast Mountains	5300 +/- 70	Lowdon and Blake, 1975
Mt. Breakenridge	Coast Mountains	5960 +/- 140	Lowdon and Blake, 1968
Near Bridge Glacier	Coast Mountains	5500 +/- 70	Blake, 1983
Sentinel Glacier	Coast Mountains	6170 +/- 150	Lowdon and Blake, 1973
Garibaldi Provincial Park	Coast Mountains	6400-5100	Koch *et al.* , 2007
Garibaldi Provincial Park	Coast Mountains	4300	Koch *et al.* , 2007
Boundary Glacier	Rocky Mountains	3880 +/- 60	Gardner and Jones, 1985
Boundary Glacier	Rocky Mountains	4050 +/- 70	Gardner and Jones, 1985
Mid-Neoglacial Advance: Tiedemann Advance (Ryder and Thompson, 1986) and Battle Mountain Advance (Alley, 1976)			
Tiedmann Glacier	Coast Mountains	3345 +/- 115	Ryder and Thomson, 1986
Tiedmann Glacier	Coast Mountains	2355 +/- 60	Ryder and Thomson, 1986
Tiedmann Glacier	Coast Mountains	2940 +/- 130	Fulton, 1971
Tiedmann Glacier	Coast Mountains	2250 +/- 130	Fulton, 1971
Gilbert Glacier	Coast Mountains	2200 - 1900	Ryder and Thomson, 1986
Frankmackie Glacier	Coast Mountains	2730 +/- 170	Lowdon and Blake, 1973
Garibaldi Provincial Park	Coast Mountains	4100-2900	Koch *et al.* , 2007
Bugaboo Glacier	Purcell Mountains	3390 +/- 80	Osborn and Karlstrom, 1986
Bugaboo Glacier	Purcell Mountains	3070 +/- 120	Osborn and Karlstrom, 1986
Peyto Glacier	Rocky Mountains	2880 +/- 170	Lowdon *et al.* , 1971
Battle Mountain	Monashee Mountains	3400 - 2300	Alley, 1976; Westgate, 1977
Natazhat Glacier	St. Elias Mountains	3300 +/- 130	Rampton, 1970
Late Neoglacial Advance: Little Ice Age, Cavell Advance (Luckman and Osborn, 1979), and Mammoth Creek Advance (Alley, 1976)			
Klinaklini Glacier	Coast Mountains	400 +/- 45	Ryder and Thomson, 1986
Klinaklini Glacier	Coast Mountains	900 +/- 40	Ryder and Thomson, 1986
Franklin Glacier	Coast Mountains	835 +/- 45	Ryder and Thomson, 1986
Bridge Glacier	Coast Mountains	680 +/- 50	Ryder and Thomson, 1986
Bridge Glacier	Coast Mountains	540 +/- 45	Ryder and Thomson, 1986
Sphinx Glacier	Coast Mountains	460 +/- 60	Ryder and Thomson, 1986
Scud Glacier	Coast Mountains	455 +/- 65	Ryder and Thomson, 1986
Scud Glacier	Coast Mountains	625 +/- 140	Ryder and Thomson, 1986
Glacier B	Coast Mountains	595 +/- 60	Ryder and Thomson, 1986
Garibaldi Provincial Park	Coast Mountains	1600-1100	Koch *et al.* , 2007
Bugaboo Glacier	Purcell Mountains	900 +/- 60	Osborn, 1986
Big Eddy Creek	Monashee Mountains	450 +/- 130	Wheeler, 1964
Kiwa Glacier	Monashee Mountains	840 +/- 80	Luckman, 1986
Mamoth Creek	Monashee Mountains	1000-800 and last 400	Alley, 1976
Robson Glacier	Rocky Mountains	450 +/- 150	Heusser, 1956
Robson Glacier	Rocky Mountains	860 +/- 50	Luckman, 1986
Robson Glacier	Rocky Mountains	900 +/- 60	Luckman, 1986
Robson Glacier	Rocky Mountains	1140 +/- 80	Luckman, 1986
Kaskawulsh Glacier	St. Elias Mountains	1750 (*calendrical age*)	Reyes *et al.* , 2006
Klutlan Glacier	St. Elias Mountains	1520 +/- 130	Rampton, 1970

above the long-term average (National Oceanic and Atmospheric Administration, 2010).

1.4.3 ENSO and PDO

ENSO is an acronym for “El Niño Southern Oscillation”, a linked ocean-atmosphere phenomenon in the equatorial Pacific Ocean. It has two components: El Niño/La Niña, the oceanic component; and the Southern Oscillation, the atmospheric component (Redmond and Koch, 1991).

An El Niño event begins with a random, slight reduction in the trade winds, which causes warm water in the western equatorial Pacific Ocean to flow eastward. The eastward flow further reduces the strength of trade winds, causing more warm water to move eastward until El Niño conditions are established. Winter in the Pacific Northwest is drier in an El Niño year, whereas it is wetter in the southwest United States. The La Niña state is the opposite of the El Niño one. It is manifested by cool sea surface temperatures in the equatorial Pacific, a wetter winter climate in the Pacific Northwest, and drier winter conditions in the southwest United States (Cayan *et al.,* 1998). ENSO effects in Yukon are similar to those in the Pacific Northwest, although with larger temperature variations (Shabbar and Khandekar, 1996).

The Southern Oscillation is the alternation of normal high and low atmospheric states over the Pacific and Indo-Australian regions. When atmospheric pressure is low over the South Pacific and high over Indonesia and Australia, Pacific trade winds weaken and upwelling of cool water slows or stops along the west coast of

South America. Sea-surface temperatures increase in the areas of weakened upwelling (Taylor, 1998). When atmospheric pressure is high over the South Pacific, strong trade winds induce upwelling and westward flow of cool water, reducing equatorial surface water temperatures.

PDO is an acronym for “Pacific Decadal Oscillation”. It is a long-term El Niño-like pattern of North Pacific climate variability, with phases that persist up to 20-30 years. The positive (warm) phase of the PDO is characterized by cooler-than-average sea surface temperatures near the Aleutian Islands and warmer-than-average sea surface temperatures along the California coast. The positive phase of the PDO enhances El Niño conditions, and the negative (cool) phase enhances La Niña conditions, in the Northern Hemisphere (Mantua *et al*., 1997).

Changes in ENSO and PDO have been related to many phenomena, including the California drought of 1987-1992 (Roos, 1994), changes in stream flow (Langbein and Slack, 1982) and snowpack (Changnon *et al*., 1993), changes in the time of the freshet (Roos, 1991; Wahl, 1992; Dettinger and Cayan, 1995), multi-decadal groundwater fluctuations (Dettinger and Schaeffer, 1995), changes in flood frequency (Webb and Betancourt, 1990; Ely *et al.*, 1994), and changes in salmon productivity (Mantua *et al.*, 1997).

The effects of ENSO and PDO can differ with elevation. PDO shifts may change the locations of regions of high and low geopotential height anomalies in the middle and upper troposphere (Moore *et al.*, 2003); these changes strengthen ENSO events at high elevations in North America. This effect has been inferred

from winter mass balance data at Wolverine Glacier, Alaska, and at Mount Logan, Yukon (Moore *et al.*, 2003).

1.5 Thesis Structure

Chapter 2 summarizes the recent history of Wheaton Glacier and its relation to climate based on analysis of sequential aerial photographs and field observations. Chapter 3 summarizes and discusses the Neoglacial history of the valley below Wheaton Glacier, especially the debris flow fan at its mouth. This part of the study is based on analysis of sedimentologic, stratgraphic, and geomorphic data collected in the field. Chapter 4 reflects on the major findings and significance of the research, and offers suggestions for future work.

2: WHEATON GLACIER

2.1 Introduction

Wheaton Glacier is located at the eastern limit of glaciers within the northern Coast Mountains. Glaciers to the west in the St. Elias Mountains have been the focus of many studies and long-term monitoring programs (for example Denton and Stuiver, 1967; Marcus and Ragle, 1970; Johnson, 1992; Spotila *et al*., 2004; Frappé-Sénéclauze and Clarke, 2007; De Paoli and Flowers, 2009), but to date no study of smaller, more isolated Yukon glaciers has been completed, making my work unique. Wheaton Glacier is distant from its precipitation source, the Pacific Ocean, which increases its sensitivity to climate change. In addition, its location near the eastern limit of glaciers in this region may make it more likely to show deterioration due to increased temperature. This sensitivity makes documentation of the historic changes in the glacier worthy of study, because they provide a unique perspective on the impacts of changing climate in the Coast Mountains of southwest Yukon.

2.2 Objectives

This study addresses two questions:

- How has Wheaton Glacier changed between the Little Ice Age and today?
- What is the relationship between the historic activity of Wheaton Glacier and regional climate? This objective addresses the relationship between

temperature and precipitation patterns; PDO and ENSO; and glacier volume and area.

2.2.1 Study Site

Wheaton Glacier is located in a cirque at the head of the Wheaton River watershed (Figure 4). A rock ridge and medial moraine divide the glacier into two lobes. The east lobe is 3 km long and is the source of a stream that flows 4 km to a debris flow fan in the trunk Wheaton River valley. The west lobe is 3 km long and terminates in a small proglacial lake. The glacier is bordered by the highest peaks in the watershed (maximum elevation 2460 m). The bedrock beneath and around Wheaton Glacier is highly fractured and jointed granite, granodiorite, and diorite. Talus covers the lower slopes adjacent to the glacier. The glacier forefield is largely unvegetated, covered by ground moraine, recessional moraines, and erratics, and is bordered by a Little Ice Age terminal moraine. The site of a former proglacial, moraine-dammed lake, inside the terminal moraine, is marked by a shoreline and a flat lake bed. Rock glaciers are common on the east side of the valley downvalley from the Little Ice Age terminal moraine.

2.3 Methods

2.3.1 Glacier Area Loss and Downwasting

Observations by staff of the Yukon Geological Survey and successive aerial photographs (1948, 1964, 1987, and 1995; Table 2) demonstrate that Wheaton Glacier has significantly thinned and retreated over the past 60 years.

Figure 4 Wheaton Glacier; photograph taken in 2007. Note the rock ridge within the west lobe that was covered by the glacier as recently as the early 1960s.

Table 2 Aerial photographs used in this study*.

Date	Photo Roll Number	Photo Numbers
1948	A11521	444-446
1964	A19425	116-117
1987	A27149	052-054
1995	A28240	087-089, 096-098

*Government of Canada aerial photographs, National Air Photo Library.

The aerial photographs were scanned using a photogrammetric scanner at the National Air Photo Library in Ottawa. I imported the digital images into a GIS using ArcView software and geo-referenced them using ground-control points collected during the 2007 field season with both differential and hand-held GPS units. I determined the aerial extents of the glacier in 1948, 1964, 1987, and 1995 in ArcView GIS, and measured the Little Ice Age extent of the glacier based on moraine and trimline features. The extent of the glacier in 2004, 2006, and 2007 is based on field surveys by the Yukon Geological Survey, Monica Bruckner (a former graduate student at Montana State University), and myself in 2007. Glacier downwasting was determined by differencing ground control points collected with a differential GPS. I collected points from the top of a rock ridge separating the two lobes of Wheaton Glacier that first became exposed in 1964 (Figure 4).

2.3.2 Bivariate Scaling Analysis and Volume Estimates

A scaling analysis based on mass and momentum conservation equations shows that glacier volume can be related by a power law to more easily observed glacier surface area (Bahr *et al.*, 1997):

$$V \alpha S^{\gamma} \qquad \text{(Equation 1)}$$

where V is glacier volume, S is glacier surface area, and γ is an exponent relating volume and surface area.

Based on a dataset of 144 glaciers worldwide, Bahr *et al*. (1997) estimated γ to be 1.36. Other authors, however, have suggested values ranging from 1.25 (Paterson, 1972) to 1.4 (Macheret *et al*., 1988). Volume estimates for this study were calculated using values of γ of 1.25, 1.36, and 1.4 to capture the potential range of values.

2.3.3 Geomorphology

Trimlines, moraines, a landslide track, rock glaciers, a bedrock ridge exposed by glacier recession, and the margins of a now-drained proglacial lake in the glacier forefield were delineated on aerial photographs and captured in the GIS (Figure 5). The delineation was field checked in the summer of 2007.

2.3.4 Lichenometry

Thalli of lichen (*Rhizocarpon geographicum*) on moraines and other features throughout the glacier forefield (Figure 6) were measured to estimate the time of glacier retreat over the past century. The methodology is modified from that of Innes (1985). At each site, the maximum diameters of 100 randomly chosen thalli were measured to the nearest millimetre to obtain a sample of the lichen population that included the largest specimens. Measurements for each sample were plotted as histograms to facilitate comparison (see Section 2.5.2 below). The average of the five largest lichen was used to estimate surface age (Figure 7). This metric was used to reduce the influence of anomalous outliers that may have existed within the site lichen population (Innes, 1985).

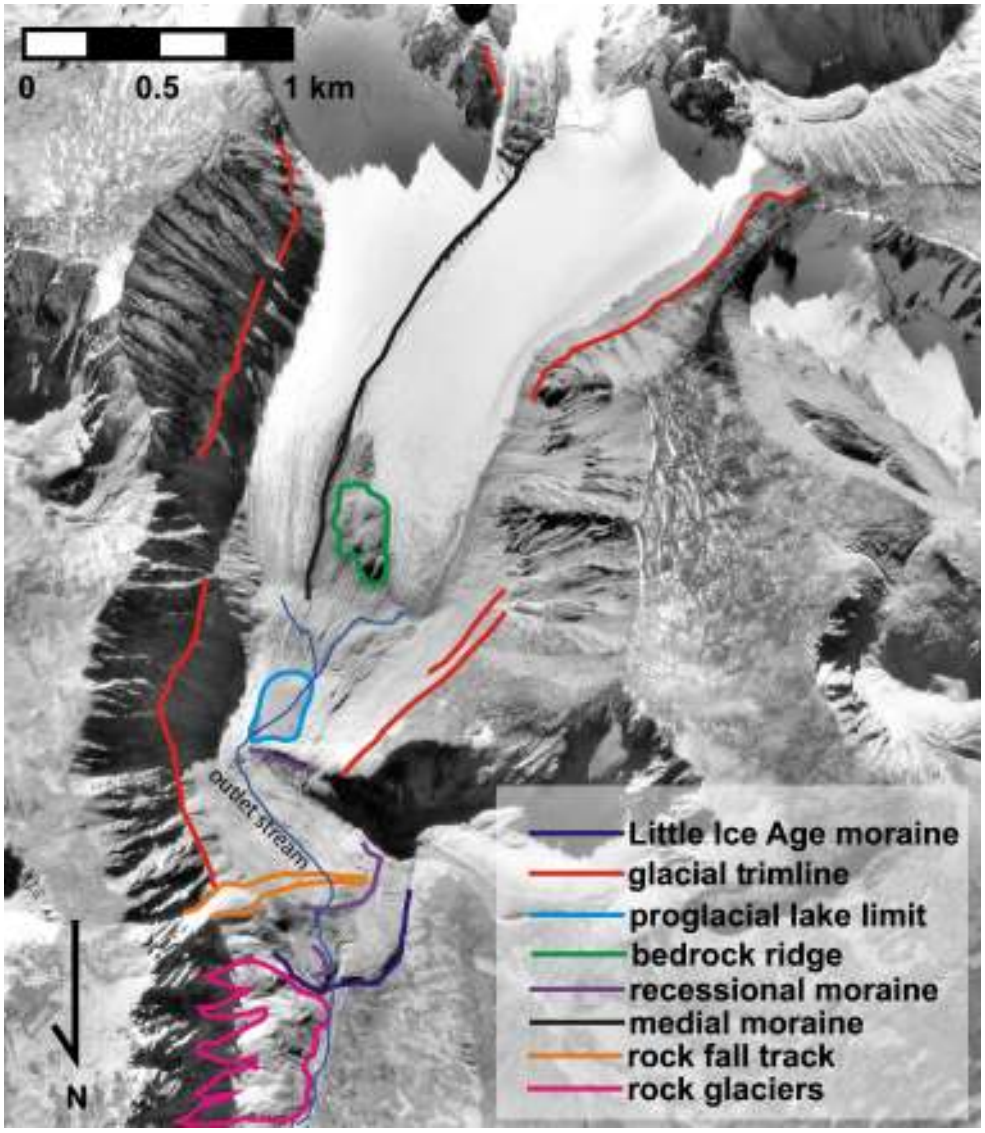

Figure 5 Location of geomorphic features in the Wheaton Glacier forefield. Features are plotted on aerial photograph A28240/88, taken in 1995.

A lichen growth curve (Figure 7) for subalpine environments in southern Yukon was constructed to estimate the ages of landforms of interest in the Wheaton River watershed. Lichens on surfaces of known age were measured in the same manner as at Wheaton Glacier. The surfaces include the Carcross-Tagish First Nations cemetery and several sites on Montana Mountain, including turn-of-the-century stone buildings and national survey points (Figure 1 and Table 3). As in

the Wheaton River watershed, each point on the growth curve represents the average of the five largest lichens at a site. An error range of +/- 20 years was estimated for lichen ages (Figure 7). Lichen growth curves have been constructed for other regions of Yukon, including the St. Elias Mountains (Rampton, 1970) and the Frances Lake map area (Dyke, 1990). Given the large differences in climate, geology, geomorphology, and elevation between these regions and the study area, and the availability of historic sites of known age near the Wheaton River watershed, I chose to construct a new lichen growth curve rather than use an existing curve.

2.3.5 Climate Analysis

Temperature and precipitation data for Whitehorse and Carcross, the two closest weather stations to the study area, were obtained from the National Climate Data and Information Archive (Environment Canada, 2009). Data exist for the period 1907-present. Yearly and seasonal temperature and precipitation averages were calculated and plotted to identify dominant trends. Comparisons were also made to records of the Pacific Decadal Oscillation (PDO), obtained from the University of Washington (JISAO, 2009), and the El Niño-Southern Oscillation (ENSO), obtained from National Oceanic and Atmospheric Administration's (NOAA) National Weather Service Climate Prediction Centre (National Oceanographic and Atmospheric Administration Climate Prediction Center, 2009).

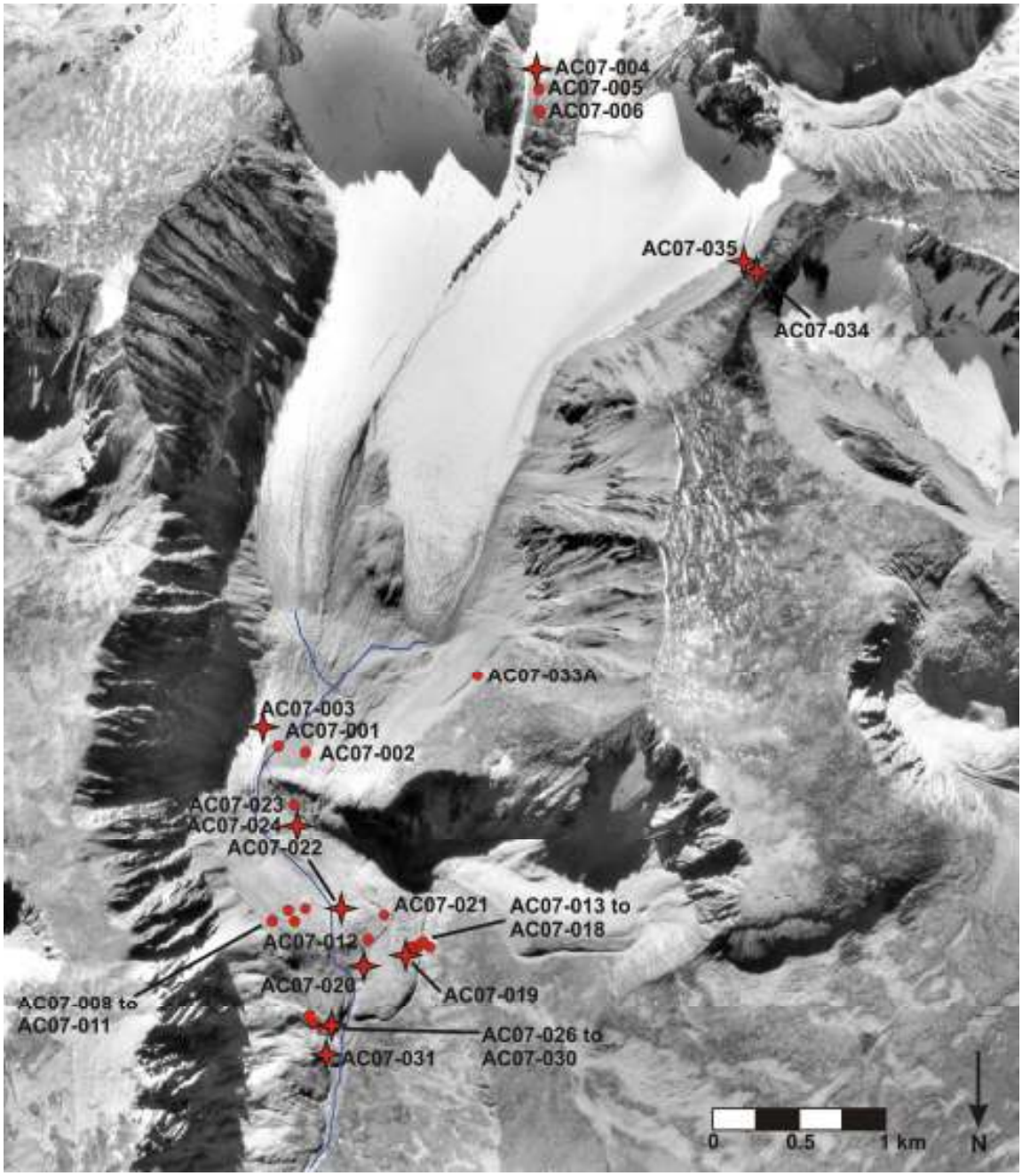

Figure 6 Locations of lichen sample sites. Histograms showing the distributions of lichen size at starred sites are shown in Figure 10. Histograms showing the distributions of lichen size at all other sites (circles) are shown in Appendix 1. Locations are plotted on aerial photograph A28240/88, taken in 1995.

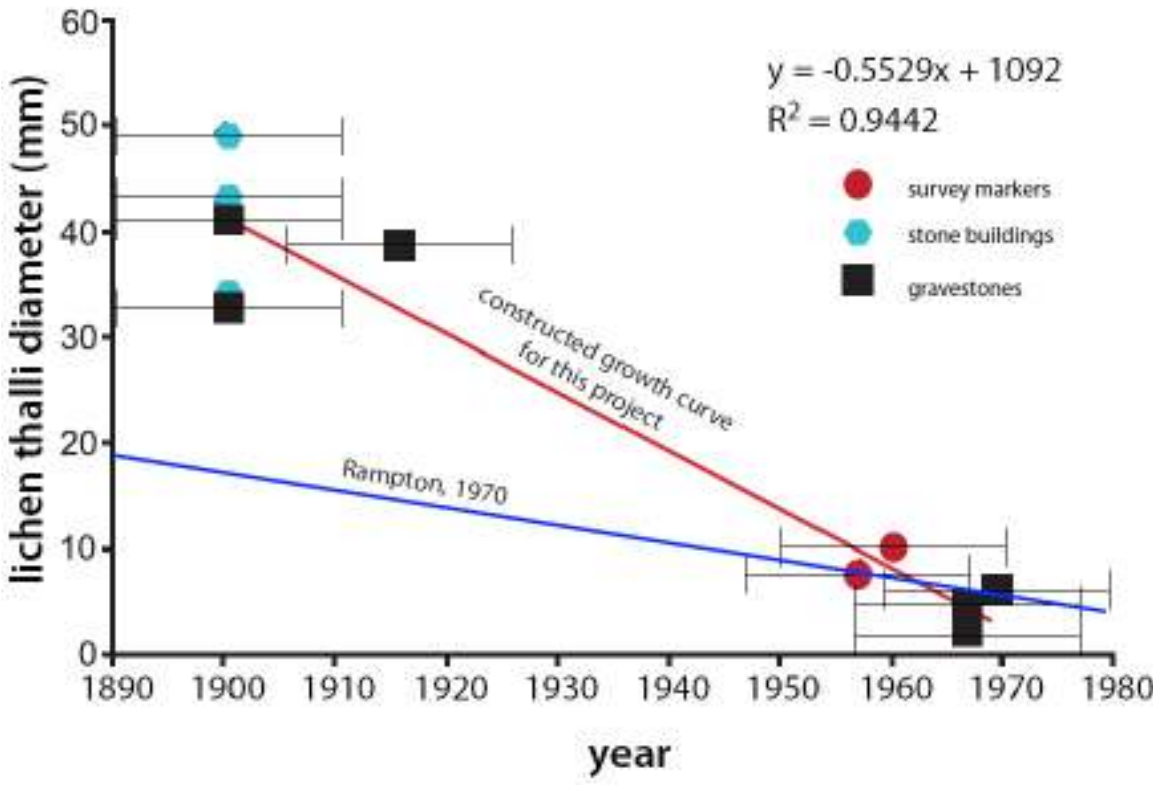

Figure 7 Lichen growth curve based on data collected from sites at Montana Mountain and Carcross. Horizontal bars are estimates of possible error for each sample. For comparison, the growth curve of Rampton (1970) is shown. The Dyke (1990) growth curve plots outside the area of the figure.

Table 3 Descriptions and locations of sites used to produce the lichen growth curve.

Site name	Description	Location
Survey markers	Geographic survey markers	520331 E, 6653114 N and 517205 E, 6657911 N
Stone buildings	Stone buildings built for mining activity at the turn of the century	516777 E, 6662429 N
Gravestones	Gravestones from the Carcross-Tagish First Nations cemetery	Undisclosed location near Carcross

Note: The exact location of the Carcross-Tagish First Nations cemetery is not provided in respect to the First Nation.

2.4 Results

2.4.1 Glacier Ice Loss

Table 3 and Figure 8 summarize changes in the area of Wheaton Glacier through time, and Table 4 and Figure 9 present glacier volume changes calculated using the bivariate scaling procedure described above.

The area of Wheaton Glacier in 2007 was 50% (1.8 km^2) less than at the offend of the Little Ice Age in the early twentieth century. Since the first aerial photographs were taken in 1948, the glacier has lost 41% (1.2 km^2) of its area.

Estimated ice volume loss between the end of the Little Ice Age and 2007 is 2.8-3.7 km^3, or 58-63%. Since 1948, the glacier has lost 48-52% (1.9-2.4 km^3) of its volume.

The top of the rock ridge separating the east and west lobes of the glacier was first exposed in 1964. The glacier downwasted 120 m in this area between 1964 and 2007 (i.e., from 1873 to 1753 m asl).

2.4.2 Geomorphology and Chronology

The Little Ice Age terminal moraine is continuous with a conspicuous trimline that delineates the glacier margin at the Little Ice Age maximum (Figure 10). Figure 11 presents a selection of lichen data from the glacier forefield (see Appendix 1 for all lichen data). Each lichen sample includes a large range of individual measurements. At sites with large lichens, the sample histogram has a broad distribution because more lichens colonize the site through time. In contrast, the histograms of sites with only small lichens have a narrow range of diameters.

Lichen mortality may also play a role at sites with a wide range of lichen diameters. Table 5 summarizes the estimated age of each measurement site based on the lichen growth curve (Figure 7). The sites range in age from 1718 +/- 20 (AC07-034) to 1969 +/- 20 (AC07-003). Outside the Little Ice Age limit, lichens range in age from 1718 +/- 20 (AC07-034) to 1902 +/- 20 (AC07-004).

Two of these sites, AC07-027 and AC07-031, are located on rock glaciers north of the Little Ice Age limit. They yielded age estimates of 1799 +/- 20 and 1786 +/- 20, respectively. The lichens sampled on the Little Ice Age moraine (AC07-013) gave an age of 1915 +/- 20. A rock fall that crossed the forefield (AC07-007 to AC07-011, AC07-021 to AC07-022) yield a range of ages, from 1748 +/- 20 to 1966 +/- 20. The oldest lichens sampled within the Little Ice Age limit, outside of the rock fall, indicate an age of 1930 +/- 20 (AC07-012). Lichens were sampled on large boulders at three sites (AC07-001 to AC07-003) within the footprint of a drained proglacial lake. They returned ages of 1968 +/- 20, 1967 +/- 20, and 1969 +/- 20, respectively.

Figures 12 and 13 show locations of the glacier terminus at several times since the Little Ice Age. From the end of the Little Ice Age to 1948, the glacier retreated approximately 1 km. The glacier margin retreated another 150 m by 1964 and became confined to the cirque that it occupies today. The glacier also thinned over this period, as is shown by the emergence of a bedrock knob at the glacier surface. Figure 12 also shows that the proglacial lake had formed by 1964. By 1987 the glacier had retreated another 800 m, the proglacial lake had drained,

Table 4 Estimated surface area of Wheaton Glacier and associated reduction in area since the Little Ice Age (LIA) and the first aerial photographs in 1948.

Date	Area (km^2)	Area Loss (since LIA)	Area Loss (since 1948)
Little Ice Age (LIA)	3.55	0 km^2 /0 %	
1948	2.98	0.57 km^2 /16.1 %	0 km^2 /0 %
1964	2.72	0.83 km^2 /23.4 %	0.26 km^2 /8.7 %
1987	2.21	1.33 km^2 /37.6 %	0.76 km^2 /25.6 %
1995	1.81	1.74 km^2 /49.1 %	1.17 km^2 /39.3 %
2004	1.78	1.76 km^2 /49.7 %	1.19 km^2 /40.0 %
2006	1.77	1.77 km^2 /50.0 %	1.20 km^2 /40.4 %
2007	1.76	1.79 km^2 /50.4 %	1.22 km^2 /40.9 %

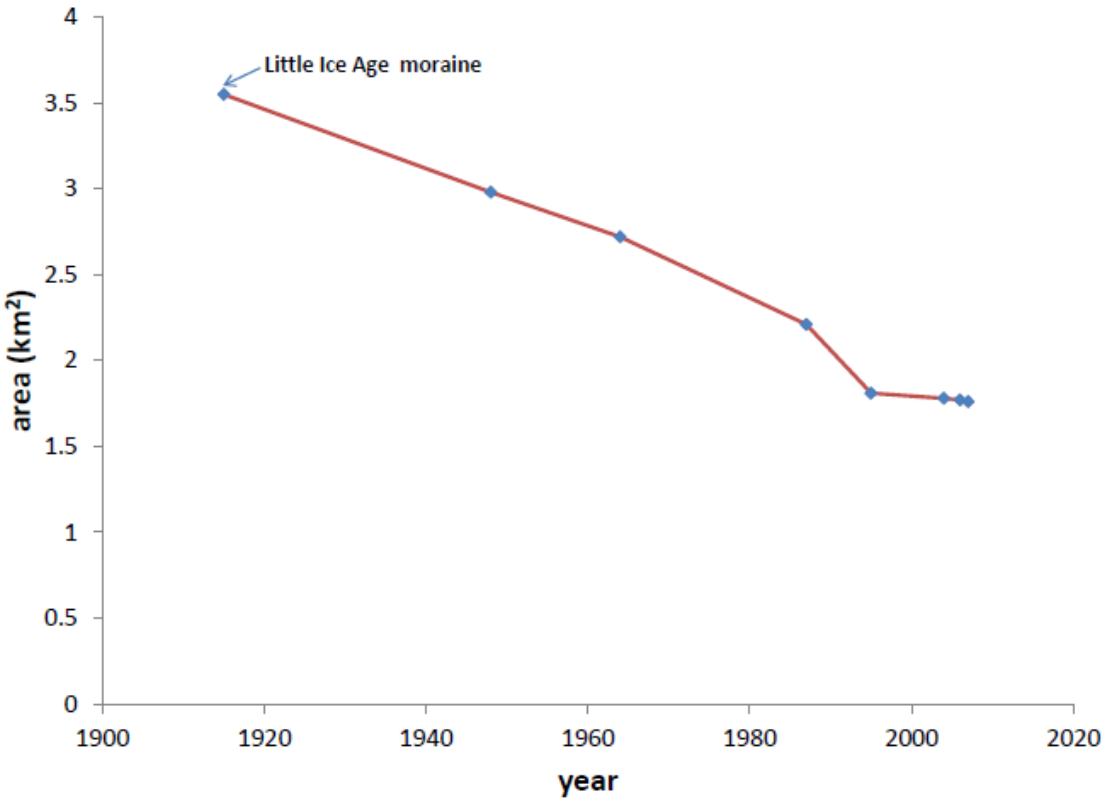

Figure 8 Change in the area of Wheaton Glacier through time. The age of abandonment of the Little Ice Age moraine is 1915, determined through lichenometry (see Section 2.5.2).

Table 5 Estimated volume of Wheaton Glacier and associated ice volume loss since the Little Ice Age (LIA) and the first aerial photography in 1948. Ice volumes were estimated using a bivariate scaling relation, with three values of ϒ (1.25, 1.36, and 1.4).

		Volume loss since:	
	Volume (km^3)	LIA	1948
ϒ = 1.25			
LIA	4.86		
1948	3.91	1.0 km^3/19.7 %	
1964	3.49	1.4 km^3/28.3 %	0.4 km^3/10.7 %
1987	2.70	2.2 km^3/44.5 %	1.2 km^3/30.9 %
1995	2.09	2.8 km^3/57.0 %	1.8 km^3/46.4 %
2004	2.06	2.8 km^3/57.6 %	1.8 km^3/47.2 %
2006	2.04	2.8 km^3/58.0 %	1.9 km^3/47.7 %
2007	2.02	2.8 km^3/58.4 %	1.9 km^3/48.2 %
ϒ = 1.36			
LIA	5.59		
1948	4.40	1.2 km^3/21.2 %	
1964	3.89	1.7 km^3/30.4 %	0.5 km^3/11.6 %
1987	2.95	2.6 km^3/47.3 %	1.5 km^3/33.1 %
1995	2.23	3.4 km^3/60.0 %	2.2 km^3/49.3 %
2004	2.20	3.4 km^3/60.7 %	2.2 km^3/50.6 %
2006	2.18	3.4 km^3/61.1 %	2.2 km^3/50.6%
2007	2.15	3.4 km^3/61.5 %	2.3 km^3/51.1 %
ϒ = 1.4			
LIA	5.88		
1948	4.60	1.3 km^3/21.6 %	
1964	4.05	1.8 km^3/31.1 %	0.5 km^3/11.9 %
1987	3.04	2.8 km^3/48.3 %	1.6 km^3/33.9 %
1995	2.29	3.6 km^3/61.1 %	2.3 km^3/50.3 %
2004	2.25	3.6 km^3/61.8 %	2.4 km^3/51.1 %
2006	2.23	3.7 km^3/62.1 %	2.4 km^3/51.6 %
2007	2.20	3.7 km^3/62.5 %	2.4km^3/52.1 %

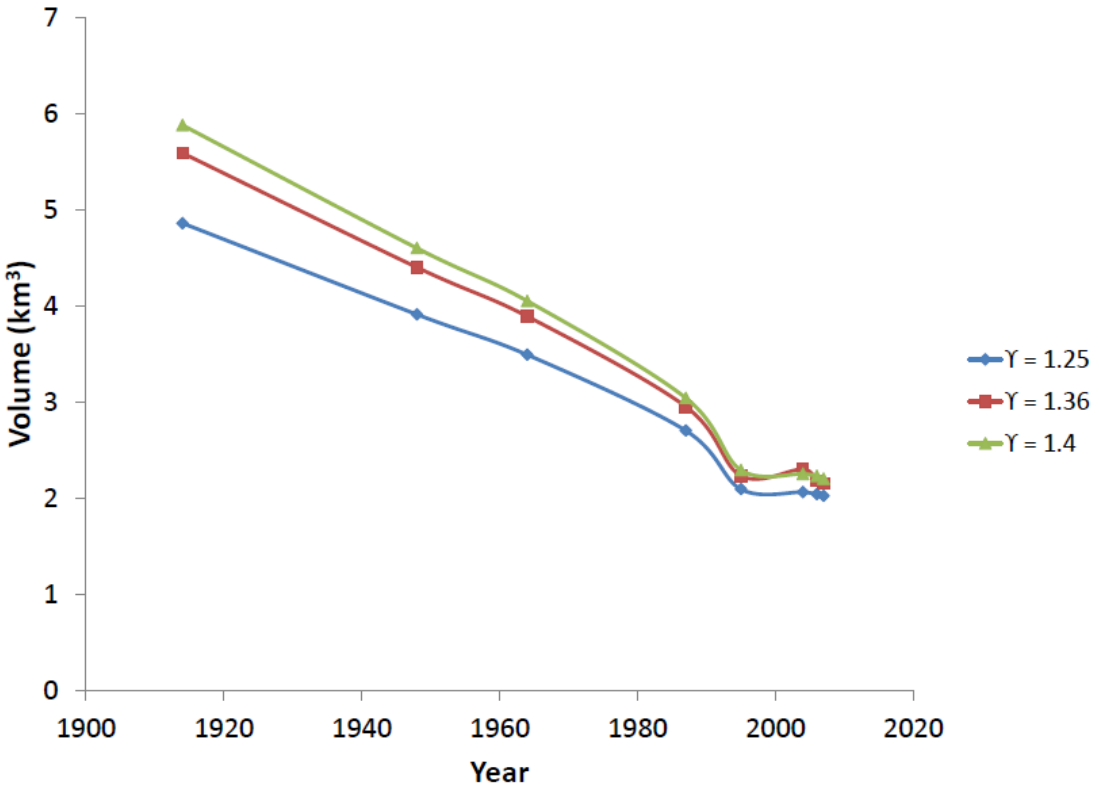

Figure 9 Change in volume of Wheaton Glacier through time. The age shown for the Little Ice Age moraine is 1915, determined through lichenometry (see Section 2.5.2).

and the aerial extent of the bedrock knob exposed at the glacier surface was larger. In 1995, the glacier margin tracked around the bedrock knob, which had become increasingly exposed, and the margin itself had retreated another 200 m. The glacier margin, mapped sequentially in 2004, 2006, and 2007, showed additional glacier retreat of 10 to 25 m between each observation period.

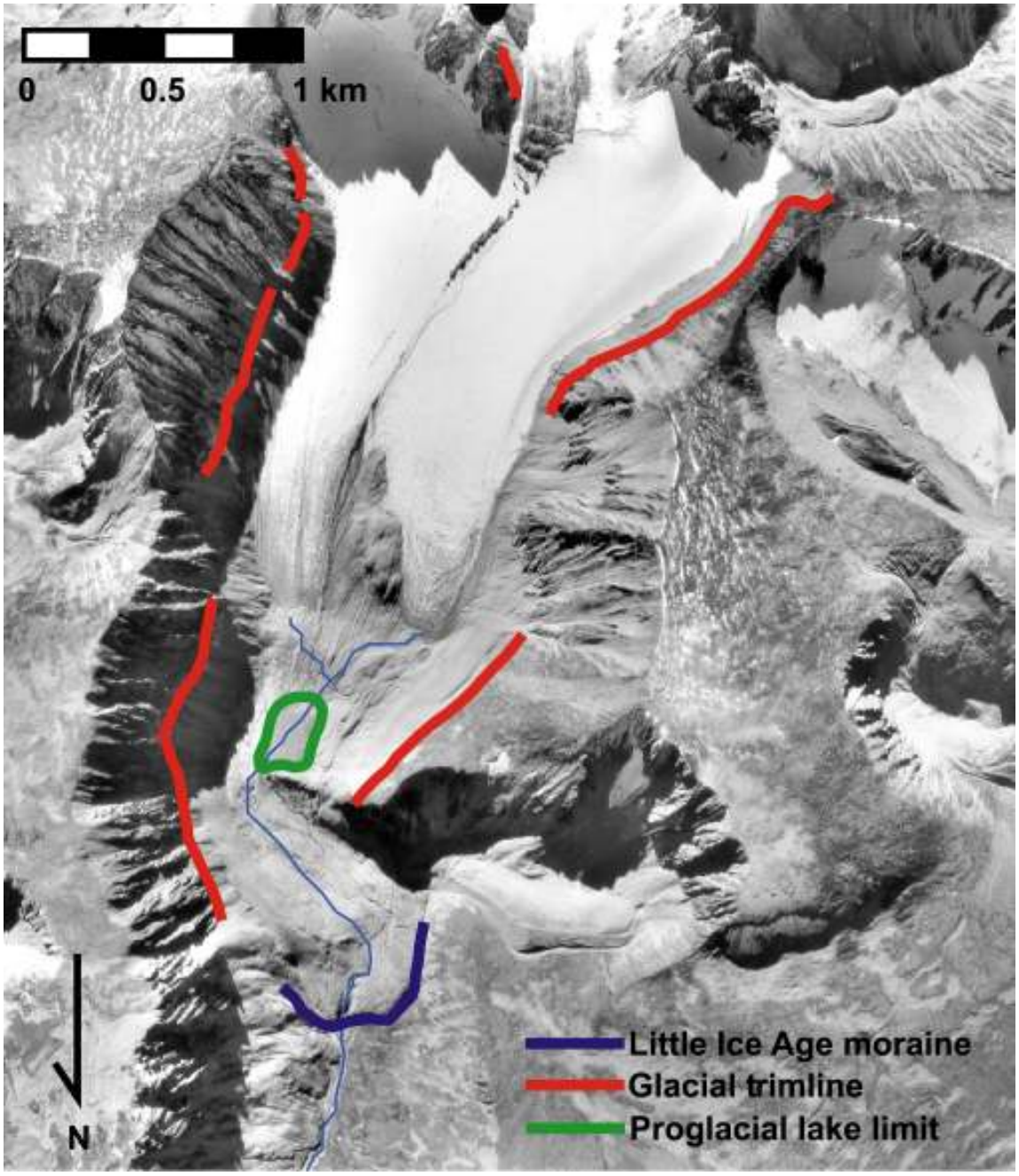

Figure 10 Locations of the Little Ice Age trimline and terminal moraine and a former proglacial lake visible on 1995 aerial photographs. Features are plotted on aerial photograph A28240/88, taken in 1995.

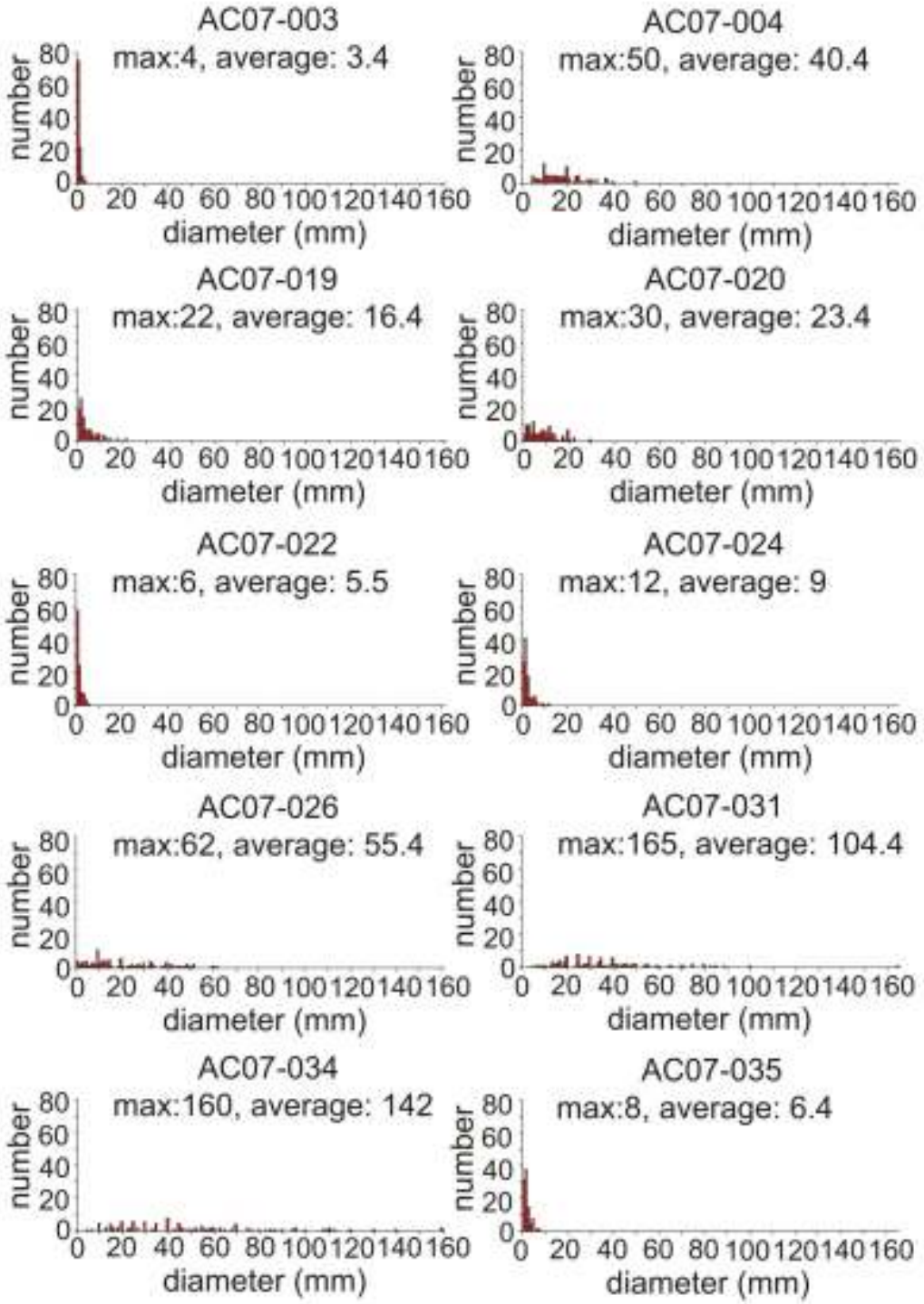

Figure 11 Histograms of the maximum diameter of lichen thalli in the Wheaton Glacier forefield and surrounding area. See Figure 6 for sample locations.

Table 6 Average long-axis diameter of the five largest lichen thalli at each sample site and ages predicted using the lichen growth curve.

Lichen site number	Average diameter of five largest lichen (mm)	Estimated age from lichen growth curve
AC07-001	4	1968
AC07-002	4.4	1967
AC07-003	3.4	1969
AC07-004	40.4	1902
AC07-005	17.4	1944
AC07-006	49	1886
AC07-007	11.4	1954
AC07-008	9.8	1957
AC07-009	8.2	1960
AC07-010	27.4	1925
AC07-011	125.8	1748
AC07-012	24.8	1930
AC07-013	33.2	1915
AC07-014	21.4	1936
AC07-015	12.8	1952
AC07-016	18.8	1941
AC07-017	17.2	1944
AC07-018	18.4	1942
AC07-019	16.4	1945
AC07-020	23.4	1933
AC07-021	8.4	1960
AC07-022	5	1966
AC07-023	13	1952
AC07-024	9	1959
AC07-026	55.4	1875
AC07-027	97.4	1799
AC07-028	92.6	1808
AC07-029	67.6	1853
AC07-030	54	1877
AC07-031	104.4	1786
AC07-033A	11.4	1954
AC07-034	142	1718
AC07-035	6.4	1963
AC07-036A	80.4	1830
AC07-036B	94.4	1804
AC07-037A	9	1959
AC07-037B	7.6	1961
AC07-040	7.4	1962

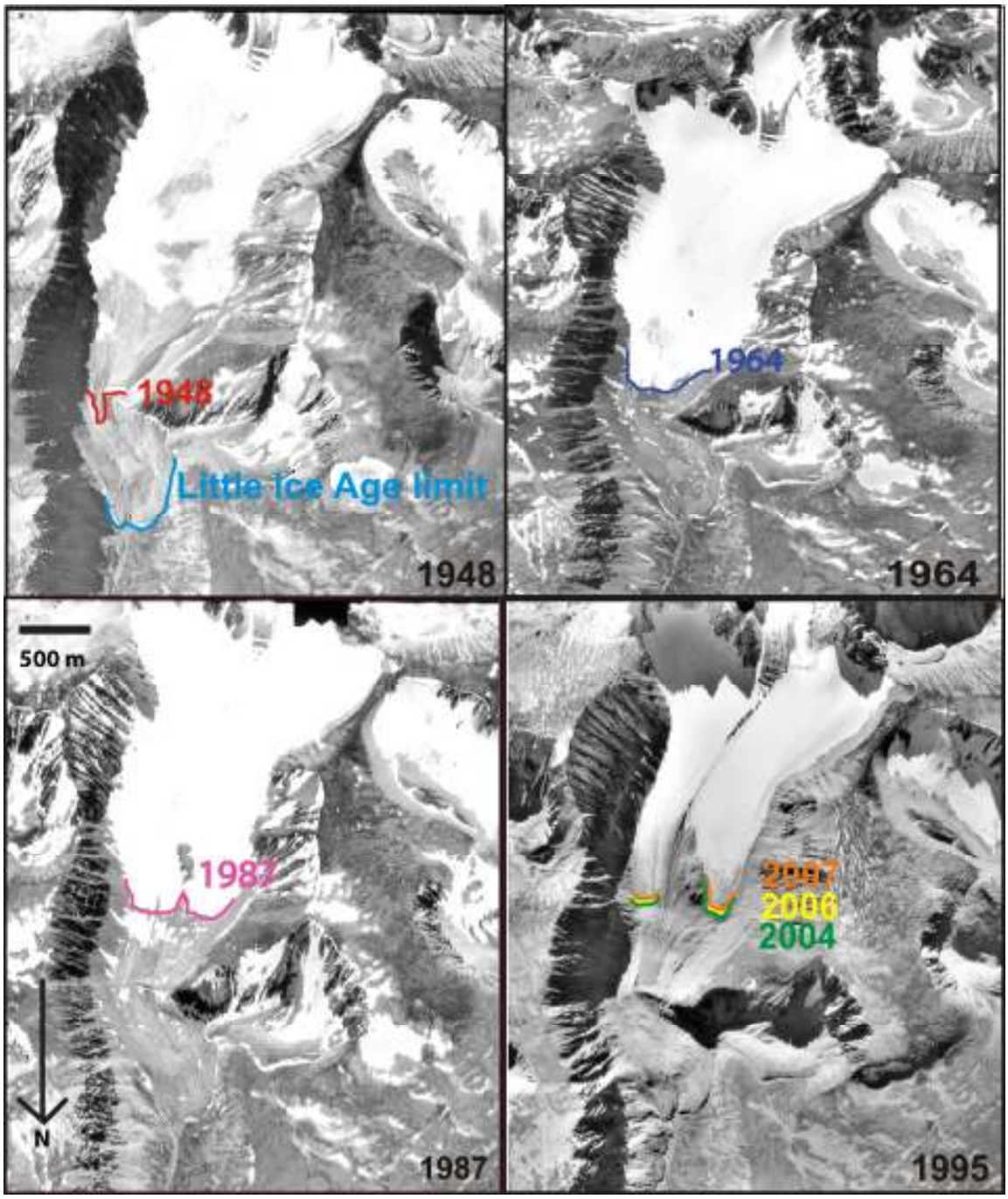

Figure 12 Margins of Wheaton Glacier at the end of the Little Ice Age and in 1948, 1964, 1987, 1995, 2004, 2006, and 2007. Features are plotted on aerial photographs A11521/445 (1948), A19425 (1964), A27149/53 (1987) and A28240/88 (1995).

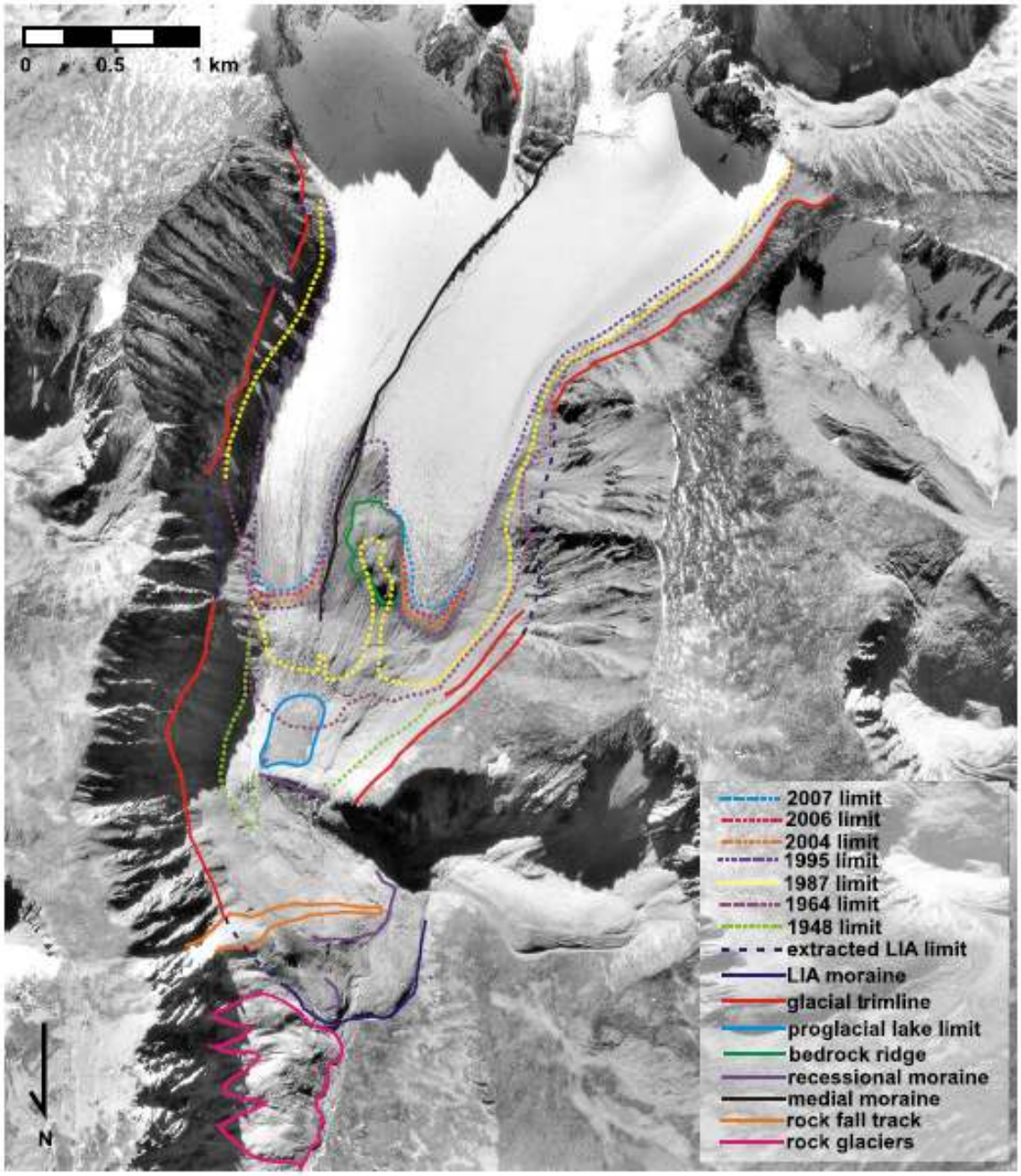

Figure 13 Wheaton Glacier and its forefield showing mapped geomorphic features, and ice limits derived from aerial photographs. Features plotted on aerial photograph A28240/88 taken in 1995.

2.4.3 Climate

The Carcross climate record is incomplete. It does, however, extend back in time beyond the Whitehorse record. As these are the only two records available for

this region, I chose to still make use of the Carcross record, despite its incomplete nature, to obtain a regional sense of climate back to 1907.

Annual average temperature at Whitehorse and Carcross increased between 1907 and 2005 (Figure 14). Temperatures rose between 1920 and 1960, decreased slightly from 1960 to 1980, and then rose steadily from 1980 onwards. Over the period of the record, annual average precipitation increased at Carcross but changed little at Whitehorse (Figure 15).

At both stations, average winter (November-February), spring (March-May), and summer (June-August) temperatures increased; and average fall (September-October) temperature decreased (Figure 16). Winter temperature displays a similar long-term pattern to annual temperature – rising from 1920 to 1960, decreasing from 1960 to 1980, and rising after 1980. Average summer and fall precipitation increased over the period of record; winter precipitation increased at Carcross, but decreased at Whitehorse; spring precipitation did not change significantly at Carcross and decreased at Whitehorse (Figure 17).

ENSO events have been associated with warm and wet weather in some areas of northwest North America (Cayan *et al*., 1998). Figure 18 shows that there is little or no relationship between ENSO events and precipitation at Carcross and Whitehorse.

There is no apparent relation between PDO phase and precipitation at Carcross and Whitehorse, but a relation may exist between PDO phase and temperature

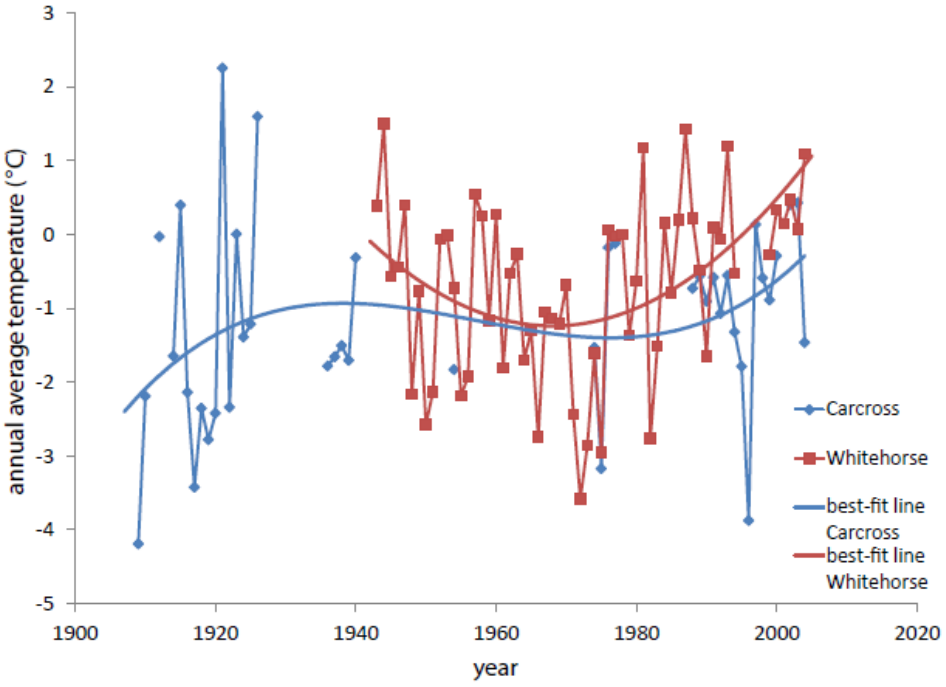

Figure 14 Annual average temperature at Whitehorse and Carcross for the period 1907-2005.

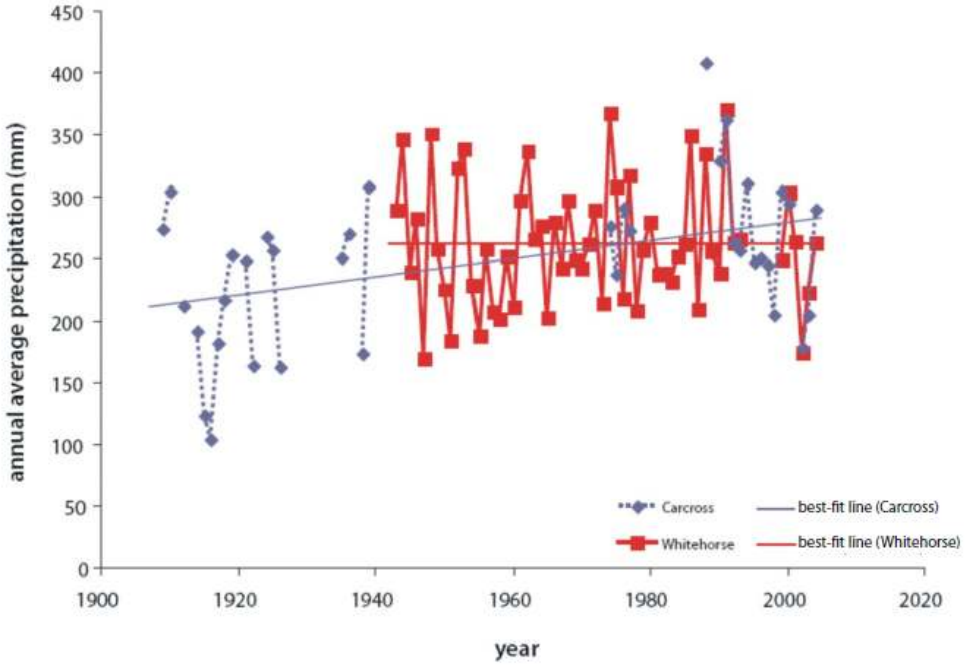

Figure 15 Annual average precipitation at Whitehorse and Carcross for the period 1907-2005.

(Figure 19). The cooler portions of the temperature record appear to correlate with negative PDO phases, most notably during the period 1960-1980. Such a

relation is surprising because the negative PDO state typically amplifies warm ENSO events, elevating temperatures and precipitation in northwest North America (Mantua *et al*., 1997). Figure 19, however, suggests that PDO may have an effect on the climate of southern Yukon and, therefore, the mass balance of Wheaton Glacier.

2.5 Discussion

Wheaton Glacier has lost 50% of its area and 58% to 63% of its volume since the end of the Little Ice Age. The rate of glacier retreat remained steadily until the 1980s, when it increased. The increase in the rate of retreat in the 1980s coincides with an increase in temperature at this time. Retreat slowed slightly in the 1990s and has remained constant since then.

Historic retreat of the glacier terminus can be approximated by the equation $y = 0.0203x + 42.44$, where y is glacier area in km^2 and x is year. If the glacier continues to retreat at its historic rate, it may disappear as early as 2090. During the 2007 field season, I observed that the previous winter's snow had ablated over the entire glacier surface. If summer melting on this scale recurs repeatedly, glacier thinning and retreat will accelerate.

2.5.1 Lichenometry and Glacier Retreat

Most of the lichen ages determined using the lichen growth curve agree with times of glacier retreat based on inspection of aerial photographs (Figure 20). Sites north of the Little Ice Age end moraine yield lichen-based ages in the 1700s

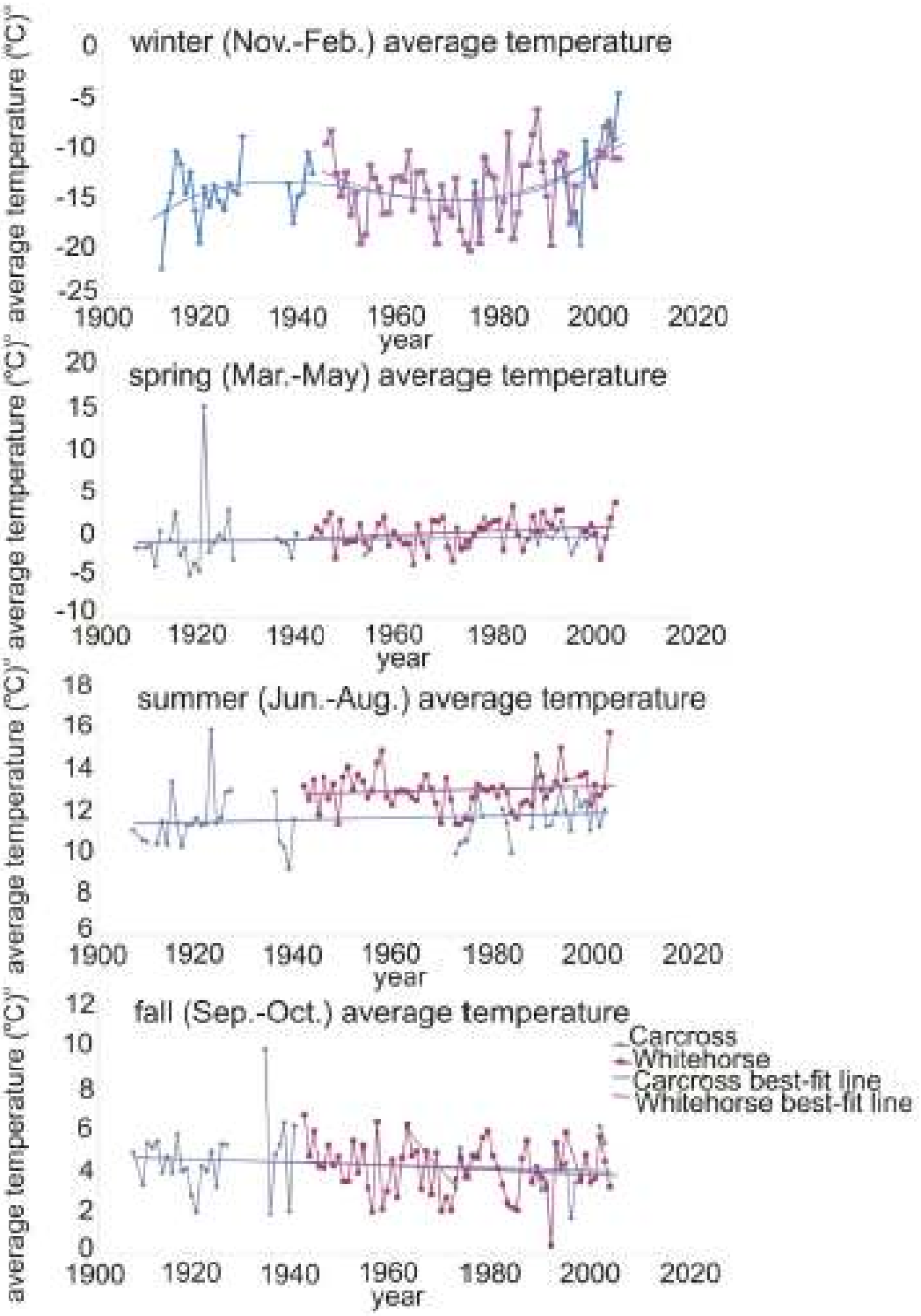

Figure 16 Average seasonal temperatures at Whitehorse and Carcross for the period 1907-2005.

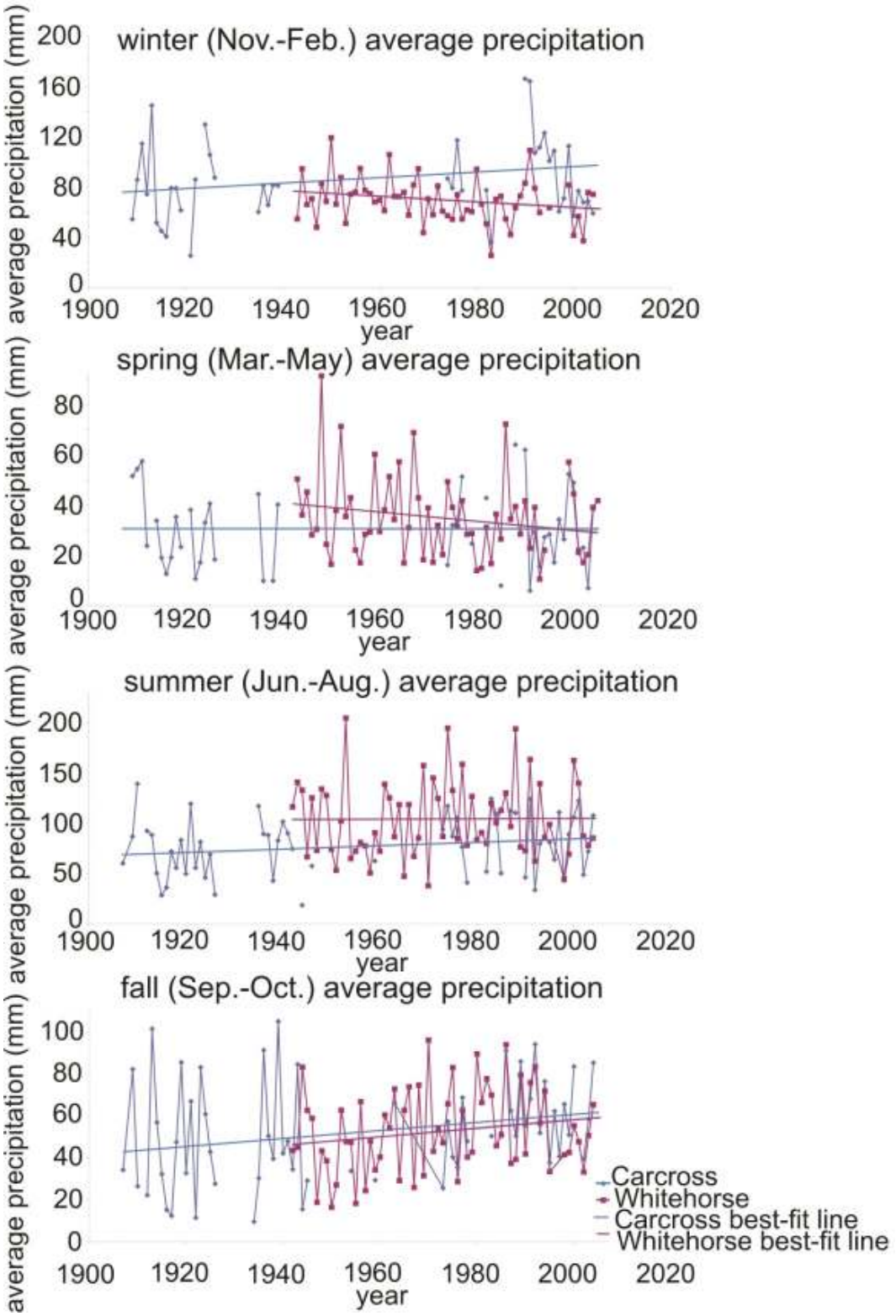

Figure 17 Average seasonal precipitation at Whitehorse and Carcross for the period 1907-2005.

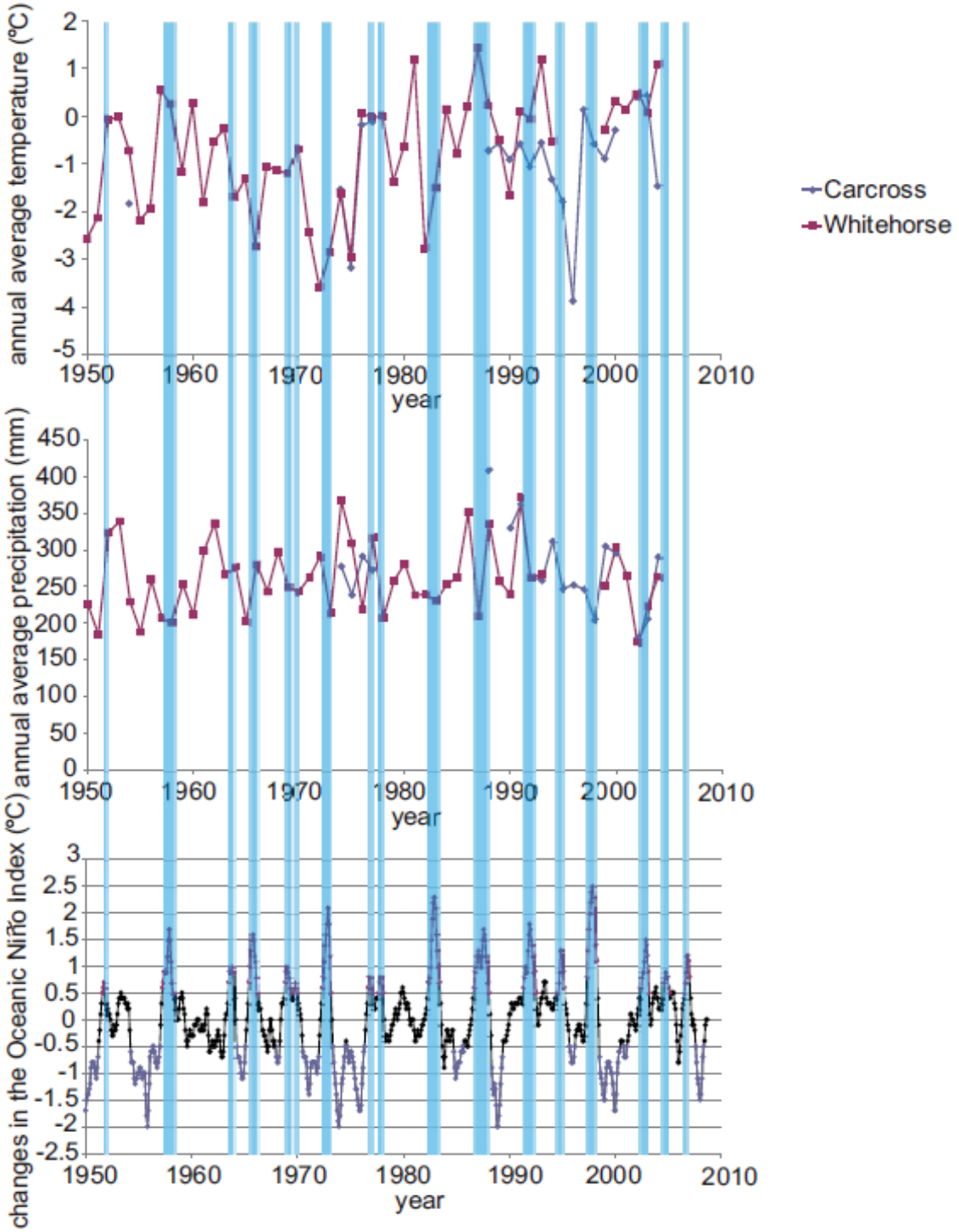

Figure 18 ENSO record and precipitation and temperature at Whitehorse and Carcross for the period 1950-2008. Shaded bars are ENSO events. ENSO data from National Oceanic and Atmospheric Administration Climate Prediction Center (2009).

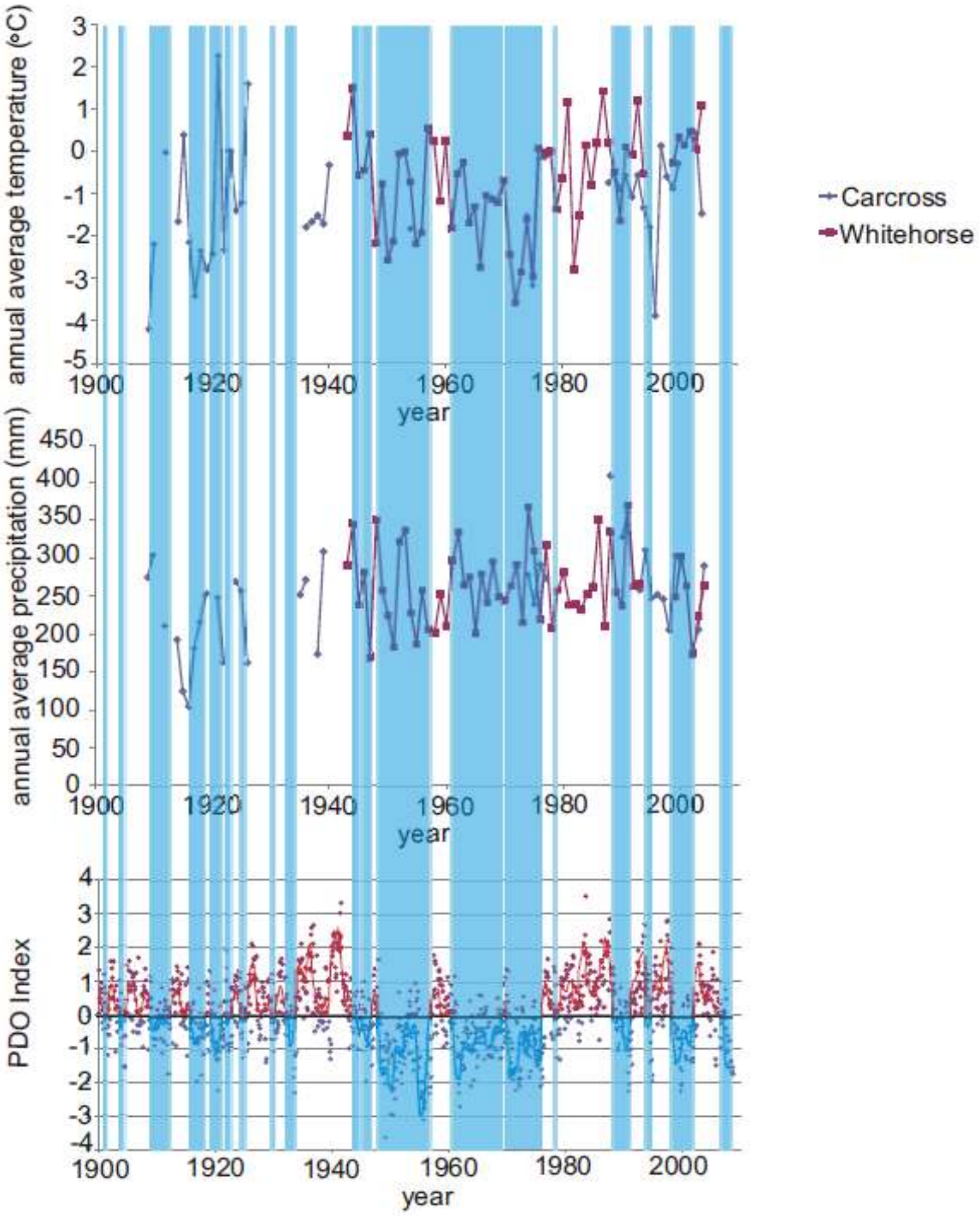

Figure 19 PDO record and precipitation and temperature for the period 1900-2008 at Whitehorse and Carcross. Shaded bars are negative PDO events. PDO data from Joint Institute for the Study of the Atmosphere and Oceans (2009).

and 1800s, and all sites inside the Little Ice Age limit are post-1900. Sites between the Little Ice Age limit and the position of the glacier terminus in 1948 give lichen ages between 1930 +/- 20 and 1945 +/- 20, with the exception of those within a rock-fall track (see below) and at site AC07-034, which may be outside the assumed Little Ice Age trimline on the southwest side of the glacier. Site AC07-034 has a lichen-based age of 1718 +/- 20. Site AC07-035, which is inside the trimline, but outside of the 1964 ice limit dates to 1963 +/- 20.

Examination of the retreat of Wheaton Glacier at a sub-decadal time scale shows the limitation of lichen analysis at this level of temporal resolution. Sites AC07-001, AC07-002, and AC07-003 lie within the remnants of a proglacial lake in the glacier forefield. The three sies are inside (north) of the 1964 ice limit, suggesting that they could be used to more tightly constrain the time of retreat. Unfortunately the estimated ages at the these sites are 1968 +/- 20, 1967 +/- 20, and 1969 +/- 20, suggesting that they should lie south, not north, of the 1964 limit. Similarly sites AC07-023 and AC07-024 date to the 1950s, but lie just north of the 1948 ice limit. These results suggest that estimated lichen ages are not accurate at a sub-decadal scale.

No lichens were found on surfaces deglacierized after 1969, suggesting that the ecesis interval for *Rhizocarpon geographicum* near Wheaton Glacier is about 40 years. Therefore, the lichen analysis could not be used to document recession of the glacier after 1970.

The general agreement between inferred lichen ages and historic retreat of Wheaton Glacier suggests that lichenometry can be used to estimate the age of

stabilization (abandonment) of the Little Ice Age moraine. The estimated lichen age at site AC07-013, on the Little Ice Age moraine, is 1915 +/- 20, suggesting that Wheaton Glacier abandoned the moraine early in the twentieth century. Four sites just outside the Little Ice Age limit, but on the valley wall (AC07-015, -016, -017, and -018) date to the 1940s and 1950s. The young ages at these sites are probably due to cryoturbation and solifluction, which are common on slopes below the terminus of Wheaton Glacier.

Sites AC07-027 and AC07-031, north of the Little Ice Age end moraine, yielded the oldest lichen ages – 1799 +/- 20 and 1786 +/- 20, respectively. Although the two sites are located on active rock glaciers, most surface blocks appear to move downslope without being overturned. Lichens become established and grow on the moving blocks.

Sites AC07-007, AC07-008, AC07-09, AC07-10, AC07-011, AC07-021, and AC07-022 are just inside the 1948 glacier margin. Their ages – 1954 +/- 20, 1957 +/- 20, 1960 +/- 20, 1925 +/- 20, 1748 +/- 20, 1960 +/- 20, and 1966 +/- 20, respectively, appear, at first glance, incongruous with their location. All of these sites, however, are within the track of a rock fall, which may explain their anomalous ages. The cluster of dates in the 1950s and 1960s suggest that the rock fall happened sometime within those two decades. The two older dates – 1925 +/- 20 (AC07-010) and 1748 +/- 20 (AC07-011) – were derived from lichens on large (> 5 m) slabs emplaced during the rock fall. These two slabs probably were transported and deposited without becoming overturned, allowing old

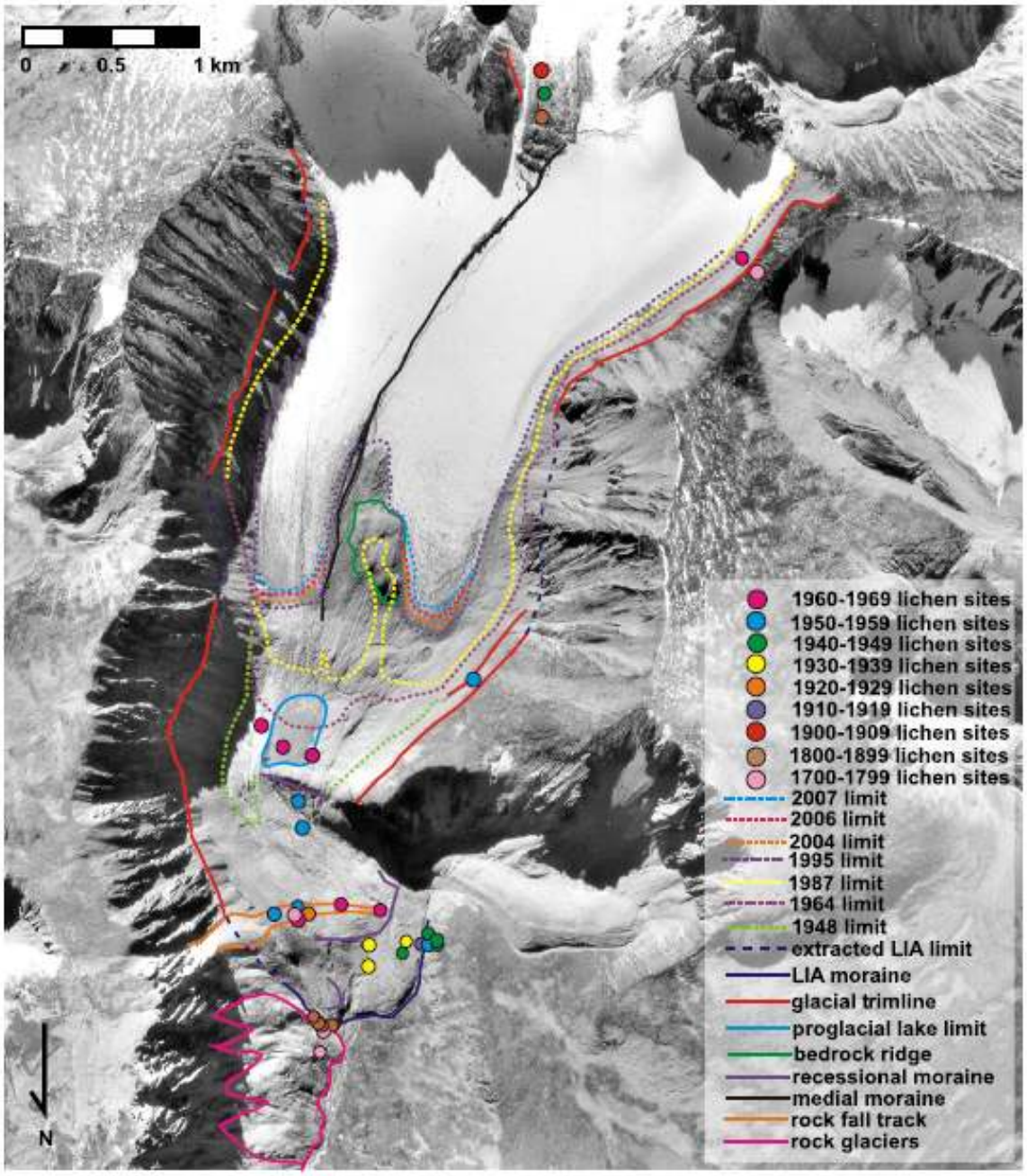

Figure 20 Wheaton Glacier and its forefield showing mapped geomorphic features, ages of lichen sites based on the lichen-growth curve, and ice limits derived from aerial photographs. Features plotted on aerial photograph A28240/88, taken in 1995.

lichens to survive the event. If so, the dated surfaces must have been exposed on the surface of the rock mass that failed in the 1950s or 1960s.

Based on this study, I conclude that lichenometry yields reliable estimates of surface ages to within about 20 years in the Wheaton Glacier forefield. The technique may be more widely applicable in other subalpine environments in southern Yukon where other dating methods are not feasible. A requirement in using the technique elsewhere in southern Yukon, however, is that a local lichen growth curve be established from surfaces of know age, using for example historical records or radiocarbon dating (Innes, 1983; McCarthy, 2003; Bradwell, 2010).

2.5.2 Link between Climate and Activity of Wheaton Glacier

The climate record shows that mean temperature in southern Yukon has increased since 1907. Average winter snowfall at Carcross has increased over this period. Average annual precipitation at Whitehorse has increased, although winter precipitation has decreased. The lower elevation, drier climate, and greater distance of Whitehorse from Wheaton Glacier make that weather station less representative of conditions at Wheaton Glacier than the Carcross station. Increases in precipitation and temperature during the historic period are consistent with trends throughout most of northern British Columbia and Yukon Territory (Egginton, 2005; Furgal and Prowse, 2008).

The documented historical increase in winter precipitation at Carcross should favour a positive regimen for Wheaton Glacier that would lead to glacier growth. In this case, however, the contemporary increase in temperature has been more significant than precipitation in affecting the glacier's mass balance. Mean temperatures at Carcross for several years in the 1920s and 1930s were 1-2°C,

the warmest temperatures on record to date. In addition, mean fall temperature at Carcross reached 10°C in the late 1930s, and the mean spring temperature reached 15°C around 1920; both of these values are far higher than normal. These abnormal conditions may explain the high rate of glacier retreat prior to 1948. Unfortunately the climate records from Carcross are incomplete between 1907 and 1975, and climate data are not available for Whitehorse until the mid-1940s.

Although ENSO has a major impact on climate in many areas of northwest North America, it does not appear to have significantly affected the climate of the southwest Yukon. ENSO events do not appear to correlate with climate fluctuations based on the Whitehorse and Carcross climate records. The lack of correlation could result from the strong rain shadow created by the St. Elias Mountains or the influence of other climate signals in the meteorological records. There appears to be some relation between PDO phase and temperature in southern Yukon, suggesting that PDO may affect the mass balance of Wheaton Glacier; unfortunately,the limited climate data cannot be used to rigorously test this hypothesis.

The increase in temperature during the twentieth and early twenty-first centuries, with its possible link to PDO phase, is the main cause of the persistent negative mass balance of Wheaton Glacier. Increased winter snowfall has not affected the activity of the glacier.

2.6 Conclusion

Wheaton Glacier has significantly thinned and retreated over the past century. Since the end of the Little Ice Age in the early twentieth century, the glacier has lost about 50% of its area and 58-63% of its volume. Climate data from Whitehorse and Carcross show that temperature in southern Yukon has increased since 1907; winter snowfall has increased at Carcross, but not at Whitehorse, over this period. Warming and its possible relation to negative PDO phases appear to be the main cause of the persistent negative mass balance of Wheaton Glacier. If temperatures continue to rise, the glacier will disappear, possibly as early as 2090.

3: DEBRIS FLOW FAN

3.1 Introduction

This study addresses the question: What has been the impact of Neoglacial activity and recent retreat of Wheaton Glacier on the valley below? Geomorphic, stratigraphic, geochronologic, and geophysical research was completed on the Wheaton debris flow fan to answer this question.

3.1.1 Debris Flows

Debris flows are fluidized mass movements (Johnson, 1970). They consist of grains ranging from clay to boulder size and water (Costa, 1988), and may contain organic material. Sediment concentrations range from 70% to 90% by weight (47% to 77% by volume) (Costa, 1988). They display laminar flow, in which both water and solid components move as a unit and have shear strengths greater than 400 dn/cm^2 (Costa, 1988).

Prerequisite conditions for debris flow initiation include an abundant supply of sediment, rain or another source of water, and relatively steep slopes (Costa, 1984). Costa (1984) and Johnson and Rodine (1984) conclude that debris flows are most commonly triggered by shallow landslides that enter stream courses. The debris become saturated by runoff from rainfall or snowmelt, and then begins to flow down the stream channel, entraining additional sediment. Sasaki *et al.* (2000) demonstrated that soil creep initiated by rainfall triggers debris flows

on steep slopes in Japan. Other studies have shown that shallow planar slides can evolve into debris flows through addition of water downslope (Shimokawa and Jitousono, 1998). Zicheng and Jing (1987) suggest that debris flows may be the cause of denudation in small drainage basins, although they occur infrequently during periods of intense rain.

Although debris flows differ greatly in their physical characteristics, some common elements can be identified. Their high viscosity and bulk density allow the transport of boulders up to tens of metres across with little turbulence (Johnson, 1970). These rheological properties account for the inverse grading in many debris flow deposits, boulder levees at the margins of their paths, their high impact forces, and their ability to stop suddenly (Johnson, 1970; Iverson, 1997; Major and Iverson, 1999).

Although debris flows typically follow pre-existing channels, their ability to construct marginal levees and to scour their own channels allows them to flow considerable distances across non-incised alluvial fans (Costa, 1984). Debris flows commonly display surge-like flow (Sharp and Noble, 1953; Pierson, 1980; Costa, 1984); each surge is characterized by a viscous, coarse-grained flow front that transitions to a more hyperconcentrated flow, and finally turbulent streamflow (Pierson and Costa, 1987). Scott's (1988) work on Mt. St. Helens has shown that flow transitions are also common along the flow path due to changing hydraulic conditions with distance from the source. These transformations occur, in part, because sediment is entrained and deposited during transit. Debris flows may

transform into hyperconcentrated flows and then to conventional water flows (Beverage and Culbertson, 1964; Pierson and Costa, 1987).

Some large debris flows travel many kilometres from their sources, but generally come to rest when they reach gentle slopes lacking channel confinement (VanDine, 1985; Rickenmann and Zimmermann, 1993, Webb and Fielding, 1999). Deposits are typically lobate sheets or channelized ribbons, ranging in thickness from several centimetres to several metres (Lawson, 1979). In section, deposits of individual flows tend to have tabular forms, commonly with concave-up, erosional bases and flat tops (Lawson, 1979). Boundaries between deposits emplaced by successive flows may have basal concentrations of clasts, interbeds of silt, sand, or gravel, or washed upper horizons (Lawson, 1979).

Episodic large inputs of coarse sediment by debris flows have a marked impact on fluvial systems. Some of the effects include out-of-channel deposition, a reduction in channel flow capacity, changes in channel pattern, and the formation of terraces (Kochel *et al*., 1997; Cenderelli and Kite, 1998; Cu, 1999; Eaton, 1999).

Researchers have reconstructed debris flow magnitudes and frequencies: by studying damage to trees (Hupp, 1984; Strunk, 1997; Baumann and Kaiser, 1999; Bollschweiler and Stoffel, 2007; Stoffel and Bollschweiler, 2009); by using historical aerial photographs (Benda and Cundy, 1990; Zimmermann, 1990; Poole *et al*., 2002), remote sensing (Knivetona *et al.,* 2000; Huggel *et al*., 2002; Crowley *et al*., 2003), eyewitness records (Rickermann and Zimmermann, 1993; Bovis and Jakob, 1999; Jakob *et al.*, 2000), newspaper accounts (Bovis and

Jakob, 1999; Cannon *et al*., 2003, 2008), stream gauge records (Caine, 1980; Cannon *et al*., 2001, 2008); and by cosmogenic (Bierman *et al*., 1995; Brown *et al*., 2002) and radiocarbon (Bovis and Jakob, 1999; Jakob *et al*., 2000; Brown *et al*., 2002) dating.

3.1.2 Effects of Recent Deglacierization on Landscape Stability

A warming climate during the past century has resulted in massive glacier ice loss in high mountains around the world (Watson *et al.,* 1996). Contemporary deglacierization, in turn, has been identified as an important factor in a range of catastrophic mountain processes (Evans and Clague, 1997; Fischer *et al.*, 2006; Huggel *et al.*, 2010b; Keiler *et al.*, 2010). For example, deglacierization is implicated in many landslides from moraines and in catastrophic outburst floods due to sudden draining of moraine- and ice-dammed lakes (Clague and Evans, 1993, 1994; Evans and Clague, 1993, 1994; Watson *et al.,* 1996; Frey *et al.*, 2010; Huggel *et al.*, 2010a; Keiler *et al.*, 2010). During the summer of 1987, numerous debris flows were triggered in the Swiss Alps by intense rainfall of unusually long duration (Zimmerman and Haeberli, 1992). The source of many of the debris flows was Little Ice Age glacial deposits exposed during recent glacier retreat. Instability was exacerbated by decay of buried ice within the moraines. Similar explanations have been offered to explain the occurrence of some recent debris flows in the southern Coast Mountains of British Columbia (Jordan, 1987), and the Mount Stephen debris flow in the Selkirk Mountains near Field, British Columbia, in 1994 (Thurber Engineering, 1994).

Debuttressing of steep rock slopes due to thinning and retreat of glaciers has been identified as an important factor in landslides adjacent to glaciers (Bovis, 1982, 1990; Evans and Clague, 1994; Fischer *et al.*, 2006; Huggel *et al.*, 2010a). Of the 31 large rock avalanches known to have occurred in the Cordillera between 1855 and 1988, 17 (55%) occurred on slopes adjacent to glaciers that had thinned and retreated in the twentieth century (Evans and Clague, 1988). Many mountain slopes that have recently been debuttressed show signs of distress, such as toe bulging, cracking, and development of antislope scarps (Evans and Clague, 1997). At Melbern Glacier in northwest British Columbia, for example, a 400-600 m lowering of the glacier surface has debuttressed adjacent slopes, causing extensive, non-catastrophic slope deformation (Clague and Evans, 1993).

Moraine-dammed lakes are common in many high mountain ranges near existing and former glaciers (Clague and Evans, 1994; Frey *et al.*, 2010; Huggel *et al.*, 2010a; Keiler *et al.*, 2010). They formed when glaciers retreated from terminal moraines built during the Little Ice Age. Moraine dams are susceptible to failure because they are steep-sided, have relatively low width-to-height ratios, and consist of poorly sorted, loose sediment. In addition, the dams and the lakes behind them commonly are bordered by steep slopes that are prone to ice avalanches and rock falls (Evans and Clague, 1997). Moraine dams generally fail by overtopping and incision. The most common triggering event is an ice avalanche from the toe of the retreating glacier. The avalanche generates waves that overtop the dam. Melting of ice cores, piping, and landslides are other

reported failure mechanisms (Evans, 1987; Clague and Evans, 1994). Several moraine-dam failures have produced large floods and debris flows in the Canadian Cordillera (Evans, 1987; Blown and Church, 1985; Clague *et al.*, 1985; Clague and Evans, 1994). In the early 1970s, for example, the moraine impounding Klattasine Lake in the central Coast Mountains of British Columbia failed, releasing approximately 1.7 x 10^6 m^3 of water and triggering a massive debris flow (estimated volume 2-4 x 10^6 m^3) that traveled 8 km to block Homathko River. In the same region, ca. 6 x 10^6 m^3 of water spilled out of Nostetuko Lake in 1983 when the moraine impounding the lake was breached (Blown and Church, 1985). The breach was initiated by waves generated by an ice avalanche into the lake. The resulting flood devastated the Nostetuko River valley and traveled more than 100 km to tidewater at the head of Bute Inlet.

3.1.3 Wheaton River Debris Flows

The fan at the mouth of the stream flowing from Wheaton Glacier records large Holocene debris flows and hyperconcentrated flows (Figure 21). A study of the deposits of these events reveals a complex history of instability during the Neoglacial interval and the twentieth century. It also provides a more complete picture of the recent history and landscape evolution in the Wheaton River watershed.

3.2 Study Site

Meltwater from Wheaton Glacier flows 6 km on an average gradient of 15° / 27% (a gradient of 22° / 40% is reached at its steepest point) down a steep-sided

Figure 21 Recent debris flood deposits on the fan at the mouth of the tributary stream draining Wheaton Glacier.

valley to the main stem of Wheaton River. The stream first flows across the forefield of Wheaton Glacier. There it crosses the floor of a former proglacial lake, a dissected recessional moraine that dammed this lake, slopes mantled by colluvium and rock-fall debris, and the dissected Little Ice Age terminal moraine, which is over 15 m high. The terminal moraine is 2 km downvalley from the current glacier terminus. After leaving the glacier forefield, the stream flows in a deeply incised channel bordered on the east by active rock glaciers and on the west by colluvium. The slow advance of the rock glaciers has deflected the stream channel against the west valley wall, which is actively being eroded. At its most incised point, the stream exposes 100 m of consolidated gravel and

diamicton in steep slopes on both sides of the channel. The overall cross-valley profile, ignoring the steeply incised section of the channel, is parabolic, with steep bare faces of jointed rock bordering gentler slopes mantled by unconsolidated sediments. As it nears the main stem of Wheaton River, the stream flows across a partially forested debris flow fan (Figure 22). Just above the apex of the fan, the depth of channel incision decreases, with exposures of, at most, 10 m of gravel and diamicton along the channel walls. Here the channel begins to be bordered by debris flow levees.

Figure 22 Fan at the mouth of the tributary valley draining Wheaton Glacier.

The fan has an area of 0.24 km^2 and its average gradient is 4° / 7%. (Figures 22 and 23). Much of the fan's surface is covered by pine, white and black spruce,

shrubs, and mosses. Linear strips of disturbed or sparse vegetation mark paths of recent debris flows and debris floods (Figure 22). Most of the fan surface is covered by boulders, some up to 4 m across, even near the distal edge of the fan (Figure 24). In areas that have not recently been disturbed by debris flows, the boulders are surrounded by trees and partially or completely covered by a thick layer of mosses. In several places, debris flow deposits have piled up at the base of living trees. The stream currently flows in a single, non-incised channel at the middle of the fan, but unvegetated debris flow deposits at the east side of the fan delineate a recently active channel there (Figure 22).

Figure 23 Aerial view to the west of the fan and wetland at the mouth of the tributary valley draining Wheaton Glacier.

The northern margin of the fan grades into a wetland with an irregular surface (Figures 23 and 25) that is partially submerged due to damming of Wheaton River by beavers. Grasses, shrubs, small alders and willows, and mosses dominate the vegetation in this area. Large debris flows have come to rest on the northern margin of the fan, which slopes about 2º / 4%.

Figure 24 Large boulder near the northern edge of the Wheaton fan.

3.3 Methods

3.3.1 Geomorphology

Debris flow deposits were differentiated from fluvial deposits using aerial photographs (Figure 26) and field mapping. The bouldery nature of deposits precluded excavating pits and trenches. At the fan apex, however, the stream has incised into the uppermost fan sediments, providing several small sections

Figure 25 **View north of the w**etland bordering the Wheaton fan.

that enabled more detailed study of the debris flow deposits. In addition, up to 1 m of fan sediments are exposed locally in the walls of the active stream channel on the upper part of the fan. Surface mapping of debris flow lobes was done in combination with lithologic and lichen analyses (see below). Near the stream channels, especially in areas subject to overbank flow, debris flow deposits showed evidence of fluvial re-working, including sorting, winnowing of fines, and re-alignment and imbrication of clasts.

The Wheaton Glacier forefield was also mapped to identify potential debris flow source areas. Several potential sources were characterized in the field, including a rock fall, rock glaciers, the Little Ice Age terminal moraine, and a breached recessional moraine (Figure 27).

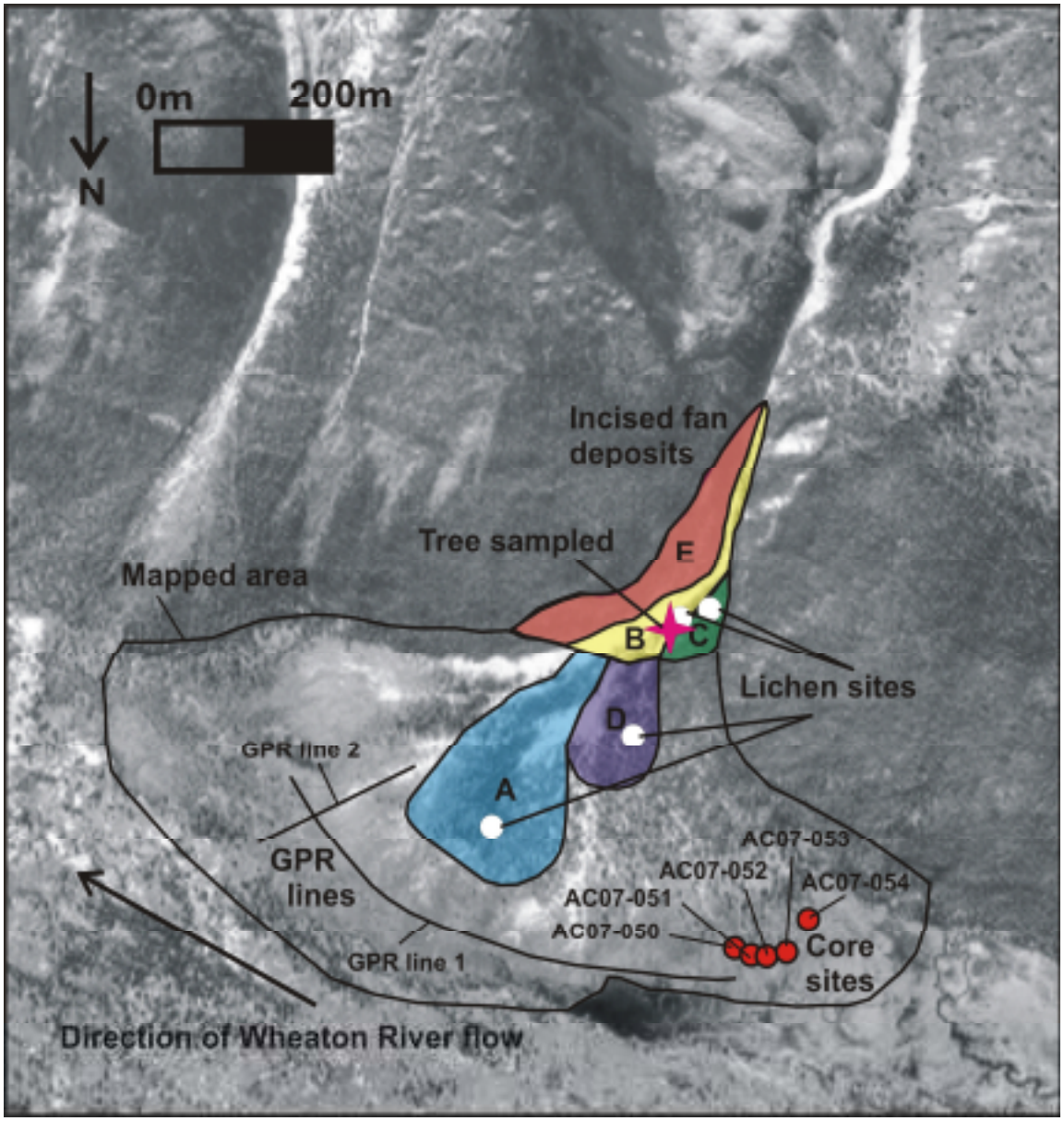

Figure 26 Aerial view of the Wheaton fan, showing locations of debris flows lobes (deposits A-D), incised fan deposits (deposit E), the part of the fan where individual debris flows could not be discriminated (uncoloured part of the mapped area), core sites, lichen sites, the location of a tree sampled for dendrochronology, and ground-penetrating radar lines. Features plotted on aerial photograph A28240/88, taken in 1995.

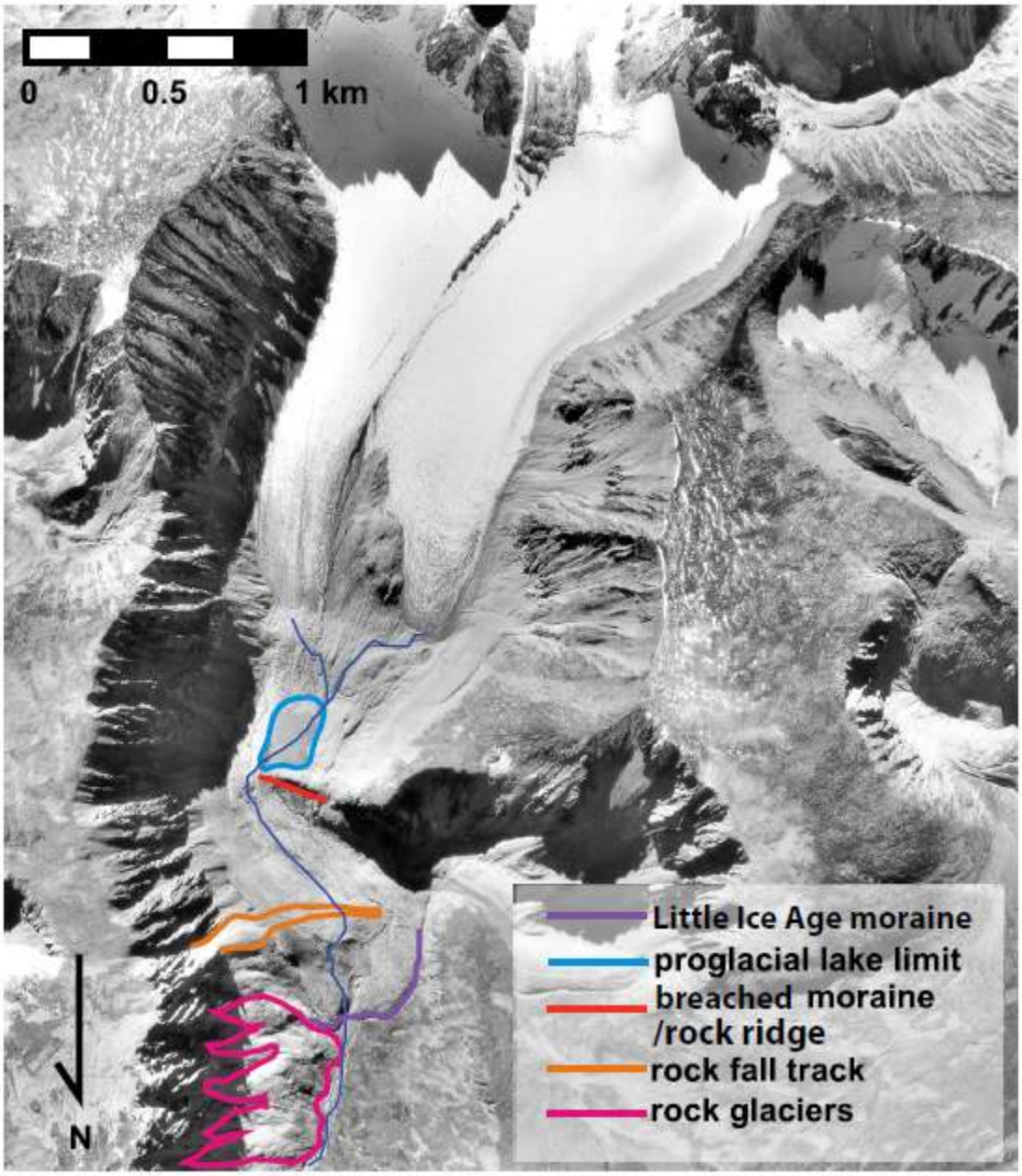

Figure 27 Aerial photograph of the Wheaton Glacier forefield, showing locations of the breached recessional moraine, a rock fall, rock glaciers, and the terminal Little Ice Age moraine. Features plotted on aerial photograph A28240/88, taken in 1995.

3.3.2 Clast Size and Lithology

The long axis of the largest 50 clasts on each debris flow deposit was measured to provide estimates of debris flow competence. The lithology and angularity of

clasts were also recorded. Clast characteristics were also documented in the forefield of Wheaton Glacier and along the valley between the glacier and the fan to provide information on possible upvalley sources of debris flows. The lithologies include granite, granodiorite, dacite, and syenite. Granite clasts were subdivided into two groups, one with abundant phenocrysts of potassium feldspar larger than 5 cm, and another with smaller and fewer feldspar crystals.

3.3.3 Lichenometry

Thalli of lichen (*Rhizocarpon geographicum*) on surface boulders on debris flow deposits were measured to estimate the time of deposition. At each site, the maximum diameter of 100 randomly chosen thalli was measured to the nearest millimetre to obtain a sample of the lichen population, including the largest specimens. Measurements for each sample were plotted as histograms to facilitate comparison. The diameter of the largest lichen thallus and the average diameter of the five largest thalli were recorded to further discriminate the samples (Innes,1985). Similar lichen measurements were made in the forefield of Wheaton Glacier and along the valley between the glacier and the fan.

3.3.4 Dendrochronology and Hydrometric Analysis

A large debris flow crossed the upper part of the fan during historic time. A tree titled and scarred by this debris flow was sampled with a hand saw to determine the age of the event (Figures 28 and 29). The sampled disk was sanded and then examined under a microscope to determine the number of rings that the tree had produced following the scarring event.

Water Survey of Canada discharge records from gauging stations on lower Wheaton and Watson rivers were examined for evidence of flooding associated with this event (Water Survey of Canada, 2009). The adjacent Wheaton and Watson River watersheds are similar in size, climate, and morphology, thus comparison of the hydrometric records from the two gauging stations allowed me to eliminate localized storm systems as possible causes of sudden increases in discharge. Precipitation records from the Carcross weather station were also examined to rule out regional rainfall events.

3.3.5 Sediment Cores

Five sediment cores, each approximately 2 m long, were collected from the distal edge of the fan (Figure 26) by pounding PVC pipe into the sediment with a sledgehammer (Figure 30). A core catcher made of galvanized tin was placed inside and at the end of each PVC pipe to prevent loss of the core during recovery. The pipe was extracted using a “come-along” attached to a strong aluminium ladder. The lowest 30 cm of one core was lost when the PVC pipe broke against a cobble or boulder at depth, but all other cores are complete. Cores were returned from the field, described, and photographed. Observations include lithology, sedimentary structures, unit contacts, and presence of fossils. Samples of plant fossils were collected for radiocarbon dating.

Forty-six organic horizons were sampled for radiocarbon dating. The samples were sieved and washed in water. Suitable plant fossils were extracted from the cores with tweezers. Macrofossils deemed suitable for dating material included

Figure 28 Debris flow B debris piled up against, and scarring, a living tree.

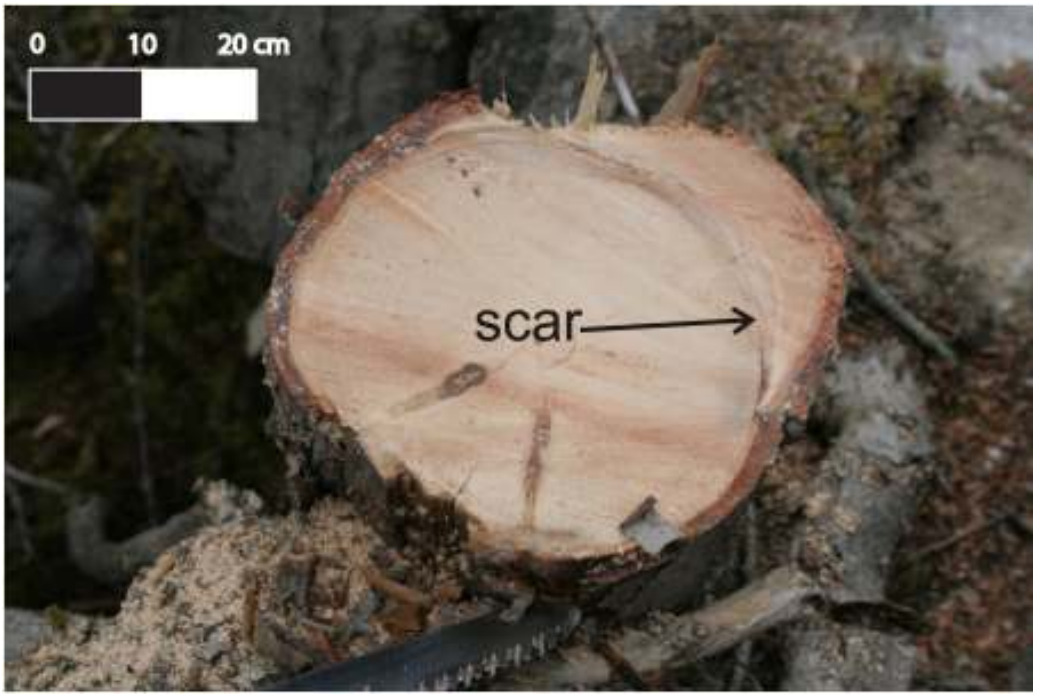

Figure 29 Cross-section of tree shown in Figure 28.

Figure 30 Collecting a core at the distal edge of the Wheaton fan.

needles, trigs, intact leaves, and a conifer cone. Accelerator mass spectrometry (AMS) radiocarbon ages were obtained on 17 samples; dating was done at the Keck Carbon Cycle AMS Facility at the University of California Irvine. Radiocarbon ages were calibrated using OxCal 4.0 (Oxford Radiocarbon Accelerator Unit, 2008).

3.3.6 Ground Penetrating Radar Survey

Ground penetrating radar (GPR) uses pulses of high-frequency electromagnetic energy to image shallow subsurface earth materials. The energy is transmitted into the ground by a radar unit as it is moved over the ground surface. A portion of the energy is reflected back to a receiver when it encounters a change in the dielectric properties of the materials, for example due to a difference in sediment type, water content, or an erosional unconformity or other contact (Davis and

Annan, 1986, 1989; Fisher *et al*., 1995; Jol *et al*., 1996). The returning energy is recorded and can then be processed and interpreted to determine stratigraphy, structure, and moisture content of the subsurface materials.

A ground penetrating radar (GPR) survey was conducted on the fan in September 2007 to determine the shallow subsurface structure of the sediments. One line, about 600 m long, was run along the perimeter of the fan (Figure 26). A second, shorter (200 m) line was run up the axis of the fan to a point where vegetation made further progress impossible. Each line was broken into 200 m segments during the survey to prevent errors in data collection.

The GPR system used in this study is a PulseEKKO 100, made by Sensors & Software Ltd. (1994). Fifty MHz antennae were used to achieve a reasonable depth of penetration (up to about 40 m) at the expense of some loss of resolution.

All GPR profiles were edited and processed using the Sensors & Software programs EKKO View Deluxe (Version 1.3). First, segments were merged to form full lines. Next, a time-zero drift correction was applied to ensure that time-zero points on each trace lined up horizontally (Sensors & Software, 2003). Next, the slowly decaying, low-frequency signal ("wow"), which is superimposed on the desired high frequency reflections, was removed using a Dewow function. Wow removal is termed the "signal saturation correction" (Sensors & Software, 2003). The magnitude of the wow depends on the proximity of the transmitter and receiver and on the electrical properties of the ground. The dewow function removes the low-frequency signal by applying a running-average filter to the

trace. A window with a width equal to one pulse width at the nominal frequency is set on the trace. The average value of all the points in this window is calculated and subtracted from the central point. The window is then moved one point along the trace and the process repeated (Sensors & Software, 2003).

The data were further processed using an Autogain filter. An automatic gain control equalizes all signals and better delineates reflecting horizons by applying a gain that is inversely proportional to the signal strength. Because the automatic gain control is inversely proportional to the signal strength, very small signals can produce very large gains. Therefore, I applied a dynamic gain-limiting scheme that changes from trace to trace. The data points between the start of the data window and the first break (time zero) are used to compute an ambient noise level. The maximum gain for the trace is the amount needed to increase the ambient noise to 'x' percent of the maximum window. This 'x' percent is entered as the Gain Max Auto variable. The external radio frequency background noise increases as the maximum gain level decreases (Sensors & Software, 2003). The automatic gain control employed in this analysis calculates and applies a gain function tailored to the input data set by calculating the decay of the average signal strength over time; no user input is required (Sensors & Software, 2003).

Finally, a horizontal filter was applied to the data. It replaces each trace with an average trace produced by integrating two or more adjacent traces. This process emphasizes flat-lying or gently dipping reflectors, while suppressing steep ones (e.g. diffraction tails or random noise) (Sensors & Software, 2003). In this study, three traces were integrated to produce the average trace.

3.4 Results

3.4.1 Geomorphology

3.4.1.1 Debris Flow Fan

Four debris flow deposits on the fan were discriminated based on surface form, lichen sizes, and lithology (Figure 26). A fifth, significantly older, deposit exposed in section adjacent to the apex of the fan was characterized sedimentologically (deposit E). The remainder of the fan surface has features indicative of debris flow activity, but individual flows could not be recognized because of thick vegetation, fluvial reworking, and lack of age control.

Debris flow deposit A is the most extensive of the five flows; its deposit dominates the lower central part of the fan to its distal margin and includes the largest clasts noted on the fan surface. Debris flow deposit B dominates the apex of the fan and the stream channel north of the apex. It has marginal levees that range from 40 to 100 cm high. Debris flow deposit B scarred the tree that I sampled to determine the age of the deposit (see Section 3.3.4). Debris flow deposit C is restricted to the west side of the fan near its apex and is largely covered by a thick carpet of mosses. Debris flow deposit D occurs on the west-central part of the fan. It has more closely spaced clasts than the deposits of the other flows; little matrix remains at the surface of the deposit. Deposit E is exposed in a section at the apex of the fan (Figure 31). Deposit E is a dark-brown, massive, matrix-supported diamicton, with a silty, medium to coarse sand matrix. Clasts are dominantly granitic, angular to subrounded, and up to about 1

m in diameter; many of them are rotten. The deposit underlies a terrace 5 m above the present stream channel and is much older than the other flows.

Figure 31 Exposure of debris flow deposit E.

3.4.1.2 Rock Fall Northeast of Wheaton Glacier

A rock fall track extends from the rock slope northeast of Wheaton Glacier (Figure 32) across the glacier forefield. The stream flowing from Wheaton Glacier crosses the rock fall debris (Figure 33). The deposit includes boulders up to 7.5 m across.

Figure 32 **Recent rock fall from a steep slope northeast of Wheaton Glacier.**

Figure 33 Part of the rock fall deposit on the east side of the stream flowing from Wheaton Glacier.

3.4.1.3 Rock Glaciers

Active rock glaciers extend into the centre of the valley downstream of the Wheaton Glacier forefield (Figure 34). The rock glaciers have steep noses that have been eroded by the stream flowing from the glacier (Figure 35).

Figure 34 Rock glaciers below the Little Ice Age end moraine of Wheaton Glacier; view north.

3.4.1.4 Proglacial Lake

A bedrock-cored recessional moraine is located approximately 1 km below the terminus of Wheaton Glacier. Aerial photographs taken in 1964 show a proglacial lake behind this composite landform (Figure 36). The moraine is deeply incised (Figure 37) and probably was breached due to sudden draining of the lake. The

lake drained prior to 1987, because it does not exist on aerial photographs taken that year.

Figure 35 Active eroding face of rock glacier below the Little Ice Age end moraine of Wheaton Glacier. The eroding face is approximately 6 m high.

The exposed floor of the former lake (Figure 37) has an area of approximately 480 m^2. Poorly developed shorelines were noted about 50 and 100 cm above the lake floor. Prior to draining, the lake at the moraine was about 2.5 m deep (marked by the washed surface), its area was about 960 m^2, and its volume, which was estimated by one half the volume of an ellipse, was about 1260 m^3.

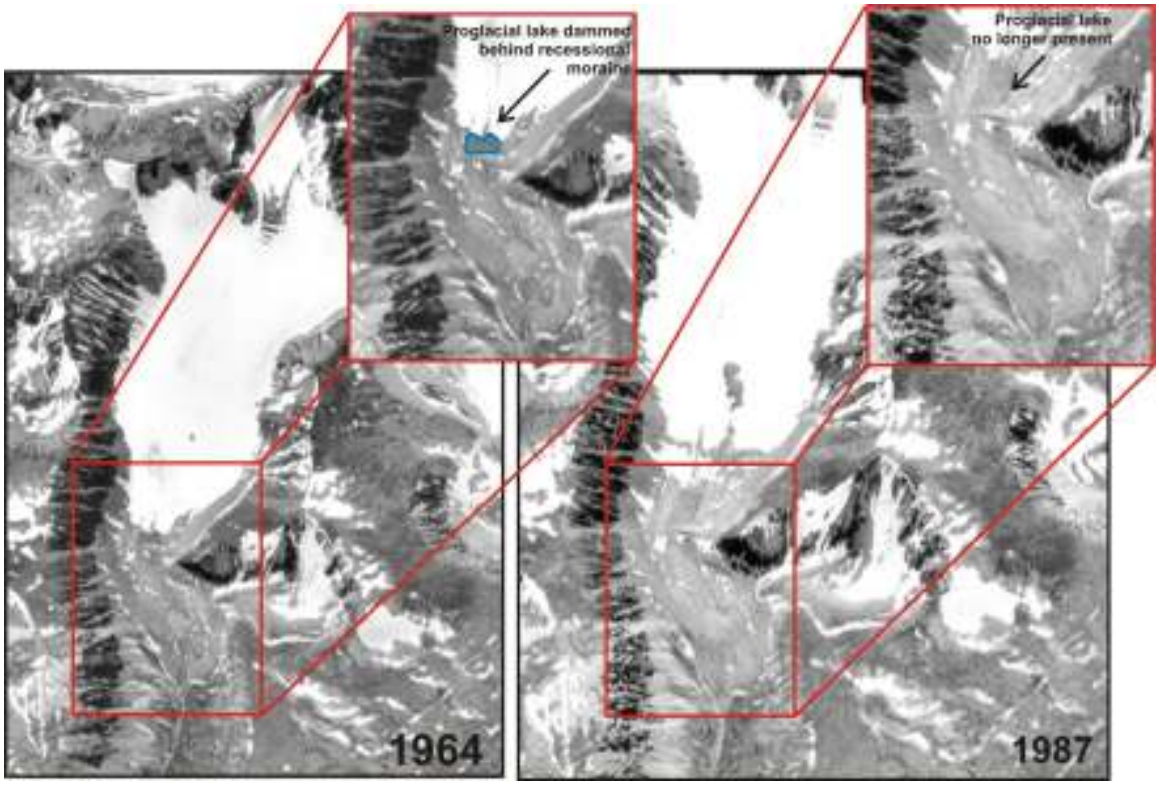

Figure 36 A moraine-dammed lake in the Wheaton Glacier forefield, which existed in 1964 (delineated on A19425/116), had drained before 1987 (delineated on A27149/53).

3.4.1.5 Little Ice Age Terminal Moraine

The Little Ice Age terminal moraine of Wheaton Glacier is located about 2 km downvalley from the present glacier margin. It is over 15 m high and is deeply incised (Figure 38). The moraine is composed of coarse, clast-supported diamicton with a matrix of pebbles and sand. Clasts are angular to subrounded and up to 3 m across.

Figure 37 Footprint of the former moraine-dammed lake in the Wheaton Glacier forefield; note dissected moraine dam in the foreground and poorly developed shorelines (red lines).

3.4.2 Lithology

Clasts in debris flow deposit A are dominantly syenite; dacite and granite clasts are also present (Figure 39). The clasts are subangular to subrounded and up to 300 cm across. Clasts in debris flow deposit B are mainly granite; syenite and orthoclase-rich granite clasts are present in small amounts (Figure 40). The clasts are angular to subrounded and up to 270 cm across. Clasts in debris flow deposit C are entirely granite. They are angular to subrounded and up to 320 cm across. Clasts in debris flow deposit D are mainly syenite and granite; gneiss and

granodiorite clasts are present in small amounts (Figure 41). The clasts are angular to subrounded and up to 220 cm across.

Figure 38 Incised Little Ice Age terminal moraine. The crest of the moraine is 15 m above the level of the stream.

The rock fall deposit in the glacier forefield is dominated by syenite and granite; granodiorite and dacite blocks are present in small amounts (Figure 42). Blocks are angular to subangular and up to 760 cm in size. The rock glaciers below the Wheaton Glacier forefield consist entirely of granite clasts. The clasts are angular to subangular and up to 300 cm across. Most clasts in the breached recessional moraine are syenite; granite, orthoclase-rich granite, and granodiorite clasts are also present (Figure 43). The clasts are angular to subrounded and up to 230 cm

in size. Clasts in the Little Ice Age terminal moraine are mainly granite and syenite, but dacite and granodiorite clasts are also present (Figure 44). The clasts are angular to subangular and up to 290 cm across.

3.4.3 Lichenometry

The largest lichen thallus found on debris flow deposit A is 160 mm in diameter; the average diameter of the five largest thalli is 113 mm (Figure 45). The estimated age of these lichens based on the lichen growth curve in Chapter 2 (Figure 7) is AD 1771 +/- 20. The maximum diameter of the largest lichen thallus found on debris flow deposit B is 111 mm; the average diameter of the five largest thalli is 93 mm (Figure 46). The estimated age of these lichens is AD 1807 +/- 20. The maximum diameter of the largest lichen thallus found on debris flow deposit C is 13 mm; the average diameter of the five largest thalli is 10 mm (Figure 47). The estimated age of these lichens is AD 1957 +/- 20. Many clasts, however, are covered with dead lichens with maximum diameters up to hundreds of millimetres. The maximum diameter of the largest lichen thallus on debris flow deposit D is 500 mm; the average diameter of the five largest thalli is 341 mm (Figure 48). The estimated age of these lichens is AD 1358 +/- 20.

The maximum diameter of the largest lichen thallus on the rock fall deposit is 10 mm; the average diameter of the five largest thalli is 8.2 mm (Figure 49). The estimated age of these lichens is AD 1960 +/- 20. This age correlates well to evidence from aerial photographs – the rock fall is not visible in the 1948 photographs, but is present in the 1964 photographs. The maximum diameter of

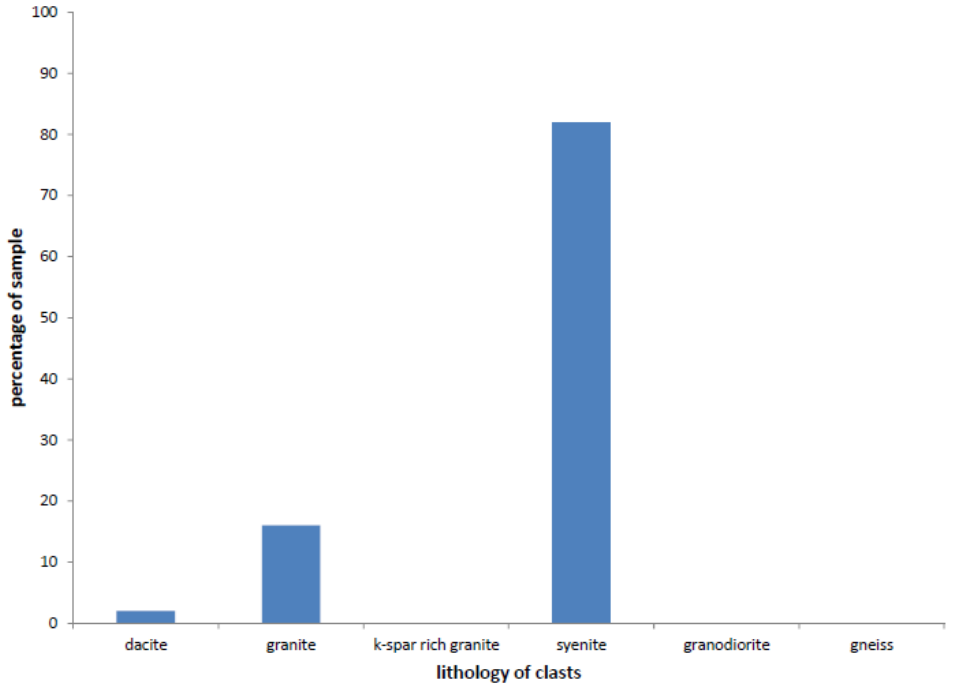

Figure 39 Lithologies of clasts in debris flow deposit A; n = 50.

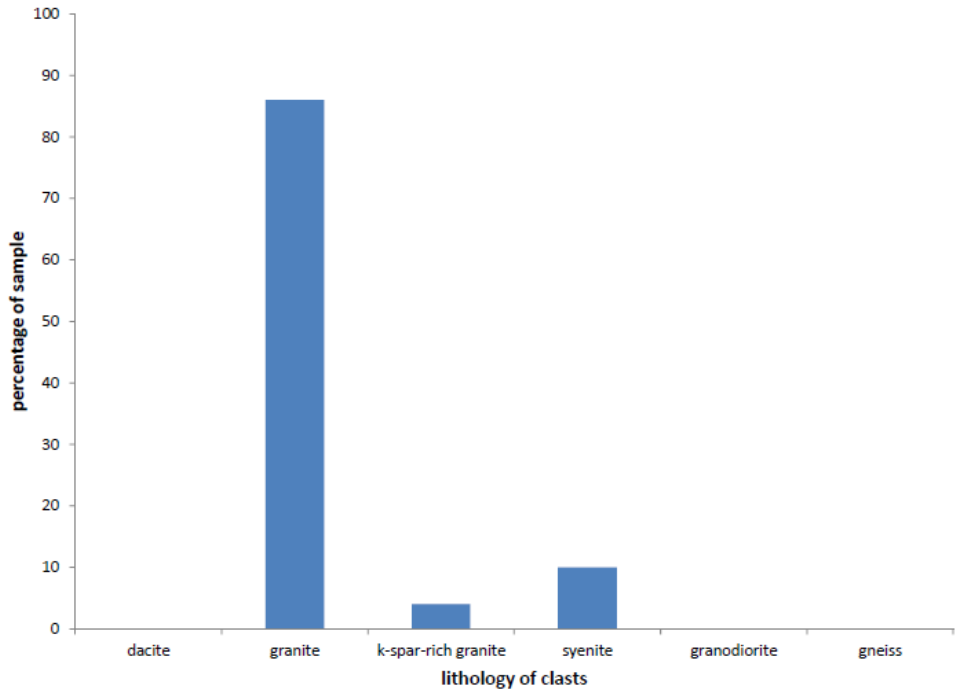

Figure 40 Lithologies of clasts in debris flow deposit B; n = 50.

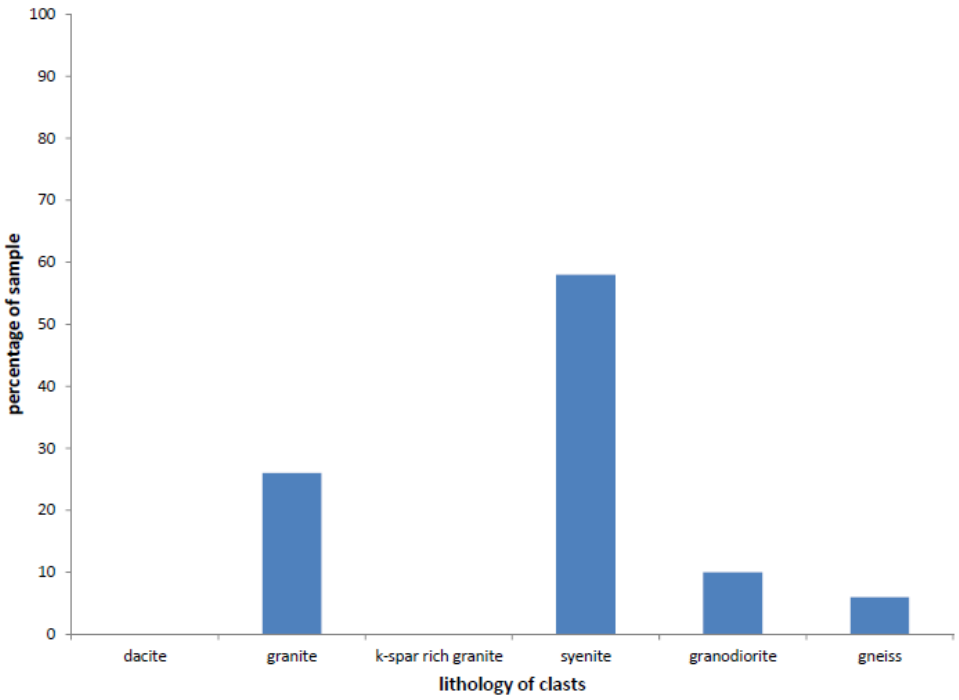

Figure 41 Lithologies of clasts in debris flow deposit D; n = 50.

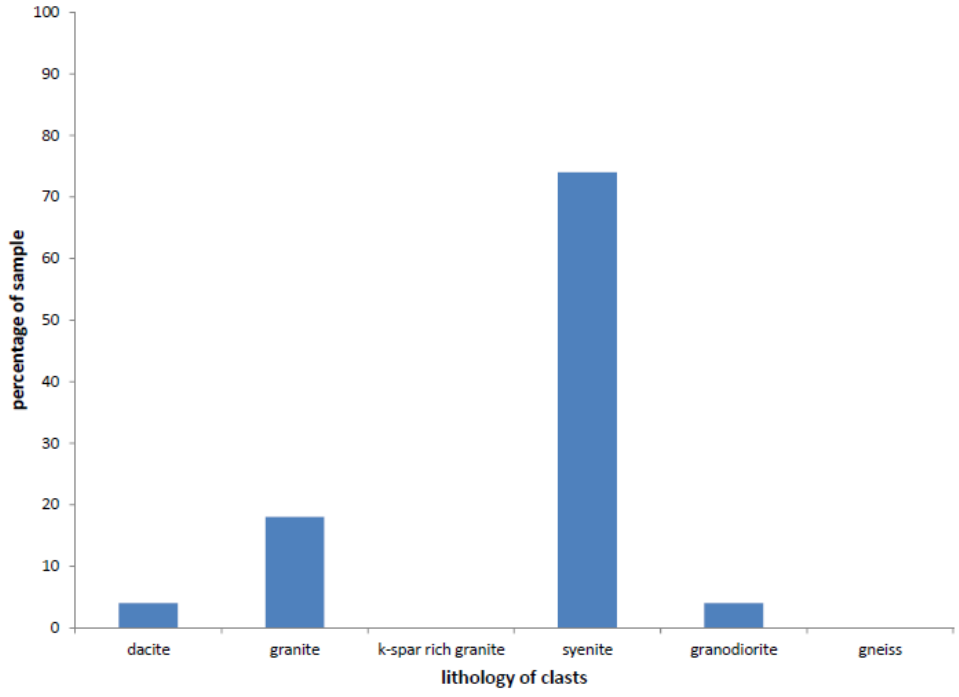

Figure 42 Lithologies of blocks in the rock fall deposit; n = 50.

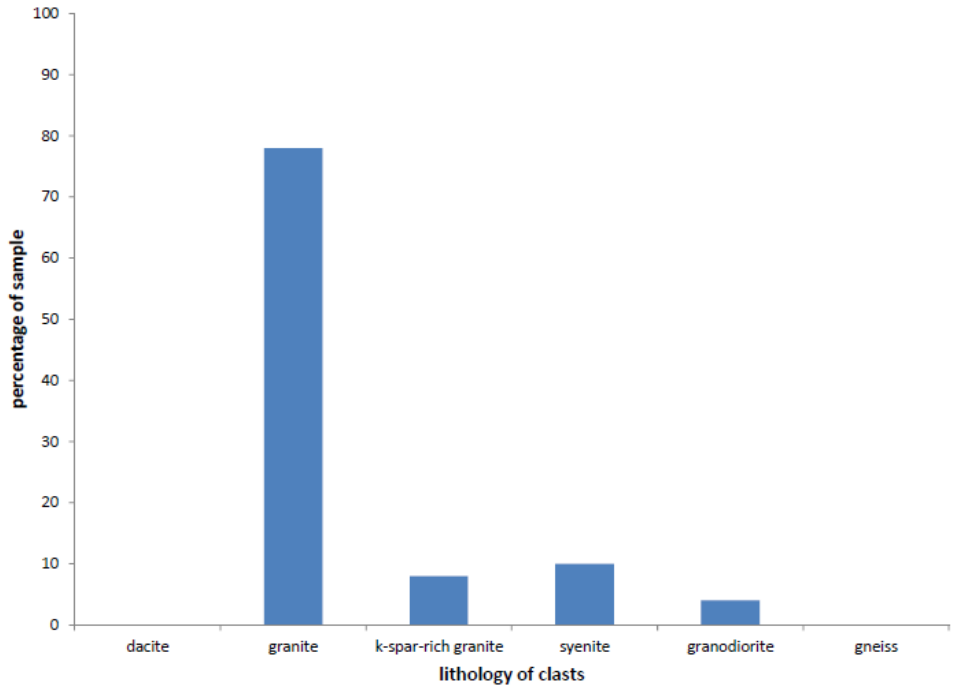

Figure 43 Lithologies of clasts in the breached recessional moraine; n = 50.

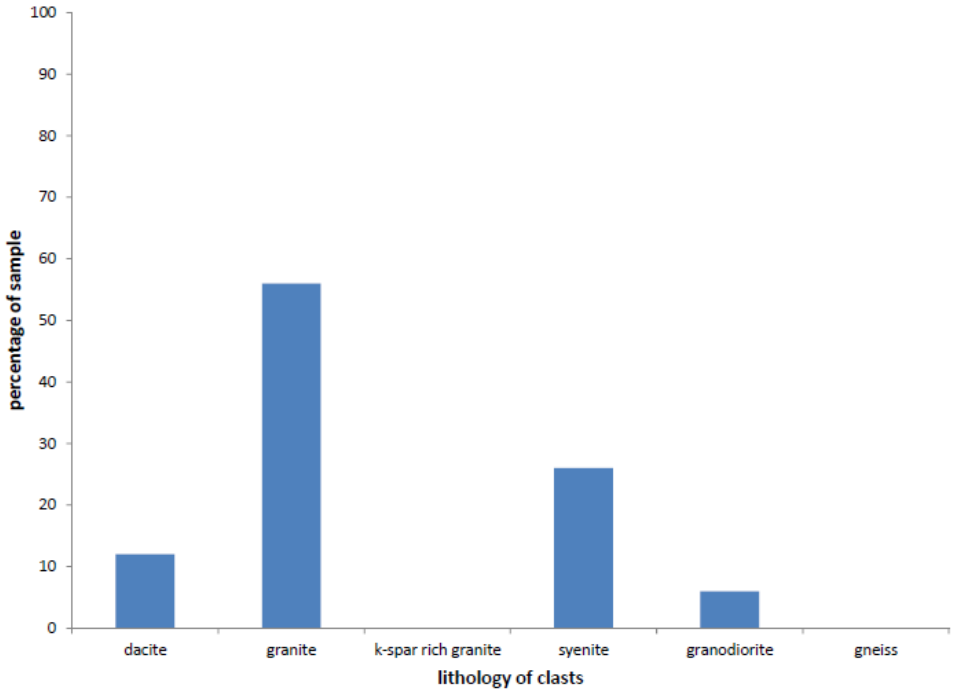

Figure 44 Lithologies of clasts in the Little Ice Age terminal moraine; n = 50.

the largest lichen thallus on the rock glaciers is 165 mm; the average diameter of the five largest thalli is 104 mm (Figure 50). The estimated age of these lichens is AD 1787 +/- 20. The maximum diameter of the largest lichen thallus above the washed surface of the incised recessional moraine is 22 mm; the average diameter of the five largest thalli is 13 mm (Figure 51). The estimated age of these lichens is AD 1952 +/- 20. No lichens were found on the proximal side of the moraine below the level of the former proglacial lake, which seems reasonable as the proglacial lake is still visible in the 1964 aerial photographs. The maximum diameter of the largest lichen thallus on the Little Ice Age terminal moraine is 36 mm; the average diameter of the five largest thalli is 33.2 mm (Figure 52). The estimated age of these lichens is AD 1915 +/- 20.

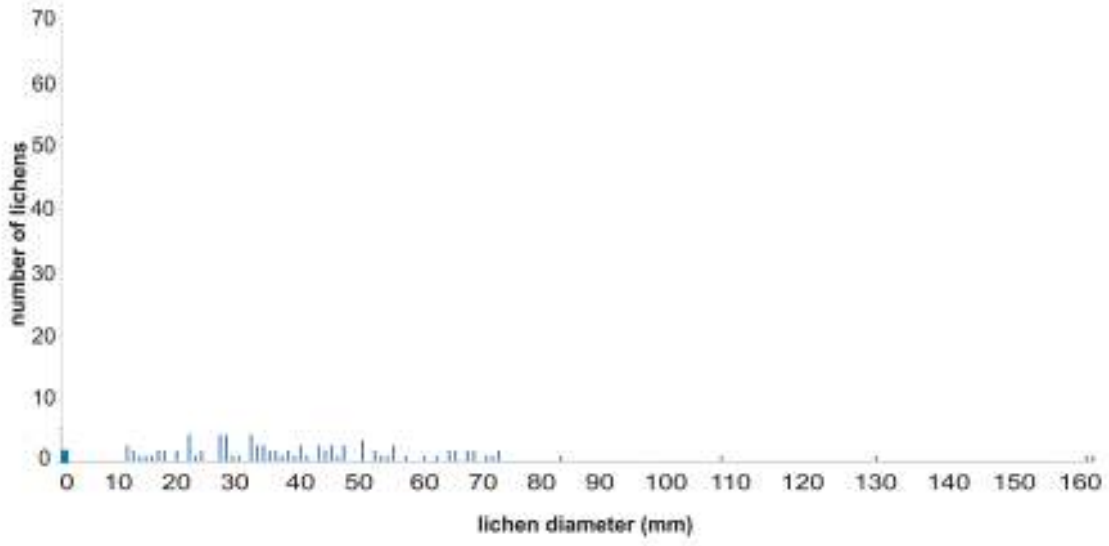

Figure 45 Distribution of lichen diameters on surface boulders of debris flow deposit A.

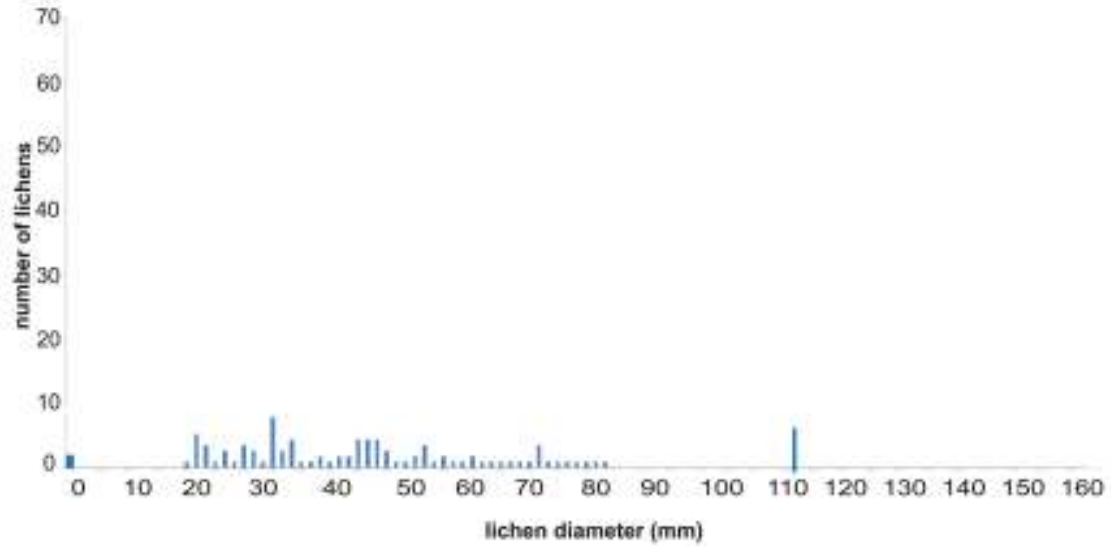

Figure 46 Distribution of lichen diameters on surface boulders of debris flow deposit B.

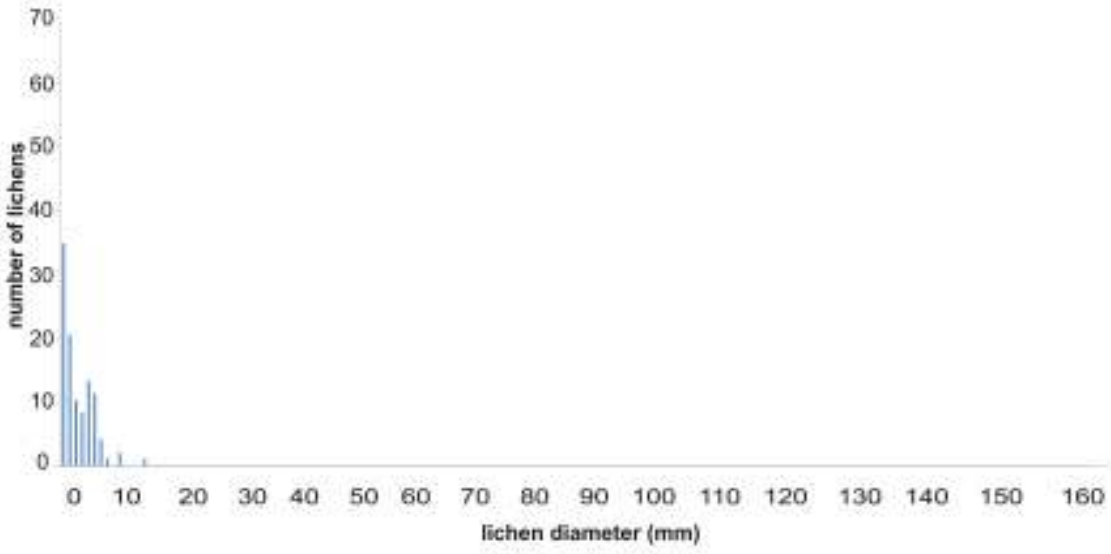

Figure 47 Distribution of lichen diameters on surface boulders of debris flow deposit C.

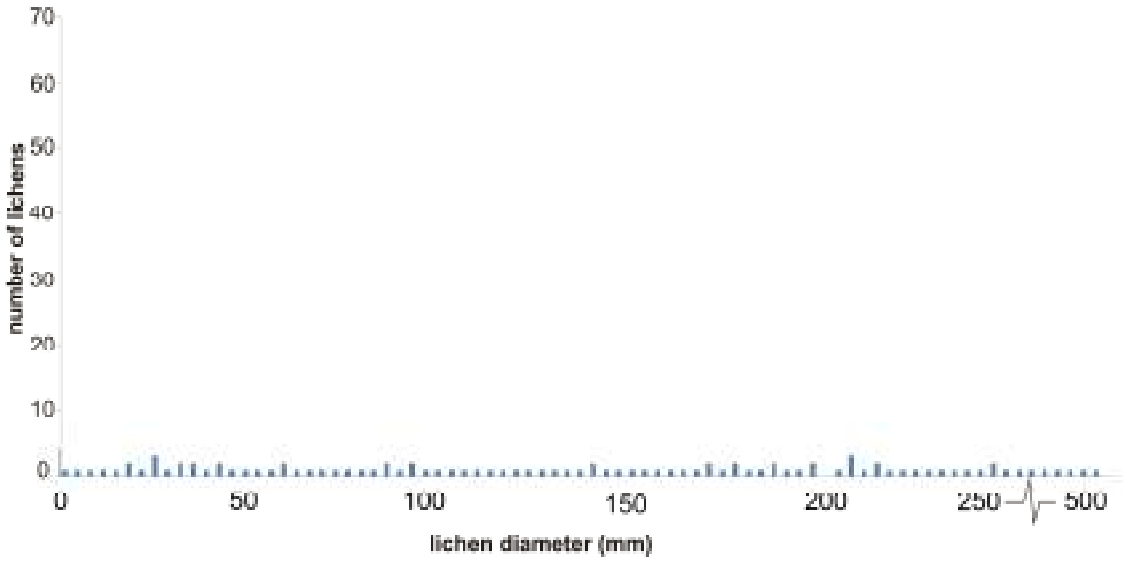

Figure 48 Distribution of lichen diameters on surface boulders of debris flow deposit D.

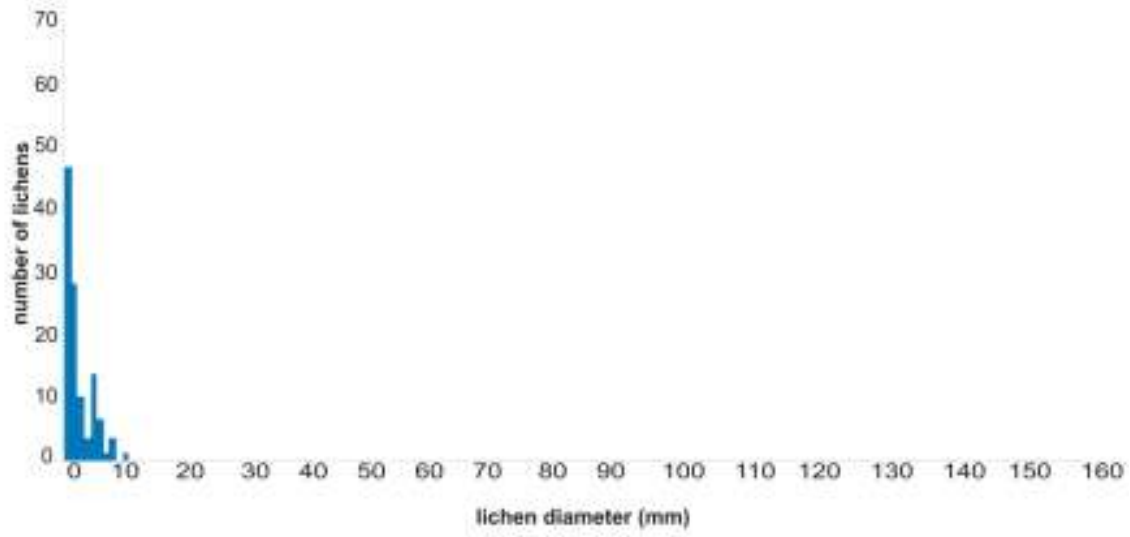

Figure 49 Distribution of lichen diameters on the rock fall deposit.

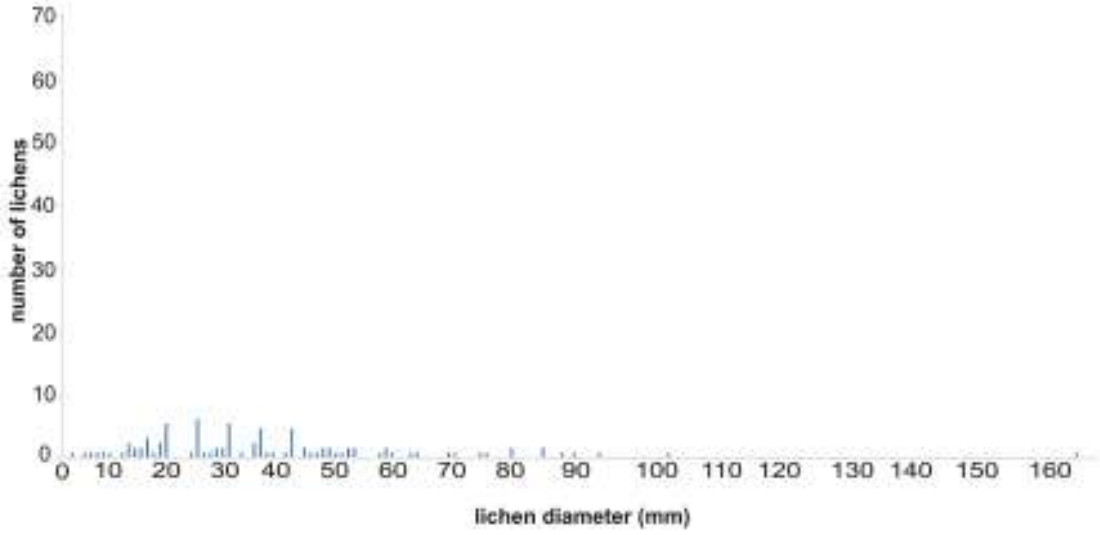

Figure 50 Distribution of lichen diameters on the rock glaciers.

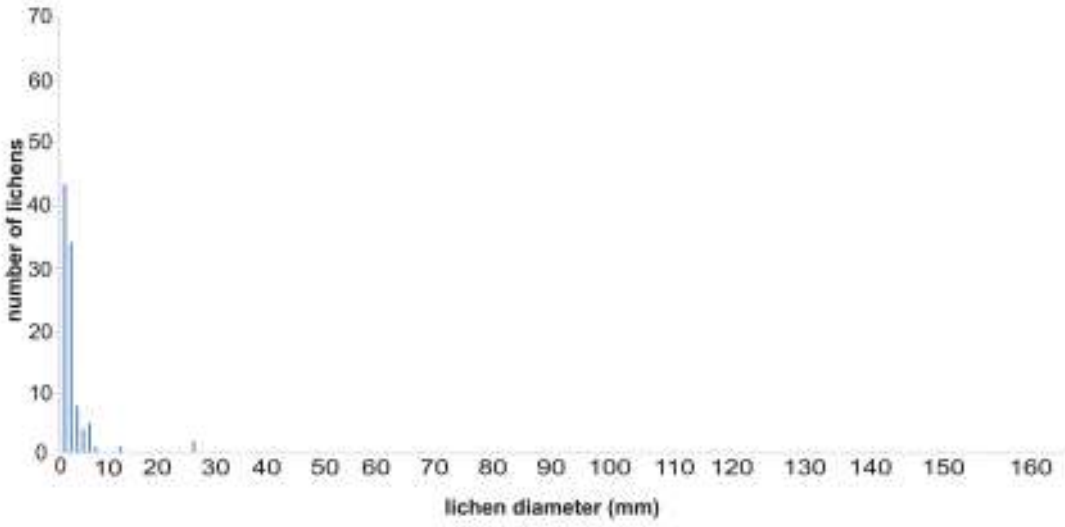

Figure 51 Distribution of lichen diameters on surface boulders of the incised recessional moraine.

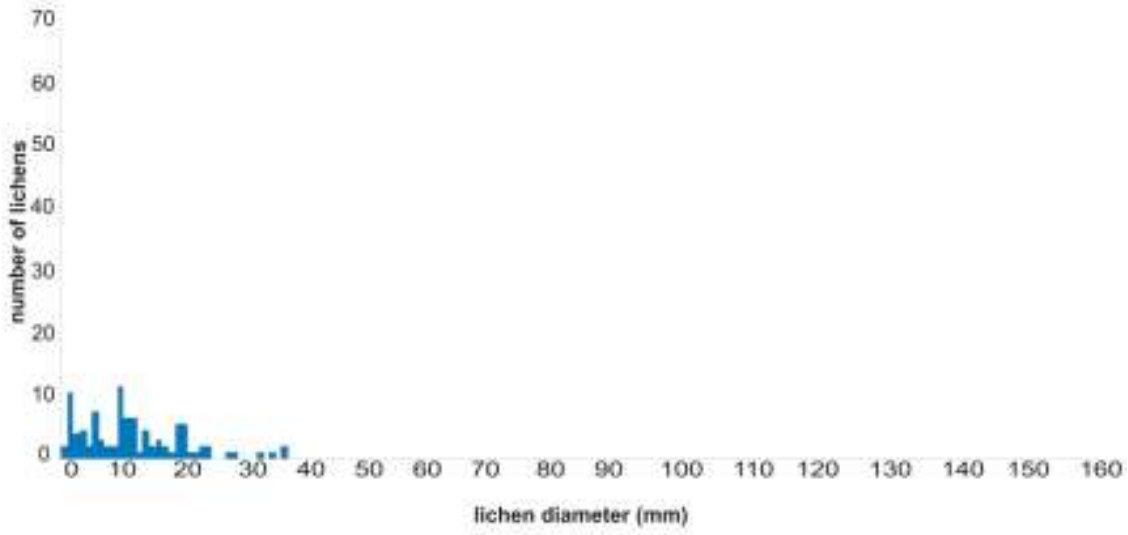

Figure 52 Distribution of lichen diameters on surface boulders of the Little Ice Age terminal moraine.

3.4.4 Dendrochronology and Hydrology

Tree-ring analysis shows that the debris flow that scarred the tree on the upper part of the fan (Figures 28 and 29) occurred in 1968. The scarred tree seeded sometime before 1802, which thus is the minimum age for debris flow B, on which the tree was growing. Because 1968 is within the period of the Water Survey of Canada records for Wheaton and Watson rivers, I searched for anomalous discharges that might be associated with the debris flow. To provide context, I also calculated mean daily discharges of Wheaton and Watson rivers for the period 1963-1973. I found two possible anomalous discharge peaks, one on October 8, 1968, and the other on October 16, 1968 (Figure 53). The two discharge spikes occurred at times where Watson River discharge decreased. Other peaks and troughs in the 1968 Wheaton and Watson River hydrographs track each other. Inspection of Whitehorse and Carcross precipitation records

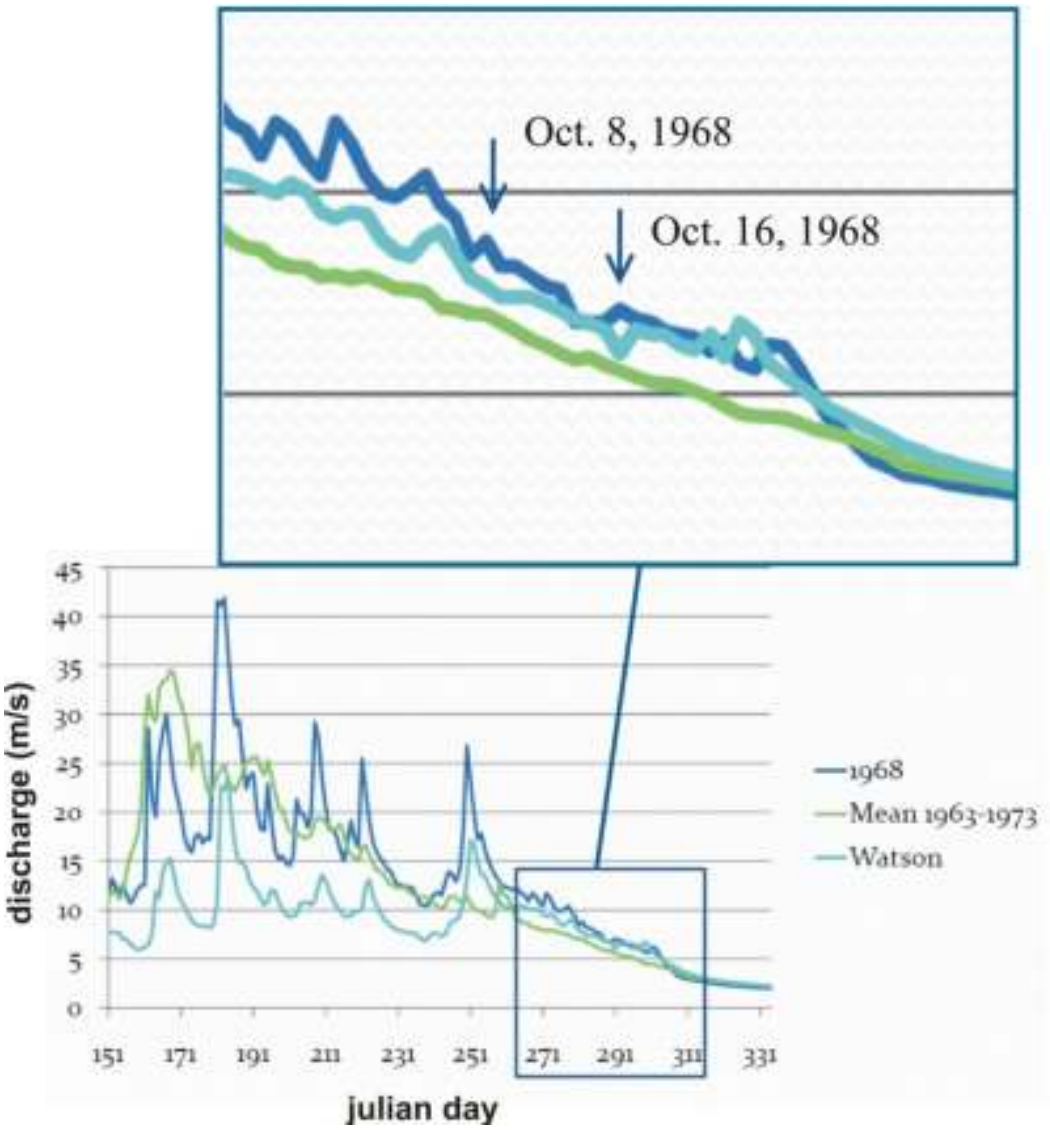

Figure 53 Hydrographs of Wheaton and Watson rivers for 1968, and mean flow of Wheaton River for the period 1963-1973. The portions of the hydrographs from September 28 to November 7, 1968 are enlarged at the top. Wheaton River discharge increases above background levels on October 8 and 16, 1968. No corresponding increases are seen in the Watson River hydrograph, suggesting that the outburst flood from the moraine-dammed lake in the Wheaton Glacier forefield may have occurred on one of these days.

revealed no rainfall on October 8 or 16 that could explain the discharge peaks in the Wheaton River record.

3.4.5 Core Stratigraphy

Each of the five cores from the distal part of the Wheaton fan contains debris flow, hyperconcentrated flow, and flood deposits separated by organic sediments that record periods of stability. Debris flow and hyperconcentrated flow deposits were identified by clasts that are coarser and more angular than those in fluvial deposits, by poor sorting, and in some instances by reverse grading. Sand units bounding these coarser deposits may be fluvial after-flow facies of debris flows or hyperconcentrated flows or, alternatively, may be unrelated fluvial deposits. Radiocarbon ages summarized in Table 6 facilitated correlation of units from core to core. Key features of the cores are presented below; detailed core logs are provided in Appendix 2.

Core AC07-050

Core AC07-050 is 197 cm long and contains sand and silt units separated by organic-rich silt horizons, some of which have been radiocarbon dated (Figure 54). Many of the sand and silt units have sharp basal contacts. The upper contacts of many of the sand and silt units in the upper part of the core are undulatory.

Core AC07-051

Core AC07-051 is 122 cm long and, like core AC07-051, contains sand and silt units separated by organic-rich silt horizons (Figure 55). The upper contacts of most of the sand and silt units are gradational. Many clasts over 2 cm in length occur between 36 cm and 68 cm. Sediments between 68 cm and 90 cm are

strongly oxidized. Coring terminated at 122 cm depth on a cobble layer; clasts up to 7 cm long were present in the core catcher.

Core AC07-052

Core AC07-052 is 198.5 cm long and contains sand and silt units separated by organic-rich silt horizons (Figure 56). The upper portion of the core is dominated by oxidized sand, and gently dipping strata occur in the lower part of the core.

Core AC07-053

Core AC07-053 is 212 cm long and contains dark grey sand and silt units separated by organic-rich silt horizons (Figure 57).

Core AC07-054

Core AC07-054 is 174 cm long and contains dark grey sand and silt units separated by organic-rich silt horizons (Figure 58). The core is strongly oxidized between 41.5 cm and 68 cm and contains pebbles larger than 1.5 cm between 77 cm and 108.5 cm.

A provisional correlation of stratigraphic units is presented in Figure 59. The surface organic horizon is easily correlated across all five cores, although its basal age differs across the fan. The organic unit in AC07-050 that yielded the radiocarbon age of 3705 ± 20 ^{14}C yrs BP probably correlates with the peat in AC07-051 dated at 3640 ± 20 ^{14}C yrs BP. The organic unit in AC07-050 dated at 3870 ± 15 ^{14}C yrs BP correlates across all cores except AC07-051, which is too young to include that horizon. Correlative dated horizons in the other cores are

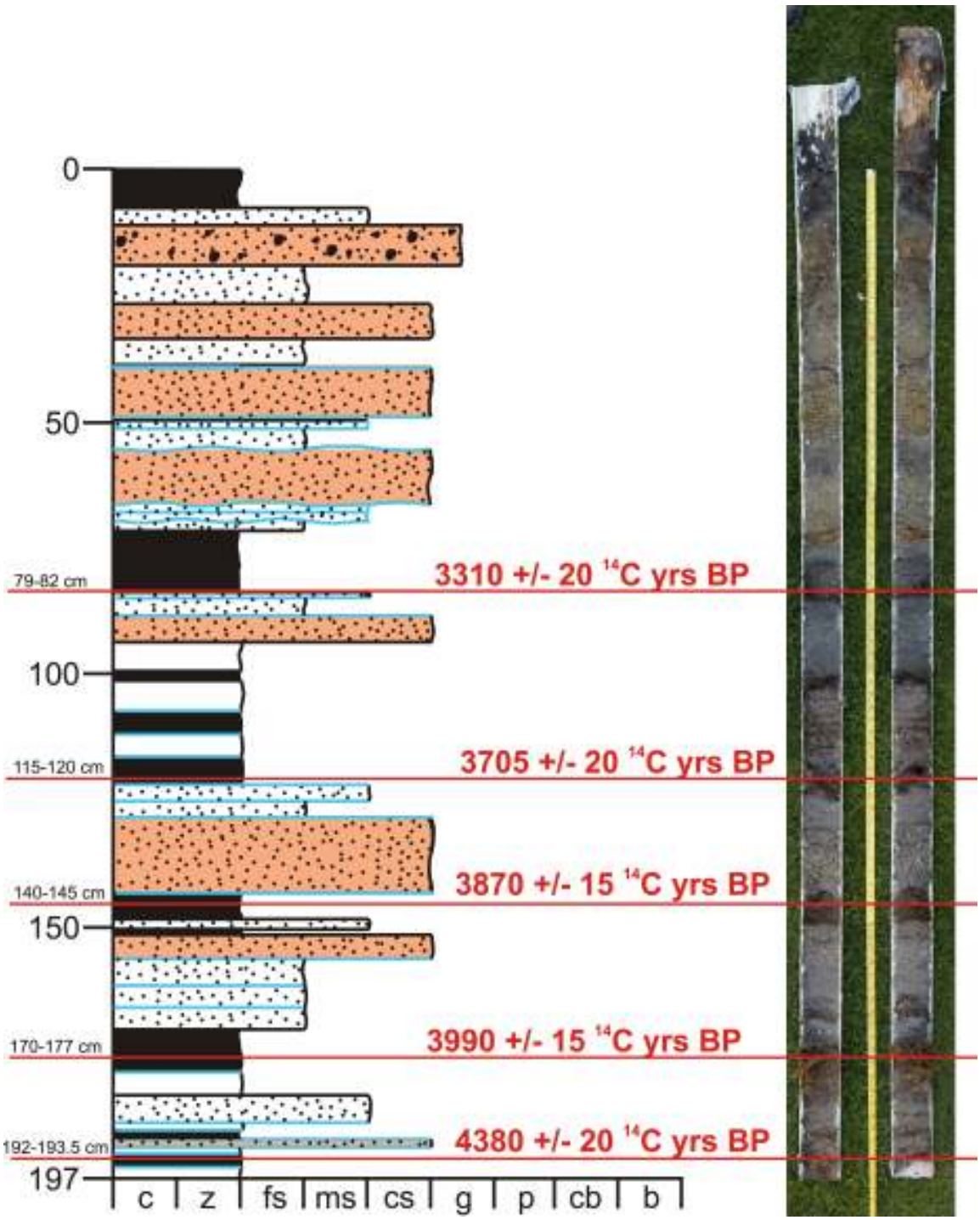

Figure 54 Stratigraphic log and photo of core AC07-050, showing depths of sampled organic horizons and radiocarbon ages. Blue lines indicate sharp basal contacts. Orange units indicate debris flow or hyperconcentrated flow deposits. c = clay, z = silt, fs = fine sand, ms = medium sand, cs = coarse sand, g = granules, p = pebbles, cb = cobbles, and b = boulders.

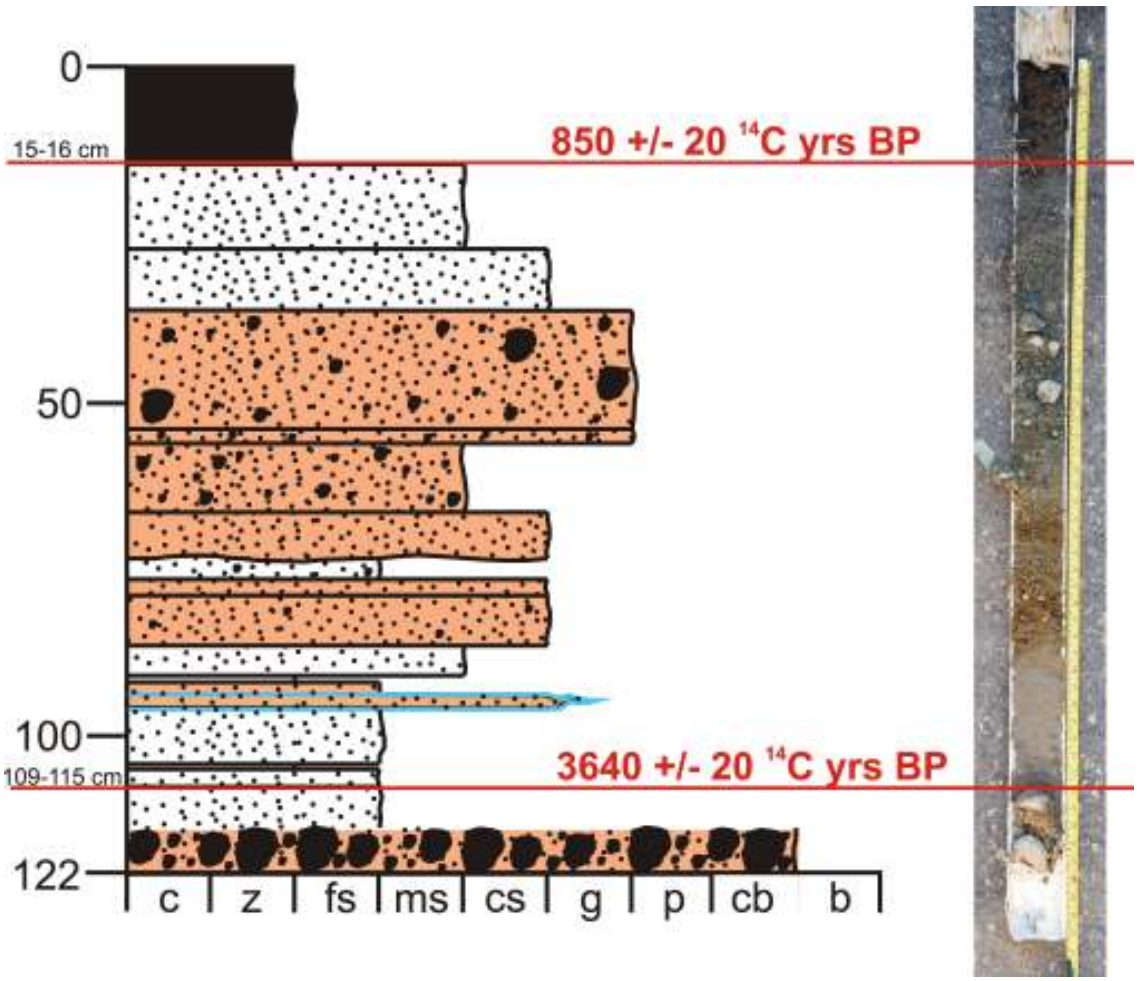

Figure 55 Stratigraphic log and photo of core AC07-051, showing depths of sampled organic horizons and radiocarbon ages. Blue lines indicate sharp basal contacts. Orange units indicate debris flow or hyperconcentrated flow deposits. c = clay, z = silt, fs = fine sand, ms = medium sand, cs = coarse sand, g = granules, p = pebbles, cb = cobbles, and b = boulders.

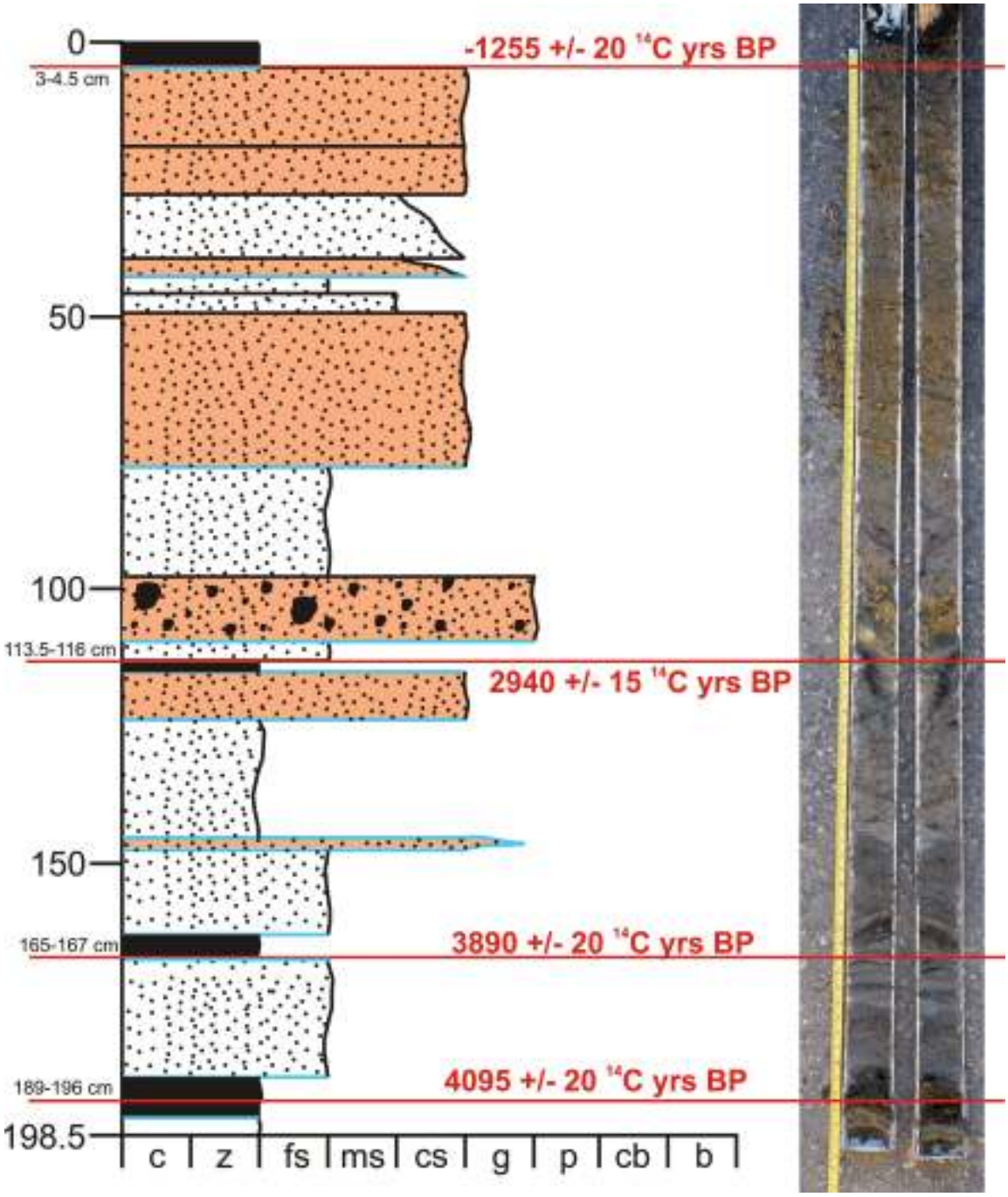

Figure 56 Stratigraphic log and photo of core AC07-052, showing depths of sampled organic horizons and radiocarbon ages. Blue lines indicate sharp basal contacts. Orange units indicate debris flow and hyperconcentrated flow deposits. c = clay, z = silt, fs = fine sand, ms = medium sand, cs = coarse sand, g = granules, p = pebbles, cb = cobbles, and b = boulders.

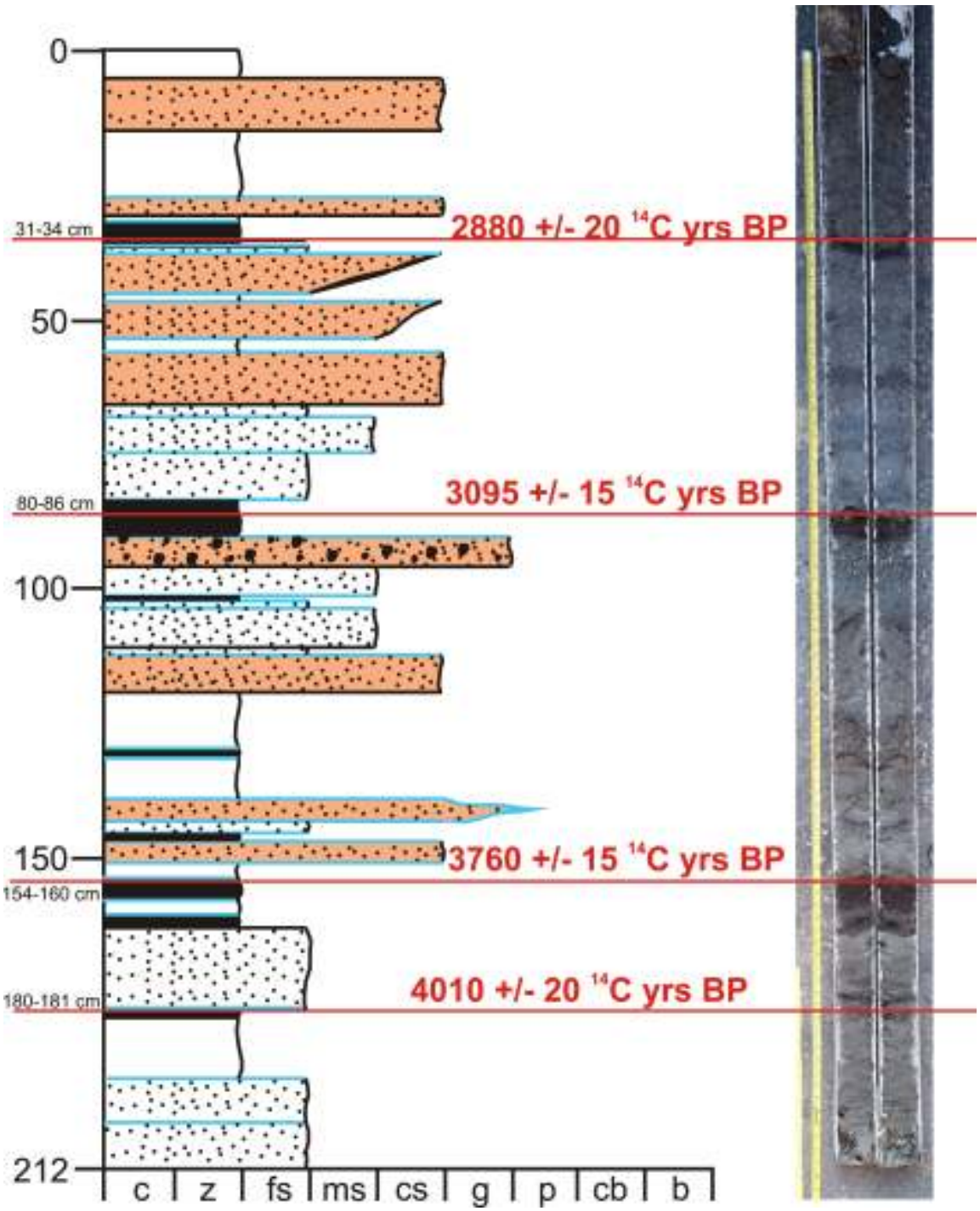

Figure 57 Stratigraphic log and photo of core AC07-053, showing depths of sampled organic horizons and radiocarbon ages. Blue lines indicate sharp basal contacts. Orange units indicate debris flow and hyperconcentrated flow deposits. c = clay, z = silt, fs = fine sand, ms = medium sand, cs = coarse sand, g = granules, p = pebbles, cb = cobbles, and b = boulders.

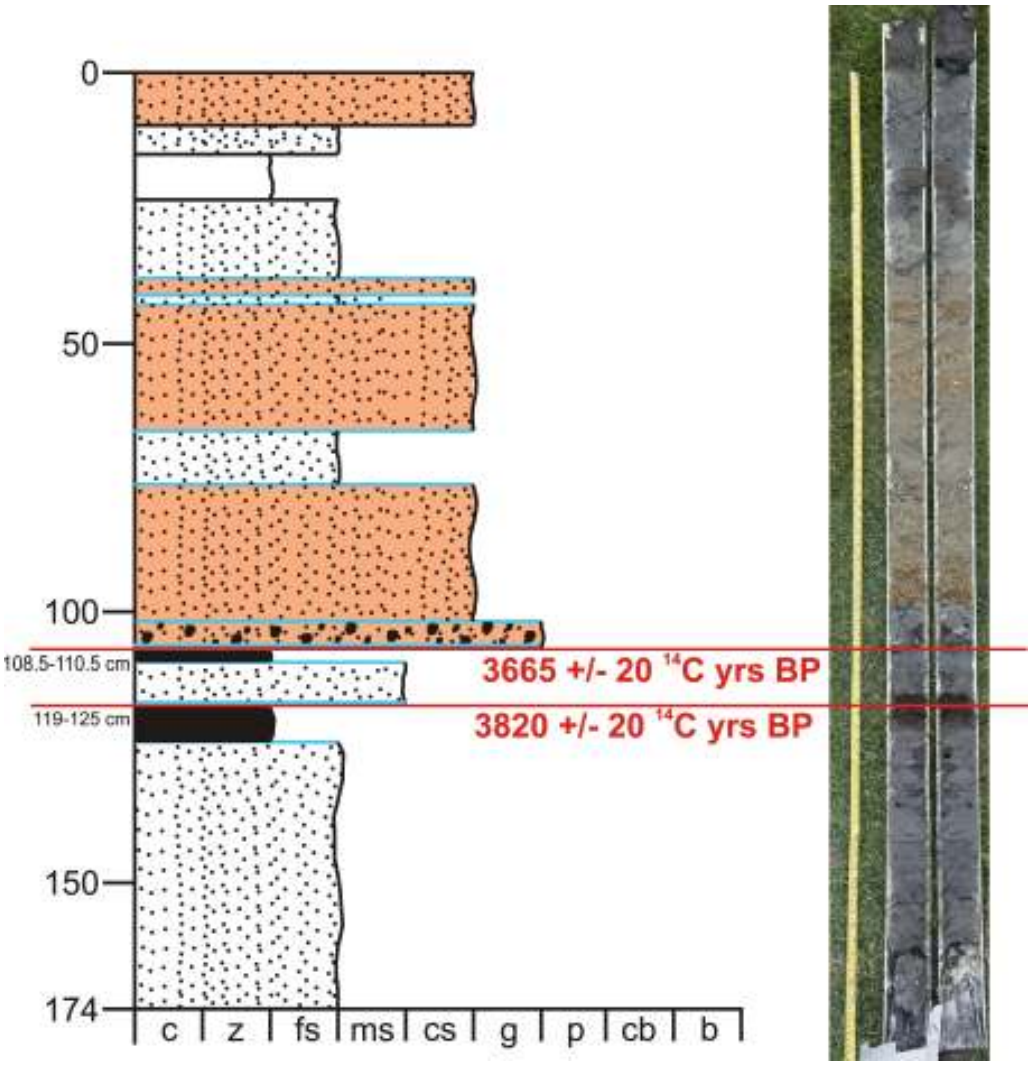

Figure 58 Stratigraphic log and photo of core AC07-054, showing depths of sampled organic horizons and radiocarbon ages. Blue lines indicate sharp basal contacts. Orange units indicate debris flow and hyperconcentrated flow deposits. c = clay, z = silt, fs = fine sand, ms = medium sand, cs = coarse sand, g = granules, p = pebbles, cb = cobbles, and b = boulders.

3890 ± 20 ^{14}C yrs BP (AC07-052), 3760 ± 15 ^{14}C yrs BP (AC07-053), and 3820 ± 20 ^{14}C yrs BP (AC07-054). The organic horizon in AC07-050 dated at 3990 ± 15 ^{14}C yrs BP correlates with horizons dated at 4095 ± 20 ^{14}C yrs BP in AC07-052 and 4010 ± 20 ^{14}C yrs BP in AC07-053. The organic horizon in AC07-052 dated

at 2940 ± 15 ^{14}C yrs BP correlates with the horizon in AC07-053 dated at 3095 ± 15 ^{14}C yrs BP.

Table 7 Radiocarbon ages of detrital plant fossils recovered from sediment cores collected on the Wheaton fan.

Name	Laboratory Number	Nature of Sample	Radiocarbon Age (BP)	Uncertainty (Reported)	Calendrical Age (BP)
AC07-050 (79-82)	40555	Twig	3310	20	3543 +/- 94
AC07-050 (115-120)	40556	Twig	3705	20	4035 +/- 120
AC07-050 (140-145)	40557	Needles	3870	15	4288 +/- 128
AC07-050 (170-177)	40649	Needles	3990	15	4470 +/- 55
AC07-050 (192-193.5)	40650	Needles	4380	20	5032 +/- 181
AC07-051 (15-16)	45016	Needles	850	20	795 +/- 111
AC07-051 (109-115)	40651	Needles	3640	20	3970 +/- 115
AC07-052 (3-4.5)	45017	Leaves	-1255	20	50 +/- 4
AC07-052 (113.5-116)	40652	Leaf	2940	15	3104 +/- 110
AC07-052 (165-167)	40653	Needles	3890	20	4291 +/- 132
AC07-052 (189-196)	40654	Needles	4095	20	4631 +/- 186
AC07-053 (31-34)	45018	Leaf	2880	20	3019 +/- 140
AC07-053 (80-86)	40655	Leaves	3095	15	3314 +/- 70
AC07-053 (154-160)	40656	Needles	3760	15	4114 +/- 122
AC07-053 (180-181)	40657	Leaves	4010	20	4596 +/- 185
AC07-054 (108-110)	40658	Needles	3665	20	4011 +/- 133
AC07-054 (119-125)	40659	Needles	3820	20	4249 +/- 159

*Accelerator mass spectrometry (AMS) radiocarbon ages determined at the Keck Carbon Cycle AMS Facility in the Earth System Science Department at the University of California Irvine. Radiocarbon ages were calibrated using OxCal 4.0 (Oxford Radiocarbon Accelerator Unit, 2008); range in calendric ages is reported at a 2 sigma level.

3.4.6 Seismostratigraphy

The GPR survey provided information on the subsurface stratigraphy of the alluvial fan to depths of 30 m, although detail is limited below a depth of about 12 m (Figures 60 and 61).

GPR line 1 (Figure 60) is located on the perimeter of the fan. Reflectors are generally parallel to the surface of the fan, but are irregular and discontinuous.

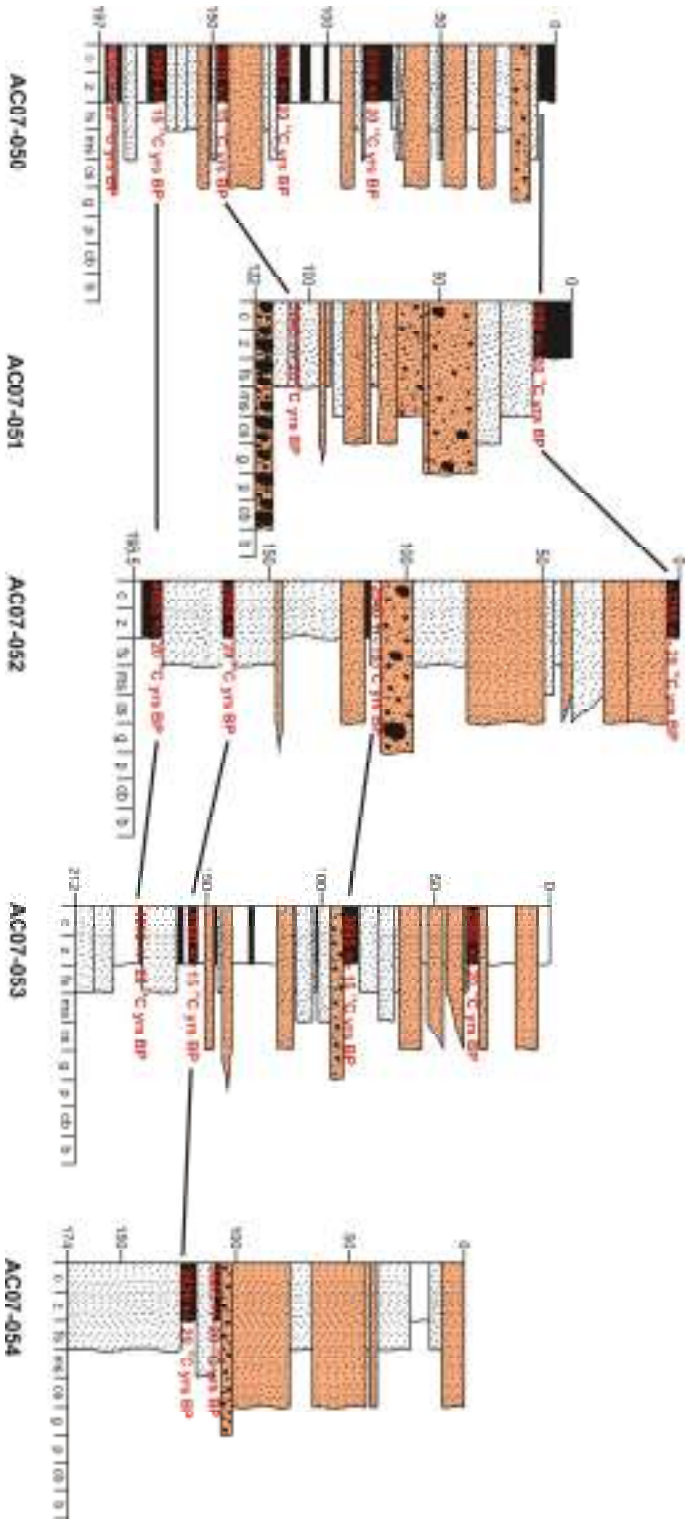

Figure 59 Correlations of radiocarbon-dated organic units in five sediment cores collected from the distal edge of the Wheaton fan. Orange units indicate debris flow deposits.

Infilled channels up to several tens of metres wide are evident below about 5 m depth. The floor of the largest of these channels is about 10 m below the fan surface.

GPR line 2 (Figure 61) extends 180 m up the axis of the fan from the periphery. Energy penetration decreases from 16 m at the edge of the fan to less than 10 m at the south end of the profile due to the coarsening of sediment in this direction. Line 2 has more reflectors than line 1. The reflectors in line 2 also are more irregular than those in line 1; they display multiple truncations, troughs, and parabolic forms attributed to boulders. A wide trough infilled with bouldery sediments occurs near the edge of the fan at a depth of about 10 m, and two overlapping rises occur at a depth of about 4-5 m near the southern end of line 2.

3.5 Discussion

Periglacial processes, extreme rainfall events, and glacier recession are affecting sediment delivery in the upper Wheaton River watershed. Sediment is moving downstream from the unstable Wheaton Glacier forefield to the fan at the mouth of the valley. Large, out-of-channel debris flows are spilling across the fan and aggrading its surface.

Ages of surfaces at sites AC07-001, AC07-002, AC07-003, AC07-023, and AC07-024 seem unreasonably young. The fan surface is 600 m lower than the glacier forefield, where the lichen growth curve has yielded reliable ages. It is likely that lichens on the fan surface grow more rapidly than those in the glacier forefield, in which case lichen ages on the fan surface are too young.

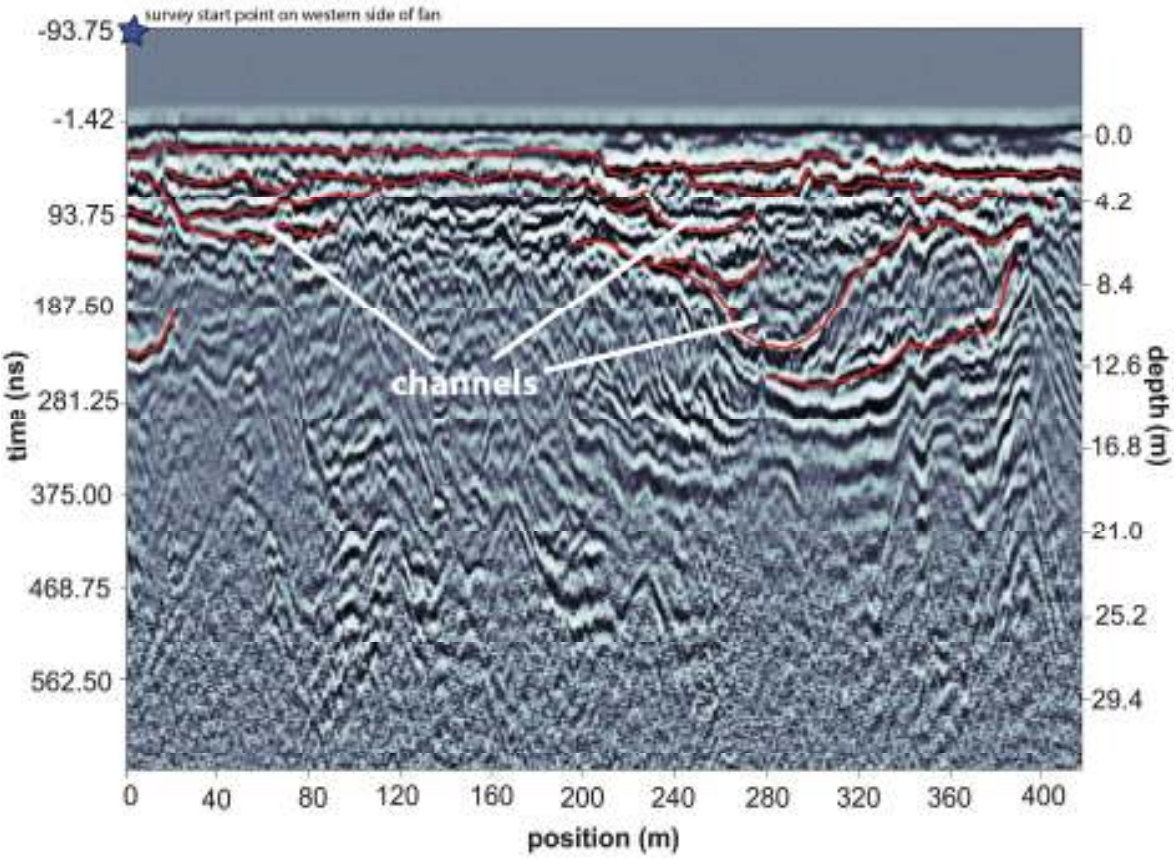

Figure 60 GPR line 1 along the perimeter of the fan (see Figure 26 for location). The zero position is at the west edge of the fan. Red lines delineate strong reflectors. Channels are highlighted.

3.5.1 Rock Fall

Debris flow deposit A and the rock fall have similar clast lithologies (Figure 62), which might suggest a possible link between the two. Lichen ages, however, rule out this possibility. The apparent lichen age of debris flow deposit A is AD 1771 +/- 20. This lichen age is supported by a minimum age of AD 1805 for the surface on which the scarred tree at the apex of the fan is located (see Section 3.5.4).

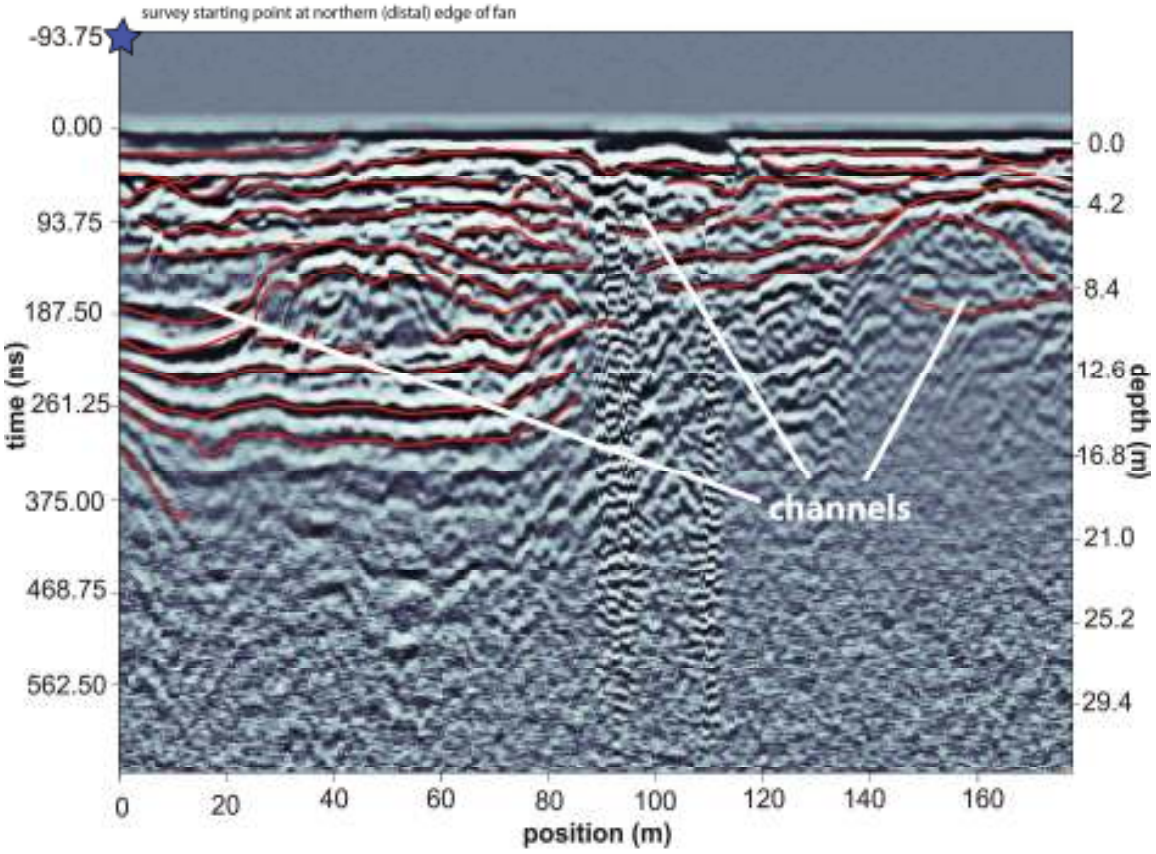

Figure 61 GPR line 2, part way up the axis of the debris flow fan (see Figure 26 for location). The zero position is located at the distal edge of the fan. Red lines delineate strong reflectors. Channels are highlighted.

The scarred tree could not have been alive at the time of debris flow A. The rock fall deposit is south of the 1948 glacier margin (see Chapter 2) and occurred about 1960 based on lichen results. The source of debris flow deposit A thus remains unknown.

3.5.2 Draining of Moraine-dammed Lake

A link between draining of the moraine-dammed lake and debris flow deposit B is suggested by similarities in the lithologies of clasts in the breached moraine and deposit B; these two deposits are the only ones found in the study area that

contain orthoclase-rich granite (Figure 63). The link is supported by evidence that the two events may have occurred at the same time. Debris flow deposit B occurred in 1968, possibly in October (see Section 3.4.1.4). The moraine-dammed

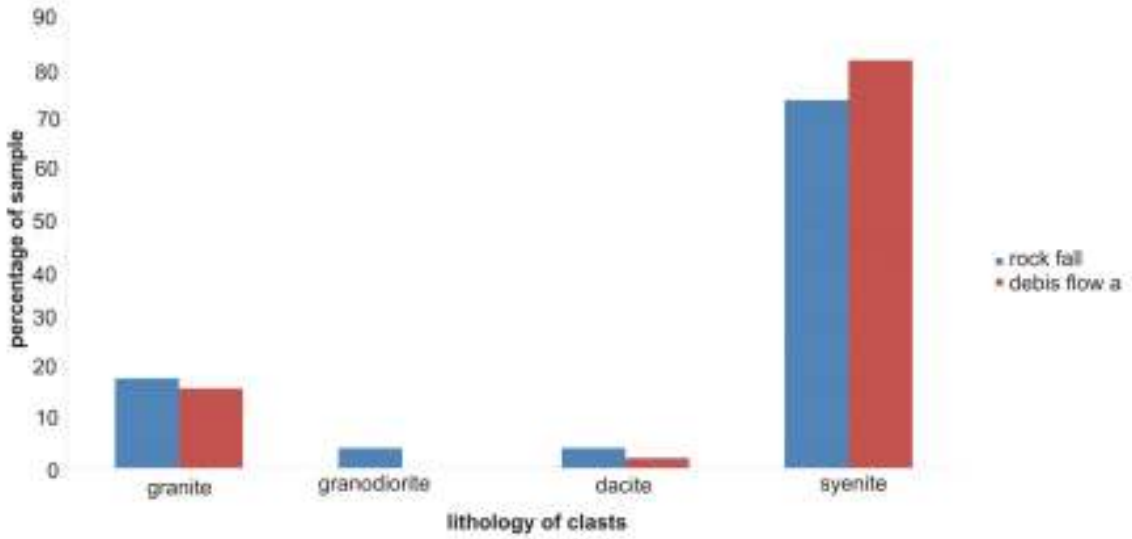

Figure 62 Comparison of lithologies of the rock fall deposit and debris flow deposit A; n = 50.

lake drained sometime between 1964 and 1987 (see Section 3.4.1.4). No lichens were found on the moraine below the uppermost level of the lake, suggesting that the lake drained after 1969 (see Chapter 2). Inspection of Wheaton River hydrograph records revealed two discharge peaks that may relate to the drainage event, one on October 8,' 1968, and the other on October 16, 1968.

Lichens on debris flow deposit B yielded an anomalously old age (AD 1809 +/- 20), given that the debris flow was dated to 1968 on the basis of damage to a tree. This dichotomy can be explained by considering the lichen data collected from the debris flow deposit. I measured 100 thalli to capture a representative

sample of lichens on each surface that I attempted to date. To measure 100 thalli on debris flow deposit B, I had to measure lichens on clasts that were not directly responsible for the damage to the dated tree. Many of these clasts may not have been deposited by debris flow B, but instead were deposited by an older debris flow. The age of this older debris flow is probably close to the time trees became established on its surface, i.e. before AD 1802. This age is similar to the age of deposit debris flow A – ca. AD 1771.

3.5.3 Rock Glaciers

The clasts of the rock glaciers and debris flow deposit C are entirely granite, suggesting a link between the two. The large, dead lichens on boulders of deposit C strengthen this link because large lichens also cover boulders on the rock glaciers. Lichens on the rock glacier boulders may have been killed when they were transported to the fan, after which a much younger lichen population became established (AD 1957 +/- 20). Similar scenarios have been reported from Southern Alps of New Zealand and the Scottish Highlands (Bull and Brandon, 1998; Innes, 1983, 1985). A date of AD 1957 +- 20 for debris flow deposit C is consistent with its geomorphic and chronological relationships to debris flow deposit B, a younger deposit closer to the apex of the fan (Figure 26). However, this date may be too young, because conifers that may be older than AD 1957 grow on the debris flow surface. This observation supports the previous statement that the iichen growth curve established for this study cannot be used at low elevations.

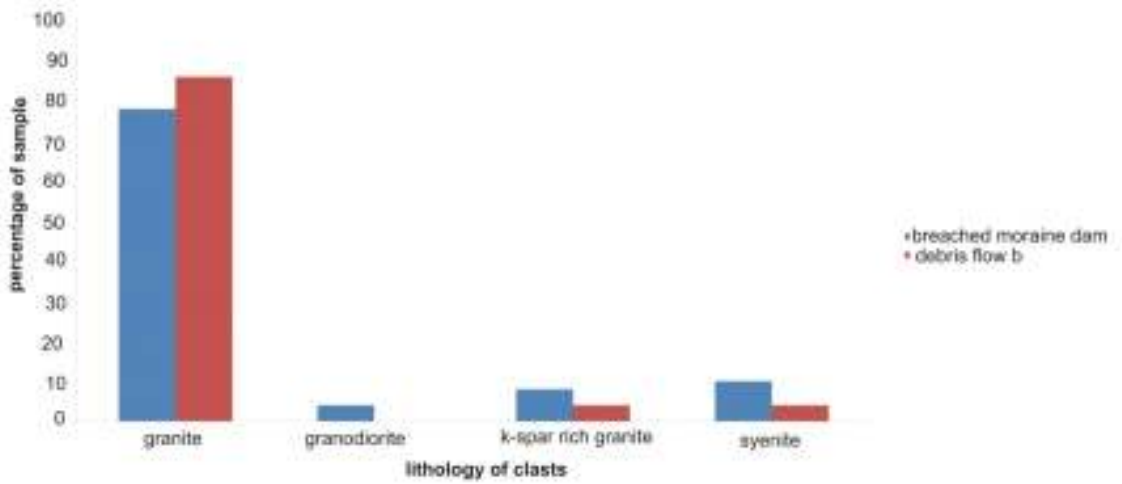

Figure 63 Comparison of lithologies of debris flow B and the breached moraine dam; n = 50.

The stream flowing from Wheaton Glacier is eroding the toe of the rock glaciers, maintaining an angle-of-repose slope. The stream channel is also deflected by the rock glaciers. Both observations indicate that the rock glaciers are active and suggest that a failure of the eroded scarp may have blocked the stream in the past. This scenario makes them potential sources of past debris flows that reached the mouth of the valley, including debris flow deposit C. The extent of these rock glaciers along the stream draining Wheaton Glacier (Figure 27) and their current activity (Section 3.4.1.3) suggest that they may be the most important source of sediment for debris flows reaching the fan.

3.5.4 Additional Debris Flow Sediment Sources and Triggers

Loose, unvegetated drift exposed as Wheaton Glacier retreated during the twentieth century may provide an additional source of sediment for debris flows. Debris flow triggers include, in addition to the sudden draining of moraine- or glacier-dammed lakes, extreme rainstorms and rain-on-snow events.

3.5.5 Core Stratigraphy

The five sediment cores reveal times of rapid sediment deposition at the periphery of the fan, alternating with periods of stability marked by accumulation of organic-rich silts. The coarse sediment layers are interpreted to be the distal deposits of debris flows, hyperconcentrated flows, and floods. The coarsest and thickest sediment layers, which tend to be massive or reversely graded and have angular clasts, are thought to be debris flow or hyperconcentrated flow deposits, whereas the few well-sorted, fine (dominantly silt and fine sand) units are attributed to floods. The area where the cores were collected shows no evidence of recent debris flow or fluvial activity, such as channels, recent fluvial deposits at the surface, or young successional vegetation.

I correlated several dated organic horizons from core to core (Figure 59). Notably, an organic-rich layer dating to about 3900 ^{14}C yrs BP is present in four of the five cores. This extensive organic-rich unit records a period of wetland development on the west side of the fan, with no significant debris flow activity. Core AC07-052 is the exception, as it does show some debris flow activity at this time. Organic deposits dated to about 4000 ^{14}C yrs BP are found in several cores and may likewise record a period of stability on the west side of the fan.

Although the cores provide no information on conditions on the central or eastern parts of the fan during the past 5000 years, they can, in combination with the GPR data, provide some sense of relative activity. The majority of surface channels are located on the central and eastern sectors of the fan. Buried paleochannels, however, are seen in the GPR records across all sectors of the

fan. The recent stability of the western sector of the fan, which is recorded by the cores, may reflect a change in the locus of debris flow deposition due to avulsion of the main channel. In this scenario, debris flow activity was focused on the fan's west side 4000 years ago, but the locus of activity shifted to the east, with occasional pulses on the west side of the fan about 3000 years ago.

My data suggest a series of large frequent debris flows occurred between 3000 and 4000 years ago on the western part of the fan. This interval is marked by glacier advances in the British Columbia Coast Mountains (Ryder and Thomson, 1986; Menounos *et al.*, 2004; Koch *et al*., 2007), Purcell Mountains (Osborn and Karlstrom, 1986), and Monashee Mountains (Alley, 1976; Westgate, 1977) and in the St. Elias Mountains of Yukon Territory (Rampton, 1970; Denton and Karlen, 1977). In particular, Osborn and Karlstrom (1986) document an advance of Bugaboo Glacier that culminated 3400-3000 years ago (see Table 1).

Church and Ryder (1972) proposed that sediment delivery from slopes to fluvial systems was high during and immediately after deglaciation, a concept they termed "paraglacial sedimentation." Deglaciation exposed large areas of unstable, poorly vegetated sediment that were rapidly transferred to streams by fluvial erosion and mass wasting, causing streams to aggrade their valleys (Church and Ryder, 1972; Church, 1983; Ashmore and Church, 2001). The flux of sediment decreased exponentially through time as the amount of erodible sediment decreased and slopes were stabilized by vegetation (Church and Ryder, 1972, Church and Slaymaker, 1989; Ballantyne and Benn, 1994, 1996). The concept of paraglacial sedimentation has been extended to Holocene glacier

advances and retreat cycles (Leonard, 1986, 1987; Ballantyne and Benn 1994; Leonard and Reasoner, 1999).

Debris flow activity on the Wheaton fan between 3000 and 4000 years ago may record climatically induced instability in the upper part of the valley, linked to the middle Neoglacial Tiedemann advance (Ryder and Thomson, 1986). The sediment cores may be preferentially capturing mid-Neoglacial debris flows. Prior to the Little Ice Age the locus of activity may have shifted eastward on the fan surface, accounting for lack of lack of Little Ice Age sediments in the cores on the west side of the fan. Alternatively, the cores may simply record typical alpine geomorphic processes, such as extreme precipitation events, and may not be linked to Neoglacial climate deterioration.

3.5.6 Ground Penetrating Radar

Many of the reflectors in the GPR profiles are discontinuous and irregular. They are truncated by other reflectors and drape underlying ones. These observations support the idea that successive debris flows covered different parts of the fan surface. The irregular forms are interpreted to be erosion surfaces and hummocky surface expression. The hyperbolic reflectors are commonly associated with underlying depressions, consistent with channels filled with coarse bouldery deposits.

Several well defined buried troughs were imaged on the central and eastern parts of the fan and at the fan's west edge. These features are interpreted to be paleo-channels of the stream flowing across the fan. They are offset laterally

from the present channels on the fan by about 20 m, suggesting that the channels shifted this distance in the intervening period.

The sediment cores and GPR profiles show that much of the fan consists of debris flow deposits that are older than 4000 years old, that is to say, deposits that are below the oldest sediments penetrated by coring. The GPR profiles image debris flow deposits related to earlier Neoglacial events or perhaps late Pleistocene deglaciation.

3.6 Conclusion

Sediment delivery in the upper Wheaton River watershed is being affected by periglacial activity, extreme precipitation events, and glacier retreat. Sediment is moving downstream from the Wheaton Glacier forefield to the fan at the mouth of the valley. Large, out-of-channel debris flows are reaching the fan and aggrading its surface. Evidence from sediment cores and a ground-penetrating radar survey suggest that debris flows have dominated sedimentation on the fan during the past several thousand years and probably the entire Holocene. Triggers identified for some of the debris flows include draining of a moraine-dammed lake, rock glacier activity, and extreme precipitation events.

4: CONCLUSIONS

4.1 Recent History of Wheaton Glacier

My research has documented the rapid loss of glacier ice in the Wheaton River watershed in the twentieth and early twenty-first centuries. The watershed contains the northeasternmost glaciers in the Coast Mountains and is particularly sensitive to climate change. Glacier ice losses were quantified by analyzing sequential aerial photographs and by applying bivariate scaling to glacier areas. Wheaton Glacier has lost 50% of its area and 58% to 63% of its volume since the end of the Little Ice Age. Wheaton Glacier retreated at a more-or-less constant rate until the 1980s, when the rate of retreat increased, before decreasing again in the 1990s. If the glacier continues to retreat at its historic rate, it may disappear as early as 2090.

Meteorological data from weather stations at Whitehorse and Carcross indicate that mean temperature in southern Yukon has increased since 1907. Temperature variations over this period appear to correlate roughly with PDO phases. Average winter snowfall at Carcross has increased over the historic period, as has average annual precipitation in Whitehorse. On a larger scale, increases in precipitation and temperature during the historic period are consistent with trends throughout most of northern British Columbia and Yukon Territory.

The documented historical increase in winter precipitation at Carcross should favour a positive regimen for Wheaton Glacier that would lead to glacier growth. In this case, however, the contemporary increase in temperature has been more significant than precipitation in affecting the glacier's mass balance.

Based on this study, I conclude that lichenometry yields reliable estimates of surface ages to within about 20 years in the Wheaton Glacier forefield. The technique may be more widely applicable in other subalpine environments in southern Yukon where other dating methods are not feasible. A requirement in using the technique elsewhere in southern Yukon, however, is that a local lichen growth curve be established from surfaces of known age, using for example historical records or radiocarbon dating.

4.2 Debris Flow History of Wheaton Fan

Recent retreat of Wheaton Glacier has caused instability in the glacier forefield. Draining of a proglacial lake triggered a debris flow that reached the fan at the mouth of the valley. Periglacial activity related to the advance of rock glaciers outside the Little Ice Age limit of Wheaton Glacier has also impacted the valley below. One debris flow, and possibly many others, are linked to these rock glaciers. It is likely that other triggers, including extreme precipitation events and rain-on-snow events, have contributed debris flows that built the fan at the mouth of the valley.

Five sediment cores reveal times of rapid sediment deposition at the western periphery of the fan, alternating with periods of stability marked by accumulation

of organic-rich silts. The coarse sediment layers are interpreted to be the distal deposits of debris flows, hyperconcentrated flows, and floods. The coarsest and thickest sediments layers, which tend to be massive or reversely graded and have angular clasts, are thought to be debris flow and hyperconcentrated flow deposits, whereas the few well-sorted, fine (dominantly silt and fine sand) units are attributed to floods. The area where the cores were collected shows no evidence of recent debris flow or fluvial activity, such as channels, recent fluvial deposits at the surface, or young successional vegetation. An organic-rich layer dating to about 3900 ^{14}C yrs BP is present in four of the five cores. This extensive organic-rich unit records a period of wetland development on the west side of the fan, with no significant debris flow activity. Organic deposits dated to about 4000 ^{14}C yrs BP and found in several cores may likewise record a period of stability on the west side of the fan.

Although the cores provide no information on conditions on the central or eastern parts of the fan during the past 5000 years, they can, in combination with the GPR data, provide some sense of relative activity. The majority of surface channels are located on the central and eastern sectors of the fan, whereas buried paleochannels are present across the entire toe of the fan. The recent stability of the western part of the fan may reflect debris flow focusing onto the central and eastern parts of the fan during the past 3000 years.

My data suggest a series of large frequent debris flows occurred between 3000 and 4000 years ago. This interval is marked by glacier advances in the Coast, Purcell, and Monashee Mountains in British Columbia and in the St. Elias

Mountains in Yukon Territory. Debris flow activity on the Wheaton fan between 3000 and 4000 years ago may record climatically induced instability in the upper part of the valley, linked to mid-Neoglacial glacier advances. The sediment cores may be preferentially capturing debris flows related to this instability. Alternatively, the debris flows recorded in the cores may reflect normal alpine environment processes, for example extreme precipitation events that are not related to glacier activity.

4.3 Significance

Most alpine glaciers worldwide have thinned and retreated in the past century. Glacier retreat in northern Canada may be amplified by the larger-than-average temperature increases that have happened at high latitudes. Thinning and retreat of Wheaton Glacier illustrate this point.

This study highlights the impact of periglacial processes on alpine streams. It also provides indirect evidence for glacier expansion 4000-3000 years ago in southern Yukon outside the St. Elias Mountains.

4.4 Suggestions for Further Research

Additional work is needed on the recent activity and mass balance of small alpine glaciers elsewhere in the Yukon to determine if the rates of retreat documented at Wheaton Glacier are typical of the region as a whole. This research is important for studies of climate change, hazard analysis, and hydrology.

Debris flow records from small steep glacierized watersheds may provide a glimpse into Holocene and historic glacier activity, and should be utilized more fully across the North.

REFERENCE LIST

Alley, N.F. 1976. Post-Pleistocene glaciations in the interior of British Columbia. *In* Geomorphology of the Canadian Cordillera and its Bearings on Mineral Deposits, Programme and Abstracts, Geological Association of Canada (Cordilleran Section), Vancouver, 6-7.

Alley, R.B., Mayewski, P.A., Sowers, T., Stuiver, M., Taylor, K.C., and Clark, P.U. 1997. Holocene climatic instability: A prominent widespread event 8200 yr. ago. Geology, 25: 483-486.

Anderson, L. 2005. Holocene climate of southwest Yukon Territory, Canada, inferred from lake-level and isotope analyses of small carbonate lakes. Ph.D. thesis, University of Massachusetts, Ann Arbor, Michigan, 171 pp.

Arctic Climate Impact Assessment (ACIA). 2005. Arctic Climate Impact Assessment. Cambridge University Press, New York, 1042 pp.

Ashmore, P. and Church, M. 2001. The impact of climate change on rivers and river processes in Canada. Geological Survey of Canada Bulletin 555, 50 pp.

Bahr, D.B., Meier, M.F., and Peckham, S.D. 1997. The physical basis of glacier volume-area scaling. Journal of Geophysical Research, 102(B9): 20355-20362.

Ballantyne, C.K. and Benn, D.I. 1994. Paraglacial slope adjustment and resedimentation following glacial retreat, Fabergstolsdalen, Norway. Arctic and Alpine Research, 26: 255-269.

Ballantyne, C.K. and Benn, D.I. 1996. Paraglacial slope adjustment during recent deglaciation and its implications for slope evolution in formerly glaciated environments. *In* Advances in Hillslope Processes, M.G. Anderson and S. Brooks (eds.). Wiley, Chichester, pp. 1173-1195.

Barlow, L.K., Sadler, J.P., Ogilvie, A.E.J., Buckland, P.C., Amorosi, T., Ingimundarson, J.H., Skidmore, P., Dugmore, A.J., and McGovern, T.H. 1997. Interdisciplinary investigations of the end of the Norse western settlement in Greenland. The Holocene, 7: 489-499.

Baumann, F. and Kaiser K.F. 1999.The Multetta debris fan, eastern Swiss Alps: A 500-year debris flow chronology. Arctic, Antarctic and Alpine Research, 31: 128-134.

Benda, L.E. and Cundy, T.W. 1990. Predicting deposition of debris flows in mountain channels. Canadian Geotechnical Journal, 27: 409-417.

Beverage, J.P. and Culbertson, J.K. 1964. Hyperconcentrations of suspended sediment. Journal of Hydraulic Division of the American Society of Civil Engineering, 90: 117-128.

Bierman, P.R., Gillespie. A.R., and Caffee, M.W. 1995. Cosmogenic ages for earthquake recurrence intervals and debris flow fan deposition, Owens Valley, California. Science, 270: 447-450.

Blake, W., Jr. 1983. Geological Survey of Canada radiocarbon dates XXIII. Geological Survey of Canada, Paper 83-7, 20 pp.

Blown, I. and Church, M. 1985. Catastrophic lake drainage within the Homathko River basin, British Columbia. Canadian Geotechnical Journal, 22: 551-563.

Bollschweiler, M. and Stoffel, M. 2007. Debris flows on forested cones—reconstruction and comparison of frequencies in two catchments in Val Ferret, Switzerland. Natural Hazards and Earth System Sciences, 7: 207–218.

Bond, J.D. 2003. Late Wisconsinan McConnell Glaciation of the Whitehorse map area (105D), Yukon. *In* Yukon Exploration and Geology 2003, D.S. Emond and L.L. Lewis (eds.). Yukon Geological Survey, Whitehorse, YT, pp. 73-88.

Bovis, M.J. 1982. Uphill-facing (antislope) scarps in the Coast Mountains, southwest British Columbia. Geological Society of America Bulletin, 93: 804-812.

Bovis, M.J. 1990. Rock-slope deformation at Affliction Creek, southern Coast Mountains, British Columbia. Canadian Journal of Earth Sciences, 27**:** 243-254.

Bovis, M.J. and Jakob, M. 1999. The role of debris supply conditions in predicting debris flow activity. Earth Surface Processes and Landforms, 24: 1039-1054.

Bradley, R.S. and Jones, P. (eds.). 1995. Climate since AD 1500. Chapman & Hall, New York, 724 pp.

Bradwell, T. 2010. Studies on the growth of *Rhizocarpon geographicum* in NW Scotland, and some implications for lichenometry. Geografiska Annaler: Series A, Physical Geography, 92: 41-52.

Brown, E.T., Bendick, R., Bourles, D.L., Gaur, V., Molnar, P., Raisbeck, G.M., and Yiou, F. 2002. Sliprates of the Karakorum fault, Ladakh, India, determined using cosmic ray exposure dating of debris flows and moraines. Journal of Geophysical Research, 107: 2192-2201.

Bull, W.B. and Branson, M.T. 1998. Lichen dating of earthquake-generated regional rock fall events, Southern Alps, New Zealand. Geological Society of America Bulletin, 110: 60-84.

Caine, N. 1980. The rainfall intensity: duration control of shallow landslides and debris flows. Geografiska Annaler, Series A, Physcial Geography, 62: 23-27.

Cannon, S.H., Bigio, E.R., and Mine, E. 2001. A process of fire-related debris flow initiation, Cerro Grande fire, New Mexico. Hydrological Processes, 15: 3011-3023.

Cannon, S.H., Gartner, J.E., Holland-Sears, A., Thurston, B.M., Gleason, J.A. 2003. Debris-flow response of basins burned by the 2002 Coal Seam and Missionary Ridge fires, Colorado. In: Boyer, D.D., Santi, P.M., and Rogers, E.P. (eds.), Engineering Geology in Colorado – Contributions, Trends, and Case Histories, Association of Engineering Geologists Special Publication, 14, 31 pp.

Cannon, S.H., Gartner, J.E., Wilson, R.C., Bowers, J.C. and Laber, J.L. 2008. Storm rainfall conditions for floods and debris flows from recently burned areas in southwestern Colorado and southern California. Geomorphology, 96: 250-269.

Carrara, P.E. 1987. Holocene and latest Pleistocene glacial chronology, Glacier National Park, Montana. Canadian Journal of Earth Sciences, 24: 387-395.

Cayan, D.R., Dettinger, M.D., Diaz, H.F., and Graham, N.E. 1998. Decadal variability of precipitation over western North America. Journal of Climate, 11: 3148-3166.

Cenderelli, D. and Kite, J.S. 1998. Geomorphic effects of large debris flows on channel morphology at North Fork Mountain, eastern West Virginia, USA. Earth Surface Processes and Landforms, 23: 1-19.

Changnon, D., McKee, T.B., and Doesken, N.J. 1993. Annual snow-pack patterns across the Rockies: Long-term trends and associated 500-mb synoptic patterns. Montana Weather Review, 121: 633-647.

Church, M. 1983. Pattern of instability in a wandering gravel bed channel. *In* Modern and Ancient Fluvial Systems, J.D. Collinson and J. Lewin (eds.). International Association of Sedimentologists Special Paper 6, pp. 169-180.

Church, M. and Ryder, J.M. 1972. Paraglacial sedimentation: A consideration of fluvial processes conditioned by glaciation. Geological Society of America Bulletin, 83: 3059-3072.

Church, M. and Slaymaker, O. 1989. Disequilibrium of Holocene sediment yield in glaciated British Columbia. Nature, 337: 452-454.

Clague, J.J. and Evans, S.G. 1993. Historic catastrophic retreat of Grand Pacific and Melbern Glaciers, St. Elias Mountains: An analogue for late Pleistocene decay of the Cordilleran Ice Sheet? Journal of Glaciology, 39: 619-624.

Clague, J.J. and Evans, S.G. 1994. Formation and failure of natural dams in the Canadian Cordillera. Geological Survey of Canada Bulletin 464, 35 pp.

Clague, J.J., Evans, S.G., and Blown, I.G. 1985. A debris flow triggered by the breaching of a moraine dammed lake, Klattasine Creek, British Columbia. Canadian Journal of Earth Sciences, 22: 1492-1502.

Costa, J.E. 1984. The physical geomorphology of debris flows. In Developments and Applications of Geomorphology, J.E. Costa and P.J. Fleisher (eds.). Springer-Verlag, Berlin, pp. 268-317.

Costa, J.E. 1988. Rheologic, geomorphic, and sedimentologic differentiation of water flood, hyperconcentrated flows, and debris flows. *In* Flood Geomorphology, V.R. Baker, R.C. Kochel and P.C. Patton (eds.). John Wiley, New York, pp. 113-122.

Crowley, J.K., Hubbard, B.E., and Mars, J.C. 2003. Analysis of potential debris flow source areas on Mount Shasta, California, by using airborne and satellite remote sensing data. Remote Sensing of Environment, 87: 345-358.

Cu, P. 1999. Impact of debris flow on river channels in the upper reaches of the Yangtze River. International Journal of Sediment Research, 14: 201-203.

Davis J.L. and Annan A.P. 1986. High-resolution sounding using ground probing radar. Geoscience Canada 13: 205–208.

Davis, J.L. and Annan, A.P. 1989. Ground-penetrating radar for high resolution mapping of soil and rock stratigraphy. Geophysical Prospecting 37: 531–551.

De Paoli, L. and Flowers, G.E.. 2009. Dynamics of a small surge-type glacier using one-dimensional geophysical inversion. Journal of Glaciology, 55: 1101-1112.

Denton, G.H. and Karlen, W. 1977. Holocene glacial and tree-line variations in the White River Valley and Skolai Pass, Alaska and Yukon Territory. Quaternary Research, 7: 63-111.

Denton, G.H. and Stuiver, M. 1966. Neoglacial chronology, northeaster St. Elias Mountains, Canada. American Journal of Science, 264: 577-599.

Denton, G.H. and Stuiver, M. 1967. Late Pleistocene glacial stratigraphy and chronology, northeastern St. Elias Mountains, Yukon Territory, Canada. Geological Society of America Bulletin, 78: 485-510.

Dettinger, M.D. and Cayan, D.R. 1995. Large-scale atmospheric forcing of recent trends toward early snowmelt runoff in California. Journal of Climate, 8: 606-623.

Dettinger, M.D. and Schaeffer, D.S. 1995. Decade-scale hydroclimatic forcing of ground-water levels in the central Great Basin, eastern Nevada. Proceedings of the American Water Resources Association Annual International Symposium, Herndon, Virginia, 1995: 195-204.

Duford, J.M. and Osborn, G.D. 1978. Holocene and latest Pleistocene cirque glaciations in the Shuswap Highland, British Columbia. Canadian Journal of Earth Sciences, 15: 865-873.

Dyke, A.S. 1990. A lichenometric study of Holocene rock glaciers and Neoglacial moraines, Frances Lake map area, southeastern Yukon Territory and Northwest Territories. Geological Survey of Canada Bulletin 394, 33 pp.

Eaton, L.S. 1999. Debris Flows and Landscape Evolution in the Upper Rapidan Basin, Blue Ridge Mountains, Virginia. Ph.D. thesis, University of Virginia, Charlottesville, VA, 154 pp.

Egginton, V. 2005. Historical Climate Variability from the Instrumental Record in Northern Brititsh Columbia and Its Influence on Slope Stability. M.Sc. thesis, Simon Fraser University, Burnaby, BC, 147 pp.

Ely, L.L., Enzel, Y., and Cayan, D.R. 1994. Anomalous North Pacific atmospheric circulation and large winter floods in the south-western United States. Journal of Climate, 7: 977-987.

Environment Canada. 2009. National Climate Data and Information Archive. http://climate.weatheroffice.gc.ca/welcome_e.html

Evans, S.G. 1987. The breaching of moraine-dammed lakes in the southern Canadian Cordillera. Proceedings, International Symposium on Engineering Geological Environment in Mountainous Areas, 2: 141-150.

Evans, S.G. and Clague, J.J. 1988. Catastrophic rock avalanches in glacial environments; in Landslides. Proceedings, 5th International Symposium on Landslides, 2: 1153-1158.

Evans, S.G. and Clague, J.J. 1993. Glacier-related hazards and climatic change. *In* The World at Risk: Natural Hazards and Climatic Change, R. Bras (ed.). American Institute of Physics Conference Proceedings, 277: 48-60.

Evans, S.G. and Clague, J.J. 1994. Recent climatic change and catastrophic geomorphic processes in mountain environments. Geomorphology, 10: 107-128.

Evans, S.G. and Clague, J.J. 1997. The impacts of climate change on catastrophic geomorphic processes in the mountains of British Columbia, Yukon and Alberta. *In* Proceedings of Responding to Global Climate Change in British Columbia and Yukon, Vancouver, BC, 27-28 February, 1997. BC Ministry of Environment, Lands and Parks and Environment Canada, pp. 7-1 – 7-13.

Fagan, B.M. 2001. The Little Ice Age: How Climate Made History, 1300-1850. Basic Books, New York, 272 pp.

Ferguson, A.J. 1978. Late Quaternary Geology of the Upper Elk Valley, British Columbia. M.Sc. thesis, University of Calgary, Calgary, AB, 118 pp.

Fischer, L., Kääb, A., Huggel, C., and Noetsli, J. 2006. Geology, glacier retreat and permafrost degradation as controlling factors of slope instabilities in a high-mountain rock wall: the Monte Rosa east face. Natural Hazards and Earth System Sciences, 6: 761-772.

Fisher, T.G., Jol, H.M., and Smith D.G. 1995. Ground-penetrating radar used to assess aggregate in catastrophic flood deposits, northeast Alberta, Canada. Canadian Geotechnical Journal 32: 871–879.

Frappé-Sénéclauze, T.-P. and Clarke, G.K.C.. 2007. Slow surge of Trapridge Glacier, Yukon Territory, Canada. Journal of Geophysical Research, 112: F03S32

Frey, H., Haeberli, W., Linsbauer, A., Huggel, C., and Paul, F. 2010. A multi-level strategy for anticipating future glacier lake formation and associated hazard potentials. Natural Hazards and Earth System Sciences, 10: 339-352.

Fulton, R.J. 1971. Radiocarbon Geochronology of Southern British Columbia. Geological Survey of Canada, Paper 71-37, 28 pp.

Furgal, C. and Prowse, T.D. 2008. Northern Canada. *In* From Impacts to Adaptation: Canada in a Changing Climate 2007, D.S. Lemmen, F.J. Warren, J. Lacroix, and E. Bush (eds.). Government of Canada, Ottawa, ON, pp. 57-118.

Gardner, J.S. and Jones, N.K. 1985. Evidence for a Neoglacial advance of the Boundary Glacier, Banff National Park, Alberta. Canadian Journal of Earth Sciences, 22: 1753-1755.

Gardner, J.S., Smith, D.J., and Desloges, J.R. 1983. The Dynamic Geomorphology of the Mt. Rae area: A High Mountain Region in Southwestern

Alberta. University of Waterloo, Department of Geography, Publication Series, No. 19, 237 pp.

Grove, J.M. 1988. The Little Ice Age. Methuen, London, 500 pp.

Grove, J.M. and Switsur, R. 1994. Glacial geological evidence for the Medieval Warm Period. Climatic Change, 30: 143-171.

Hare, P.G., Greer, S., Gotthardt, R., Farnell, R., Bowyer, V., Schweger, C., and Strand, D. 2004. Ethnographic and archaeological investigations of alpine ice patches in southwest Yukon, Canada. Arctic, 57: 260-272.

Hart, C.J.R. and Radloff, J.K. 1990. Geology of the Whitehorse, Alligator Lake, Fenwick Creek, Carcross and Part of Robinson Map Areas (105D/11, 6, 3, 2 and 7). Indian and Northern Affairs Canada, Yukon Region, Open File 1990-4, 113 pp.

Heusser, C.J. 1956. Postglacial environments in the Canadian Rocky Mountains. Ecological Monographs, 26: 253-302.

Huggel, C., Kääb, A., Haeberli, W., Teysseire, P., and Paul, F. 2002. Remote sensing based assessment of hazards from glacier lake outbursts: a case study in the Swiss Alps. Canadian Geotechnical Journal, 39: 316-330.

Huggel, C., Kääb, A. and Schneider, J.-F. 2010a. Climate and geomorphic risks in high mountain environments. EOS, Transactions, American Geophysical Union, 91: 103.

Huggel, C., Salzmann, S., Allen, J., Caplon-Auerbach, L., Fischer, W., Haeberli, C., Larson, D., and Wessels, R. 2010b. Recent and future warm extreme events and high-mountain slope stability. Philosophical Transactions of the Royal Society A, 368: 2435-2459.

Hupp, C.R. 1984. Dendrogeomorphic evidence of debris flow frequency and magnitude at Mount Shasta, California. Environmental Geology and Water Science, 6: 21-28.

Innes, J.L. 1983. Lichenometric dating of debris flow activity in the Scottish Highlands. Earth Surface Processes and Landforms, 8: 579-588.

Innes, J.L. 1985. Lichenometry. Progress in Physical Geography, 9: 187-254.

Intergovernmental Panel on Climate Change (IPCC). 2007. Climate Change 2007: Impacts, Adaptation and Vulnerability. Contribution of Working Group II to the Fourth Assessment Report of the Intergovernmental Panel on Climate Change. Cambridge University Press, Cambridge, UK, 976 pp.

Iverson, N.R. 1997. The physics of debris flows. Reviews of Geophysics, 35: 245-296.

Jakob, M., Anderson, D., Fuller, T., Hungr, O., and Ayotte, D. 2000. An unusually large debris flow at Hummingbird Creek, Mara Lake, British Columbia. Canadian Geotechnical Journal, 37: 1109-1125.

Johnson, A. 1970. Physical Processes in Geology. Freeman, Cooper and Co., San Francisco, CA, 577 pp.

Johnson, P.G. 1992. Stagnant glacier ice, St. Elias Mountains, Yukon. Geografiska Annaler, Series A, Physical Geography, 74: 13-19.

Johnson, A.M. and Rodine, J.R. 1984. Debris flow. *In* Slope instability, D. Brunsden and D.B. Prior (eds.). John Wiley, New York, pp. 257-361.

Joint Institute for the Study of the Atmosphere and Oceans (JISAO). 2009. PDO Index Monthly Values: January 1900-Present, http://jisao.washington.edu/pdo/PDO.latest

Jol, H.M., Smith, D.G., and Meyers R.A. 1996. Digital ground-penetrating radar (GPR): A new geophysical tool for coastal barrier research (examples from the Atlantic, Gulf and Pacific coasts, U.S.A.). Journal of Coastal Research 12: 960–968.

Jordan, P. 1987. Impacts of mass movement events on rivers in the southern Coast Mountains, British Columbia. *In* The Impact of Climate Change on Catastrophic Geomorphic Processes: Summary Report. Environment Canada, Inland Waters Directorate, Water Resources Branch, Report IWD-HQ-WRB-SS-87-3, 62 pp.

Kaufman, D.S., Ager, T.A., Anderson, N.J., Anderson, P.M., Andrews, J.T., Bartlein, P.J., Brubaker, L.B., Coats, L.L., Cwynar, L.C., Duvall, M.L., Dyke, A.S., Edwards, M.E., Eisner, W.R., Gajewski, K., Geirsdóttir, A., Hu, F.S., Jennings, A.E., Kaplan. M.R., Kerwin, M.W., Lozhkin, A.V., MacDonald, G.M., Miller, G.H., Mock, C.J., Oswald, W.W., Otto-Bliesner, B.L., Porinchu, D.F., Rühland, K., Smol, J.P., Steig, E.J., and Wolfe, B.B. 2004. Holocene thermal maximum in the western Arctic (0-180^{o} W). Quaternary Science Reviews, 23: 529-560.

Keiler, M., Knight, J., and Harrison, S. 2010. Climate change and geomorphological hazards in the eastern European Alps. Philosophical Transactions of the Royal Society A, 368: 2461-2479.

Kniveton, D.R., DeGraff, P.J., Granica, K., and Hardy, R.J. 2000. The development of a remote sensing based technique to predict debris flow

triggering conditions in the French Alps. International Journal of Remote Sensing, 21: 419-434.

Koch, J., Osborn, G.D., and Clague, J.J. 2007. Pre-'Little Ice Age' glacier fluctuations in Garibaldi Provincial Park, Coast Mountains, British Columbia, Canada. The Holocene, 17: 1069-1078.

Kochel, R.C., Eaton, L.S., Daniels, N., and Howard, A.D. 1997. Impact of the 1995 debris flow on geomorphic evolution of Blue Ridge debris fans, Madison County, Virginia. Geological Society of America, Abstracts with Program, 29(4): 410.

Lambert, M.B. 1974. The Bennett Lake Cauldron Subsidence Complex, British Columbia and Yukon Territory. Geological Survey of Canada, Bulletin 227, 213 pp.

Langbein, W.B. and Slack, J.R. 1982. Yearly Variation in Runoff and Frequency of Dry Years for the Conterminous United States, 1911-79. U.S. Geological Survey, Open File Report 82-571, 85 pp.

Lawson, D.E. 1979. Sedimentological Analysis of the Western Terminus Region of the Matanuska Glacier, Alaska. U.S. Army Corps of Engineers, Cold regions Research and Engineering Laboratory, Report 79-9, 132 pp.

Lemmen, D.S., Warren, F.J., Lacroix, J., and Bush, E. (eds.). 2008. From Impacts to Adaptation: Canada in a Changing Climate 2007. Government of Canada, Ottawa, ON, 448 pp.

Leonard, E.M. 1986. Use of lacustrine sedimentary sequences as indicators of Holocene glacial history, Banff National Park, Alberta, Canada. Quaternary Research, 26: 218-231.

Leonard, E.M. 1997. The relationship between glacial activity and sediment production: evidence from a 4450-year varve record of neoglacial sedimentation in Hector Lake, Alberta, Canada. Journal of Paleolimnology, 17: 319-330.

Leonard, E.M. and Reasoner, M.A. 1999. A continuous Holocene glacial record inferred from proglacial lake sediment in Banff National Park, Alberta, Canada. Quaternary Research, 51: 1-13.

Lowdon, J.A. and Blake, W., Jr. 1968. Geological Survey of Canada radiocarbon dates VII. Radiocarbon, 10: 207-245.

Lowdon, J.A. and Blake, W., Jr. 1973. Radiocarbon Dates XIII. Geological Survey of Canada, Paper 73-7, 61 pp.

Lowdon, J.A. and Blake, W., Jr. 1975. Radiocarbon Dates XV. Geological Survey of Canada, Paper 75-7, 32 pp.

Lowdon, J.A., Robertson, I.M. and Blake, W., Jr. 1971. Geological Survey of Canada Radiocarbon Dates XI. Geological Survey of Canada, Paper 71-7, 69 pp.

Luckman, B.H. 1986. Reconstruction of Little Ice Age events in the Canadian Rocky Mountains. Géographie physique et Quaternaire, 40: 17-28.

Luckman, B.H. 2000. The Little Ice Age in the Canadian Rockies. Geomorphology, 32: 357-384.

Luckman, B.H. and Osborn, G.D. 1979. Holocene glacier fluctuations in the middle of the Canadian Rockies. Quaternary Research, 11: 52-77.

Macheret, Y.Y., Cherkasov, P.A., and Bobrova, L.I. 1988. The thickness and volume of the Dzhungarsky Alatau glaciers from the data of airborne radio echo sounding (in Russian). Data of Glacial Studies, 62: 59-71.

Major, J.J. and Iverson, R.M. 1999. Debris-flow deposition effects of pore-fluid pressure and friction concentrated at flow margins. Geological Society of America Bulletin, 111: 1424-1434.

Mantua, N.J., Hare, S.R., Zhang, Y., Wallace, J.M., and Francis, R.C. 1997. A Pacific interdecadal climate oscillation with impacts on salmon production. Bulletin of the American Meteorological Society, 78:1069-1079.

Marcus, M.G. and Ragle, R.H. 1970. Snow accumulation in the Icefield Ranges, St. Elias Mountains, Yukon. Arctic and Alpine Research, 2: 277-292.

Mathewes, R.W. 1985. Paleobotanical evidence for climatic change in southern British Columbia during late-glacial and Holocene time. *In* Climatic Change in Canada 5, Critical Periods in the Quaternary Climatic History of Northern North America, C.R. Harington (ed.). National Museums of Canada, National Museum of Natural Sciences, Syllogeus Series, 55: 397-422.

Mayewski, P.A., Meeker, L.D., Twickler, M.S., Whitlow, S., Yang, Q., Lyons, W.B., and Prentice, M. 1997. Major features and forcing of high-latitude Northern Hemisphere atmospheric circulation using a 11,000-year-long glaciochemical series. Journal of Geophysical Research, 102: 26345-26365.

MacDonald, B.W.D. 1990. Geology and Genesis of the Mount Skukum Epithermal Gold-silver Deposits, Southwestern Yukon Territory (105D/3, 6). Indian and Northern Affairs Canada, Exploration and Geological Services Division, Bulletin 2, 100 pp.

McCarthy, D. 2003. Habitat selection and ecology of *Xanthoria elegans* (Link) Th. Fr. in glacier forefields: implications for lichenometry. Journal of Biogeography, 24: 363-373.

Menounos, B., Koch, J., Osborn, G., Clague, J.J., and Mazzucchi, D. 2004. Early Holocene glacier advance, southern Coast Mountains, British Columbia, Canada. Quaternary Science Reviews, 23: 1543-1550.

Moore, G.W.K., Alverson, K., and Holdsworth, G. 2003. The impact that elevation has on the ENSO signal in precipitation records from the Gulf of Alaska region. Climate Change, 59: 101-121.

National Oceanic and Atmospheric Administration (NOAA). 2010. State of the Climate Global Analysis Annual 2009. http://www.ncdc.noaa.gov/sotc/?report=global&year=2009&month=13&submitted=Get+Report

National Oceanic and Atmospheric Administration Climate Prediction Centre (NOAA CPC). 2009. Changes to the Oceanic Nino Index (ONI) http://www.cpc.ncep.noaa.gov/products/analysis_monitoring/ensostuff/ensoyears.shtml

Osborn, G. 1985. Holocene tephrostratigraphy and glacial fluctuations in Waterton Lakes and Glacier National Parks, Alberta and Montana. Canadian Journal of Earth Sciences, 22: 1093-1101.

Osborn, G. 1986. Lateral moraine stratigraphy and Neoglacial history of Bugaboo Glacier, British Columbia. Quaternary Research, 26: 171-178.

Osborn, G. and Karlstrom, E.T. 1986. Holocene fluctuations of the Bugaboo Glacier, British Columbia, inferred from superposed tills and paleosols. Geological Society of America, Abstracts with Programs, 18: 712.

Osborn, G. and Luckman, B.H. 1988. Holocene glacier fluctuations in the Canadian Cordillera (Alberta and British Columbia). Quaternary Science Reviews, 7: 115-128.

Oxford Radiocarbon Accelerator Unit (ORAU), 2008. OxCal 4, http://c14.arch.ox.ac.uk/embed.php?File=oxcal.html

Paterson, W.S.B. 1972. Laurentide Ice Sheet: Estimated volumes during Late Wisconsin. Reviews of Geophysics, 10: 885-917.

Pellatt, M.G. and Mathewes, R.W. 1994. Paleoecology of post-glacial treeline fluctuations on the Queen Charlotte Islands, Canada. Ecoscience, 1: 71-81.

Pierson, T.C. 1980. Erosion and deposition by debris flows at Mount Thomas, New Zealand. Earth Surface Processes and Landforms, 5: 227-247.

Pierson, T.C. and Costa, J.E. 1987. A rheologic classification of subaerial sediment-water flows. *In* Debris Flows/Avalanches: Process, Recognition, and Mitigation, J.E. Costa and G.F. Wieczorek (eds.). Geological Society of America, Reviews in Engineering Geology, 7: 1-12.

Porter, S.C. and Denton, G.H. 1967. Chronology of neoglaciation in the North American Cordillera. American Journal of Science, 265: 177-210.

Pride, M.J. 1985. Interlayered sedimentary and volcanic sequence of the Mount Skukum volcanic complex. *In* Yukon Exploration and Geology. Department of Indian and Northern Affairs, Yukon Region, Exploration and Geological Services Division, pp. 94-105.

Pride, M.J. and Clark, G.S. 1985. An Eocene Rb-Sr isochron for rhyolite plugs, Skukum area, Yukon Territory. Canadian Journal of Earth Sciences, 22: 1747-1753.

Ramage, J.M., McKenney, R.A., Thorson, B., Maltais, P., and Kopczynski, S.E. 2006. Relationship between passive microwave-derived snowmelt and surface-measured discharge, Wheaton River, Yukon Territory, Canada. Hydrological Processes, 20: 689-704.

Rampton, V. 1970. Neoglacial fluctuations of the Natazhat and Klutlan Glaciers, Yukon Territory, Canada. Canadian Journal of Earth Sciences, 7: 1236-1263.

Redmond, K.T. and Koch, R.W. 1991. Surface climate and stream-flow variability in the western United States and their relationship to large scale circulation indices. Water Resources Research, 27: 2381-2399.

Reyes, A.V., Luckman, B.H., Smith, D.J., Clague, J.J. and VanDorp, R.D. 2006. Tree-ring dates for the maximum Little Ice Age advance of Kaskawulsh Glacier, St. Elias Mountains, Canada. Arctic, 59: 14-20.

Rickenmann, D. and Zimmermann, M. 1993. The 1987 debris flows in Switzerland: Documentation and analysis. Geomorphology, 8:175-189.

Roos, M. 1991. A trend of decreasing snowmelt runoff in northern California. Proceedings, 59th Western Snow Conference, Juneau, AK, pp. 29-36.

Roos, M. 1994. Is the California drought over? Proceedings, 10th Annual Pacific Climate (PACLIM) Workshop, Pacific Grove, CA, pp. 123-128.

Ryder, J.M. and Thomson, B. 1986. Neoglaciation in the southern Coast Mountains of British Columbia: Chronology prior to the late-Neoglacial maximum. Canadian Journal of Earth Sciences, 23: 237-238.

Sasaki, Y., Fujii, A., and Asai, K. 2000. Soil creep processes and its role in debris slide generation; field measurements on the north side of Tsukuba Mountain in Japan. Engineering Geology, 56: 163-183.

Scott, K.M. 1988. Origins, Behaviour, and Sedimentology of Lahars and Lahar-runout Flows in the Toutle-Cowlitz River System. U.S. Geological Survey, Professional Paper 1447-A, 74 pp.

Sensors & Software. 2003. EKKO_View Enhanced and EKKO_View Deluxe user's guide. Sensors & Software Ltd., Mississauga, ON, 132 pp.

Sensors & Software Ltd. 1994. PulseEKKO 100 User's Guide, Version 1.1, Technical Manual 25. Sensors & Software Ltd., Mississauga, ON, 130 pp.

Shabbar, A. and Khandekar, M. 1996. The impact of El Nino-Southern Oscillation on the temperature field over Canada. Atmosphere and Ocean, 34: 401-416.

Sharp, R.P. and Noble, L.H. 1953. Mudflow of 1941 at Wrightwood, southern California. Geological Society of America Bulletin, 64: 547-560.

Shimokawa, E. and Jitousono, T. 1998. A study of the change from landslide to debris flow at Harihara, Southern Kyu-sh. Journal of Natural Disaster Science, 20: 75-81.

Smith, C.A.S., Meikle, J.C., and Roots, C.F. (eds.). 2004. Ecoregions of the Yukon Territory: Biophysical Properties of Yukon Landscapes. Agriculture and Agri-Food Canada, PARC Technical Bulletin No. 04-01, 313 pp.

Spotila, J.A., Buscher, J.T., Meigs, A.J. and Reiners, P.W. 2004. Long-term glacial erosion of active mountain belts: example of the Chugach-St. Elias Range, Alaska, 32: 501-504.

Stoffel, M. and Bollschweiler, M. 2009. Tree-ring reconstruction of past debris flows based on a small number of samples – Possibilities and limitations. Landslides, 6(3): 225-230.

Strunk, H. 1997. Dating of geomorphological processes using dendrogeomorphological methods. Catena, 31: 137–151.

Stuiver, M., Deevey, E.S., and Gralenski, L.J. 1960. Yale natural radiocarbon measurements V. American Journal of Science, Radiocarbon Supplement, 2: 49-61.

Taylor, B. 1998. Effect of El Niño Southern Oscillation (ENSO) on British Columbia and Yukon Winter Weather. Environment Canada, Pacific and Yukon Region, Aquatic and Atmospheric Science Division, Vancouver, BC, 120 pp.

Taylor, K.C., Mayewski, P.A., Alley, R.B., Brook, E.J., Gow, A.J., Grootes, P.M., Meese, D.A., Saltzman, E.S., Severinghaus, J.P., Twickler, M.S., White, J.W.C., Whitlow, S., and Zielinski, G.A. 1997. The Holocene-Younger Dryas transition recorded at Summit, Greenland. Science, 278: 825-827.

Thurber Engineering. 1994. Mount Stephen Snow/Debris Defences; An Assessment of Current Conditions and Future Debris Flow Potential. Thurber Engineering Ltd., report to CP Rail and Parks Canada.

VanDine, D.F. 1985. Debris flows and debris torrents in the southern Canadian Cordillera. Canadian Geotechnical Journal, 22: 44-68.

Wahl, K.L. 1992. Evaluation of trends in runoff in the western United States: Managing water resources during global change. Proceedings, 28th Annual Conference and Symposium, American Water Resources Association, Reno, NV, pp. 701-710.

Water Survey of Canada. 2009. Archived hydrometric data. http://www.wsc.ec.gc.ca/hydat/H2O/index_e.cfm?cname=main_e.cfm.

Watson, R.T., Zinyowera, M.C., and Moss, R.H. (eds.). 1996. Climate Change 1995. Impacts, Adaptations and Mitigation of Climate Change: Scientific-Technical Analyses. Contribution of Working Group ll to the Second Assessment Report of the Intergovernmental Panel on Climate Change. Cambridge University Press, Cambridge, 879 pp.

Webb, J.A. and Fielding, C.R. 1999. Debris flow and sheet flood fans on the northern Prince Charles Mountains, East Antarctica. *In* Varieties of Fluvial Form, A.J. Miller and A. Gupta (eds.). John Wiley, New York, pp. 317-341.

Webb, R.H. and Betancourt, J.L. 1990. Climatic Variability and Flood Frequency of the Santa Cruz River, Pima County, Arizona. U.S. Geological Survey, Open-File Report 90-553, 69 pp.

Westgate, J.A. 1977. Identification and signature of late Holocene tephra from Otter Creek, southern British Columbia. Canadian Journal of Earth Sciences, 14: 2593-2600

Wheeler, J.O. 1964. Selkirk and Monashee Mountains: Recent glacier fluctuations. Canadian Geophysical Bulletin, 17: 126-127.

Zicheng, K. and Jing, L. 1987. Erosion processes and effects of debris flow. *In* Erosion and Sedimentation of the Pacific Rim, R.L. Beschta *et al.* (eds.). International Association of Hydrological Sciences Publication, 165: 233-242.

Zimmmerman, M. 1990. Debris flows 1987 in Switzerland: geomorphology and meteorological aspects. International Association of Hydrological Sciences Publication, 194: 387-393.

Zimmerman, M. and Haeberli, W. 1992. Climatic change and debris flow activity in high mountain areas - a case study in the Swiss Alps. Catena Supplement 22: 59-72.

APPENDICES

Appendix 1: Sample lichen diameter histograms

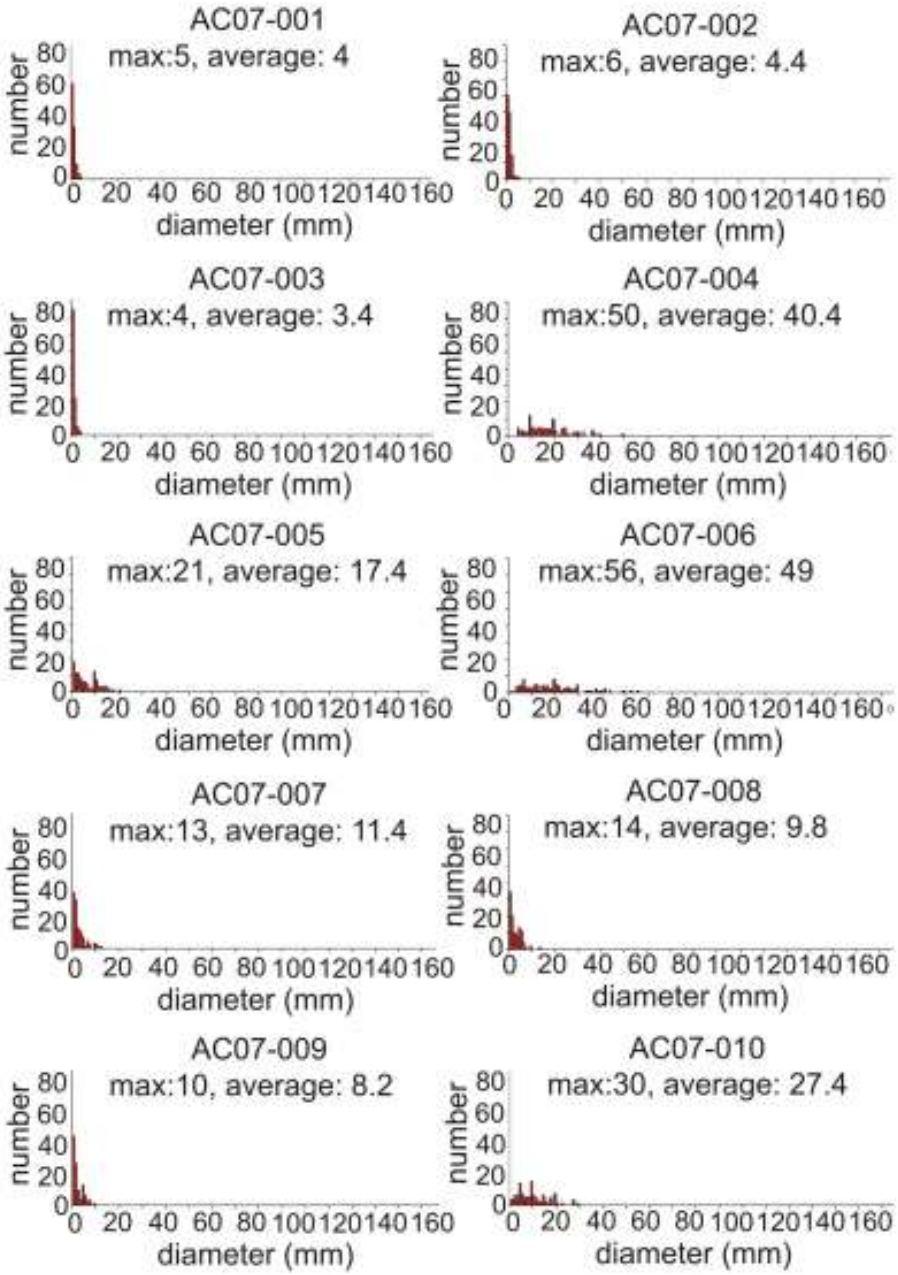

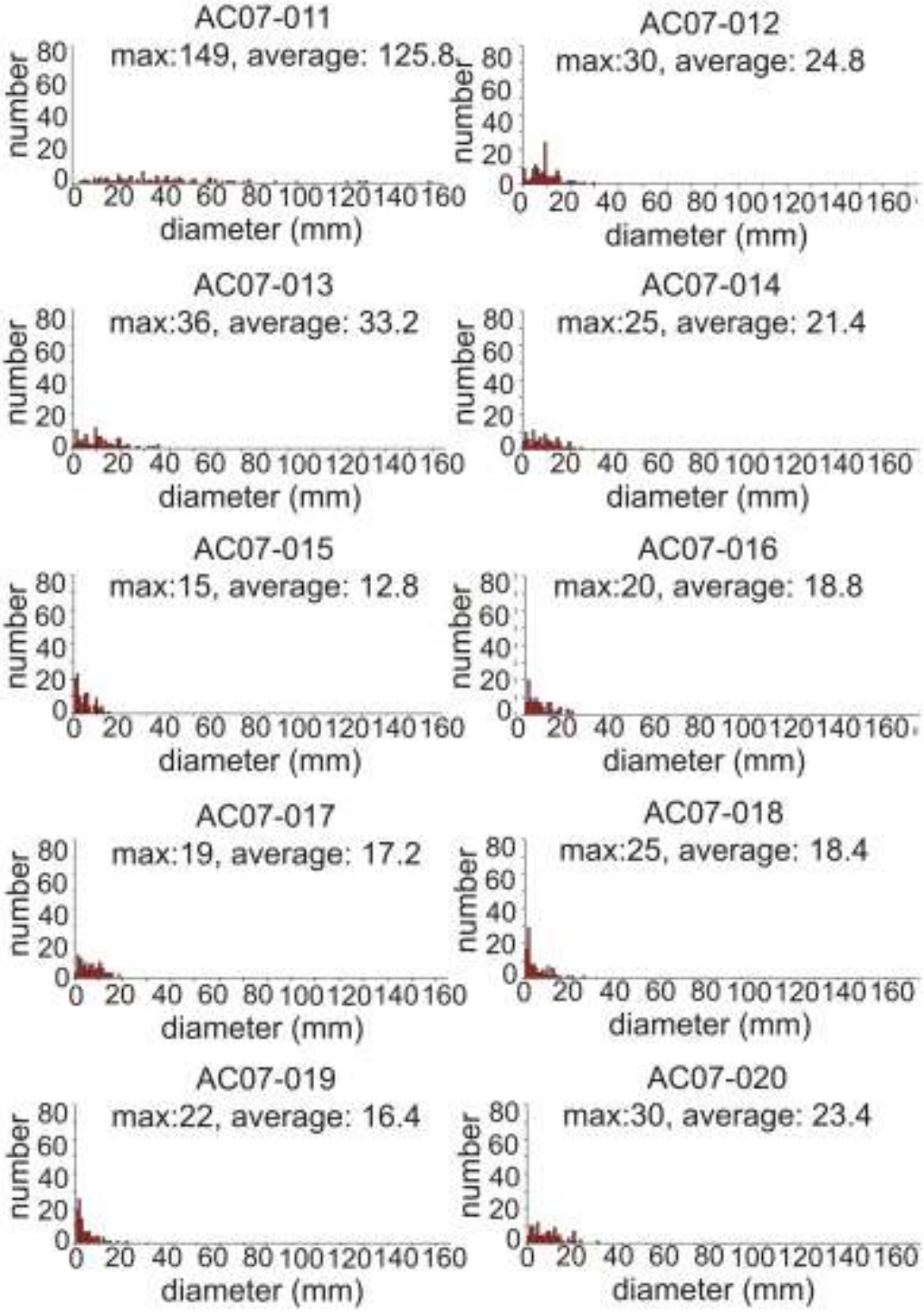
AC07-011
max:149, average: 125.8
AC07-012
max:30, average: 24.8
AC07-013
max:36, average: 33.2
AC07-014
max:25, average: 21.4
AC07-015
max:15, average: 12.8
AC07-016
max:20, average: 18.8
AC07-017
max:19, average: 17.2
AC07-018
max:25, average: 18.4
AC07-019
max:22, average: 16.4
AC07-020
max:30, average: 23.4
number
diameter (mm)
0 20 40 60 80 100 120 140 160
0 20 40 60 80

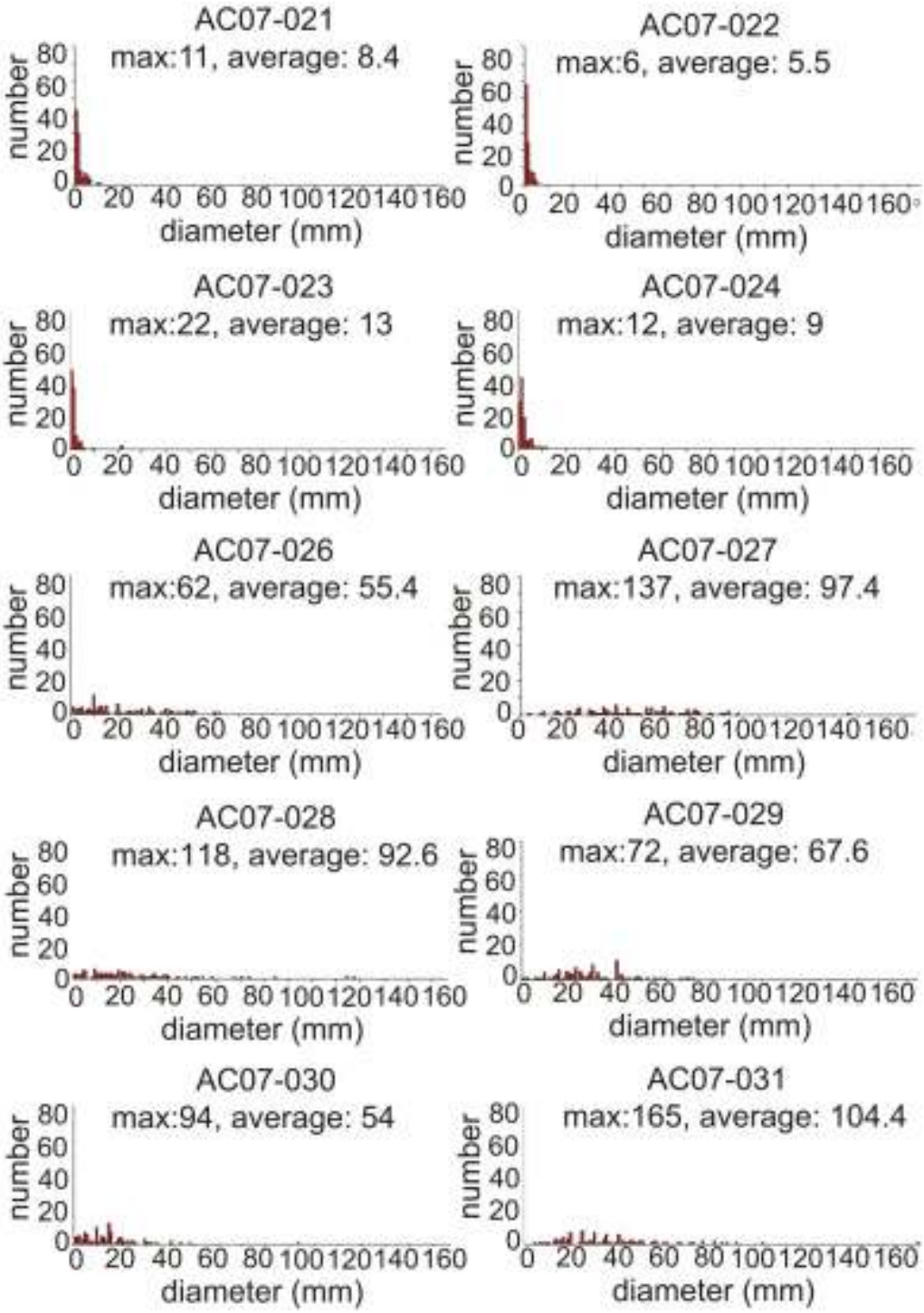
AC07-021
max:11, average: 8.4
AC07-022
max:6, average: 5.5
AC07-023
max:22, average: 13
AC07-024
max:12, average: 9
AC07-026
max:62, average: 55.4
AC07-027
max:137, average: 97.4
AC07-028
max:118, average: 92.6
AC07-029
max:72, average: 67.6
AC07-030
max:94, average: 54
AC07-031
max:165, average: 104.4
number
diameter (mm)
0 20 40 60 80 100 120 140 160
0 20 40 60 80

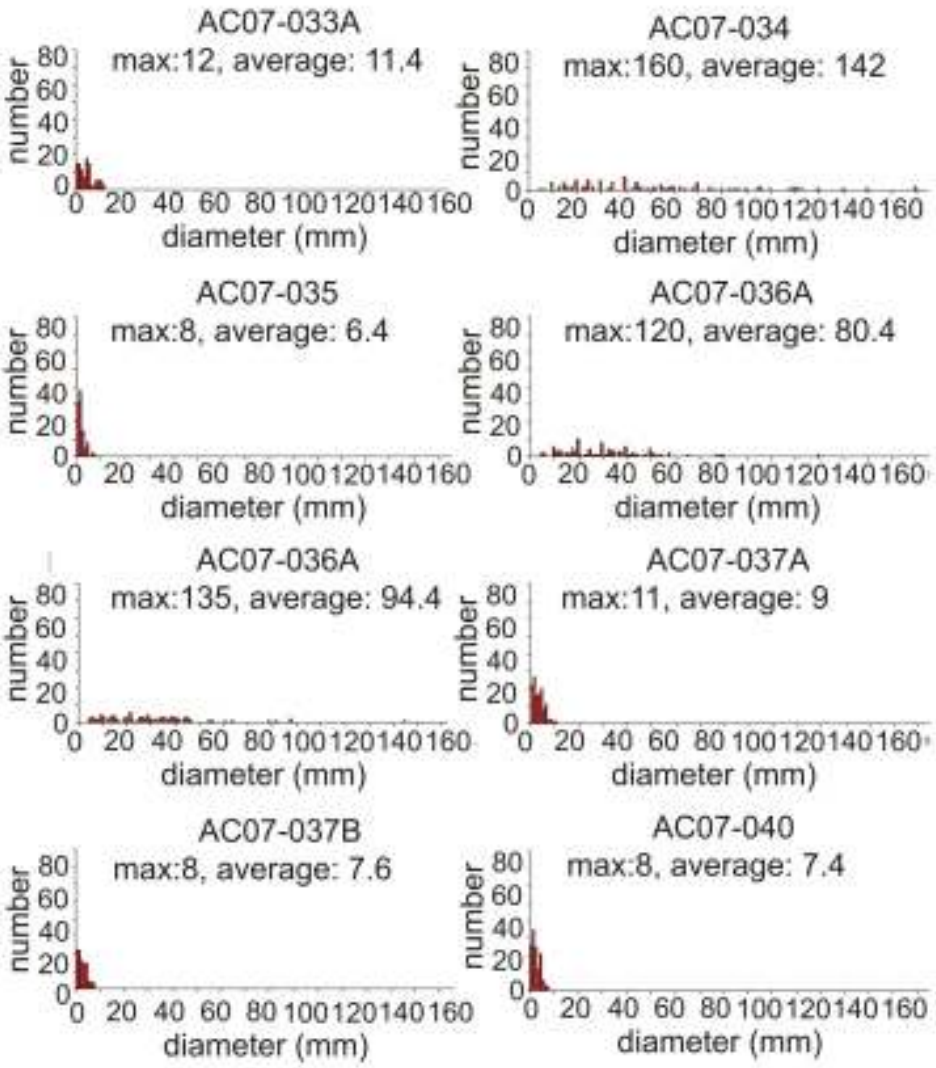
AC07-033A
max:12, average: 11.4
AC07-034
max:160, average: 142
AC07-035
max:8, average: 6.4
AC07-036A
max:120, average: 80.4
AC07-036A
max:135, average: 94.4
AC07-037A
max:11, average: 9
AC07-037B
max:8, average: 7.6
AC07-040
max:8, average: 7.4
number
diameter (mm)
0 20 40 60 80 100 120 140 160
0 20 40 60 80

Appendix 2: Sediment core logs

Core AC07-050 (Figure 52)

0-7 cm: brown to black, organic-rich silt and minor fine sand; gradational basal contact

7-12 cm: fine to medium sand; gradational basal contact

12-20.5 cm: oxidized coarse sand and gravel; subangular to subrounded clasts up to 3 cm; gradational basal contact

20.5-27 cm: grey, silty fine sand with minor oxidation; gradational basal contact

27-33 cm: grey-brown, fine to coarse sand; minor oxidation near the base of the unit; gradational basal contact

33.5-37 cm: grey, laminated, very fine sand; alternating oxidized and un-oxidized laminations; sharp basal contact

37-37.25 cm: black, organic-rich silt; sharp basal contact

37.25-48 cm: grey-brown, coarse to very coarse sand; minor oxidation; sharp basal contact

48-48.5 cm: grey-brown silt with thin black organic laminations near base of unit; sharp basal contact

48.5-51 cm: grey, fine to medium sand; sharp basal contact

51-56 cm: dark grey, very fine sand; undulatory sharp basal contact

56-67 cm: grey-brown, laminated, fine to coarse sand; undulatory sharp basal contact

67-69 cm: strongly oxidized, medium sand; gradational basal contact; oxidation is strongest in two undulatory laminae

69-71 cm: dark-grey, medium sand; undulatory gradational basal contact

71-73 cm: dark-grey, silty very fine sand; yellow laminations between 72 and 72.5 cm; sharp basal contact

73-82 cm: dark-grey to black, organic-rich silt with wood fragments, one of which yielded a radiocarbon age of 3310 ± 20 ^{14}C yrs BP; sharp basal contact

82-83 cm: dark-grey, medium sand; gradational basal contact

83-85 cm: dark-grey, massive, fine sand; gradational basal contact

85-90 cm: dark-grey, coarse sand; gradational basal contact

90-96 cm: dark-grey, thinly laminated silt; sharp basal contact

96-98 cm: black, organic-rich horizon with abundant wood fragments; sharp basal contact

98-115 cm: dark-grey, clayey silt with organic detritus between 103 and 108 cm; sharp basal contact

115-120.5 cm: black, organic-rich horizon with abundant wood fragments, one of which yielded a radiocarbon age of 3705 ± 20 ^{14}C yrs BP; sharp basal contact

120.5-123 cm: grey medium sand; sharp basal contact

123-126.5 cm: dark-grey, very fine sand; sharp basal contact; some organic detritus at 126-126.5 cm.

126.5-140 cm: very coarse sand; sharp basal contact

140-145.5 cm: dark-brown, organic-rich clayey-silt; needles dated at 3870 ± 15 ^{14}C yrs BP; sharp basal contact

145.5-148.5 cm: dark-grey, massive medium sand; gradational basal contact

148.5-149 cm: dark-brown, organic-rich medium sand; gradational basal contact

149-154 cm: grey, medium to coarse sand; gradational basal contact

154-161 cm: dark-grey, massive fine sand; patchy oxidation; sharp basal contact

161-165 cm: dark-grey to black, organic-rich, silty very fine sand; common plant detritus at 163-165 cm; sharp basal contact

165-169.5 cm: grey, silty very fine sand, becoming darker with depth; sharp basal contact

169.5-177 cm: dark brown, organic-rich horizon; needles dated at 3990 ± 15 ^{14}C yrs BP; gradational basal contact

177-182 cm: dark-grey silt with organic-rich laminations; sharp basal contact

182-186 cm: dark-grey medium sand; gradational basal contact

186-187 cm: dark-grey silt; sharp basal contact

187-188.5 cm: brown, organic-rich horizon becoming darker with depth; contains granitic granules; sharp basal contact

188.5-190.5 cm: brown-grey, medium to coarse sand; sharp basal contact

190.5-192 cm: dark-grey silt; sharp basal contact

192-193.5 cm: dark-brown, organic-rich horizon; needles dated at 4380 ± 20 ^{14}C yrs BP; gradational lower contact

193.5->197 cm: dark grey silt

Core AC07-051 (Figure 53)

0-16 cm: dark-brown, rooty, organic-rich peat and mud; gradational basal contact; the lowest 1 cm of the unit yielded a radiocarbon age of 850 ± 20 ^{14}C yrs BP from needles

16-28 cm: dark-grey medium sand with some roots intruding from the overlying unit; gradational basal contact

28-36 cm: dark-grey coarse sand; gradational basal contact

36-54 cm: dark-grey sand and gravel; gravel consists of subangular to subrounded granitic clasts up to 5 cm across; gradational basal contact

54-57 cm: brown coarse sand and gravel with a silt matrix; maximum clast size 1 cm; gradational basal contact

57-68 cm: brown-grey, fine to medium sand and gravel; maximum clast size 3 cm; gradational basal contact

68-74 cm: orange-brown, strongly oxidized, coarse sand; undulatory gradational basal contact

74-77 cm: grey, slightly oxidized, fine sand with minor granules; gradational basal contact

80-86 cm: red-brown, strongly oxidized, medium to coarse sand with minor pebbles up 1 cm; gradational basal contact

86-90 cm: orange-brown, oxidized, fine to medium sand; gradational basal contact

90-90.5 cm: dark brown silt with minor very fine sand; gradational basal contact

90.5-92 cm: grey fine sand; gradational basal contact

92-94.5 cm: oxidized coarse sand; pinches out within the core; wavy, sharp basal contact

94.5-104.5 cm: grey, well-sorted fine sand; minor oxidation; irregular laminations; sharp basal contact

104.5-105.5 cm: grey-brown, massive silt; gradational basal contact

105.5-109 cm: grey, very fine sand; irregular undulatory gradational basal contact

109-115 cm: organic-rich, silty very fine sand draped over the large clasts that define the layer below; needles yielded a radiocarbon age of 3640 ± 20 ^{14}C yrs BP

115-122 cm: very coarse sand and gravel; clasts are dominantly subrounded granitic rocks up to 7 cm in diameter; underlying sediments were lost when the PVC pipe broke on large clasts in this unit

Core AC07-052 (Figure 54)

0-4.5 cm: dark-brown, rooty silt; leaves at 3-4.5 cm returned a radiocarbon age of -1255 ± 20 ^{14}C yrs BP; sharp basal contact

4.5-20 cm: grey-brown, medium to coarse sand; gradational basal contact

20-28.5 cm: oxidized, orange-brown, medium to coarse sand and gravel; clasts are granitic and up to 1 cm across; gradational basal contact

28.5-38.5 cm: grey-brown, fining-upward, medium to coarse sand; gradational basal contact

38.5-41.5 cm: grey-brown, fining-upward, medium to coarse sand; sharp basal contact

41.5-45 cm: dark grey, massive fine sand; gradational basal contact

45-49.75 cm: orange-brown, oxidized, fine to medium sand; gradational basal contact

49.75-79 cm: orange-brown, oxidized, bedded, medium to coarse sand; sharp basal contact

79-97.5 cm: grey-brown, fine sand with plant detritus at 93 cm; sharp basal contact

97.5-111 cm: orange-brown, oxidized, very coarse, sand and gravel; clasts are granitic, subangular to subrounded, and up to 7 cm across; sharp basal contact

111-113.5 cm: dark-grey silty fine sand; gradational basal contact

113.5-116 cm: black, organic-rich silt with some peat laminae; a leaf retrieved from the unit returned a radiocarbon age of 2940 ± 15 ^{14}C yrs BP; sharp basal contact

116-125 cm: grey coarse sand; sharp basal contact

125-145 cm: dark-grey sandy silt with common plant detritus; sharp basal contact

145-147.5 cm: grey coarse sand; sharp basal contact

147.5-165.5 cm: dark-grey, silty sand with a thin lamina of plant detritus at 151 cm; sharp basal contact

165.5-167 cm: red-brown peat; needles from within the unit yielded a radiocarbon age of 3890 ± 20 ^{14}C yrs BP; sharp basal contact

167-189 cm: light- to dark-grey, laminated, silty fine sand; alternating organic-rich and organic-poor laminae 0.5-1 cm thick; sharp basal contact

189-196 cm: dark-brown peat and woody detritus; needles concentrated in the lower 5 cm of the unit yielded a radiocarbon age of 4095 ± 20 ^{14}C yrs BP; sharp basal contact

196->198.5 cm: dark-grey massive silt

Core AC07-053 (Figure 55)

0-5.5 cm: grey-brown silt with some organic detritus; gradational basal contact

5.5-16 cm: dark-grey, medium to coarse sand; gradational basal contact

16-28 cm: dark-grey massive silt; sharp basal contact

28-31 cm: coarse sand; gradational basal contact

31-31.5 cm: dark-grey, massive silt; sharp basal contact

31.5-34 cm: black peaty silt; a leaf from the unit yielded a radiocarbon age of 2880 ± 20 ^{14}C yrs BP; sharp basal contact

34-36.5 cm: dark-grey, massive, silty, very fine sand; sharp basal contact

36.5-44 cm: dark-grey, upward-coarsening, fine to coarse sand; sharp basal contact

44-45.5 cm: dark-grey massive silt; sharp basal contact

45.5-53.5 cm: dark-grey, upward-coarsening, medium to coarse sand; sharp basal contact

53.5-56.5 cm: dark-grey massive silt; sharp basal contact

56.5-67 cm: dark-grey, medium to coarse sand with scattered plant detritus; gradational basal contact

67-69.5 cm: dark-grey, silty very fine sand with a sharp basal contact

69.5-75.5 cm: grey medium sand with scattered plant detritus; sharp basal contact

75.5-80.5 cm: dark-grey, laminated, very fine sand with some plant detritus; sharp basal contact

80.5-86 cm: dark-brown peat; leaves from within the unit yielded a radiocarbon age of 3095 ± 15 ^{14}C yrs BP; sharp basal contact

86-95 cm: poorly sorted coarse sand and gravel; subangular to subrounded clasts; gradational basal contact

95-101 cm: dark-grey, medium sand; sharp basal contact

101-101.5 cm: dark-brown peat; sharp basal contact

101.5-102.5 cm: dark-grey, massive, silty, very fine sand; sharp basal contact

102.5-112 cm: grey fine to medium sand with scattered plant detritus; gradational basal contact

112-113 cm: massive, dark grey, silty fine sand with a sharp basal contact

113-120.5 cm: grey, very coarse sand with subrounded granitic clasts up to 2 cm across; gradational basal contact

120.5-130.5 cm: dark-grey, weakly laminated, sandy silt with common plant detritus; sharp basal contact

130.5-132 cm: dark-brown peat; sharp basal contact

132-139 cm: dark-grey silt with fine sand laminations approximately 0.25 cm thick and scattered plant detritus including wood; sharp basal contact

139-142 cm: grey, medium to coarse sand; sharp basal contact; unit pinches out within the core

142-144 cm: dark-grey, very fine sand; sharp basal contact

144-145 cm: black silty peat; sharp basal contact

145-151 cm: grey, medium to very coarse sand; sharp basal contact

151-154 cm: grey-brown silt; sharp basal contact

154-160 cm: dark-brown peat; needles from within the unit returned a radiocarbon age of 3760 ± 15 ^{14}C yrs BP; sharp lower contact

160-162 cm: dark-brown massive silt; gradational basal contact

162-165 cm: black silty peat; sharp basal contact

165-180 cm: dark-grey, laminated, very fine sand; sharp basal contact

180-181 cm: dark-brown peat; leaves from within the unit yielded a radiocarbon age of 4010 ± 20 ^{14}C yrs BP; sharp basal contact

181-190.5 cm: dark-grey, laminated silt; plant detritus at 182 cm; gradational basal contact

190.5-200 cm: dark-grey, thinly laminated, fine sand with abundant plant detritus at base of unit; sharp basal contact

200->212 cm: grey, massive, fine sand

Core AC07-054 (Figure 56)

0-10.5 cm: dark-grey, medium to coarse sand; gradational basal contact

10.5-16 cm: dark-grey, fine sand; gradational basal contact

16-24 cm: grey-brown silt with some plant detritus; gradational basal contact

24-37 cm: grey, laminated fine sand; alternating oxidized and un-oxidized laminae; sharp basal contact

37-40 cm: coarse sand; sharp basal contact

40-41.5 cm: grey-brown, very fine sand; sharp basal contact

41.5-68 cm: orange-brown to grey-brown, thinly laminated, medium to coarse sand; upper part of unit is strongly oxidized; sharp basal contact

68-77 cm: grey-brown, laminated very fine sand; sharp basal contact

77-102 cm: grey-brown coarse sand with minor gravel; clasts up to 1.5 cm in diameter; oxidation increases downward; sharp basal contact

102-108.5 cm: dark-grey, coarse sand and gravel; subangular to subrounded, clasts up to 4 cm in diameter; sharp basal contact

108.5-110.5 cm: dark-brown, peaty silt; needles from within the unit yielded a radiocarbon age of 3665 ± 20 ^{14}C yrs BP; sharp basal contact.

110.5-119 cm: dark-grey, fine to medium sand with scattered plant detritus; sharp basal contact

119-125.5 cm: dark-brown, peaty silt; needles from within the unit yielded a radiocarbon age of 3820 ± 20 ^{14}C yrs BP; sharp basal contact

125.5->174 cm: dark-grey, laminated, very fine sand and silt with scattered plant detritus